Neural coding of representations of self-location

Benjamin William Towse

Thesis submitted to UCL for the Degree of Doctor of Philosophy in Computational Neuroscience

I, Benjamin William Towse, confirm that the work presented in this thesis is my own. Where information has been derived from other sources, I confirm that this has been indicated in the thesis.

ABSTRACT

Grid cells in the hippocampal formation fire when the animal visits nodes of a triangular grid covering its environment. Their activity may represent the animal's spatial location for use in memory and navigation. I used simulations to investigate grid cells' encoding of self-location, showing that some properties of in-vivo firing patterns are adaptive for fidelity. In a related project, I found evidence suggesting medial entorhinal cortex cells may participate in non-local representations of remembered, planned or imagined routes, foreshadowing more recent work.

First, I simulated firing patterns in modular grid cell systems with different parameters (e.g. grid scales, orientations), and assessed how well they encode self-location under different conditions (e.g. spatial uncertainty, environment size). I demonstrated that grid cell system parameters affect precision (within the smallest grid scale) and accuracy (including mis-localisation to the wrong repeating unit of a grid) differently.

I showed that grid scale expansion partially mitigates the effect of spatial uncertainty on accuracy, supporting the hypothesis that the temporary expansion experimentally observed in rats exploring novel environments may be an adaptive response to uncertainty.

In an environment with anisotropic spatial information, I showed that aligning the grid-patterns with the axis in which more information is available improves performance, matching collaborators' findings that grid-patterns in humans virtually navigating such environments are aligned that way.

I showed how self-localisation error in larger environments is influenced by the relation between the modules' scales. In the presence of spatial uncertainty, absolute

predictions of capacity break down, and accuracy varies sharply and irregularly with the ratio between modules' scales. This, and the observed biological variability of the ratio, make some theoretical predictions of optimised values for the ratio implausible.

In sum, I have demonstrated how biologically-inspired simulations can help interpret grid cell firing patterns and explore the adaptiveness of neural coding schemes.

IMPACT STATEMENT

Animal brains must encode and use information representing not just individual sensory experiences, but generalised, high-level concepts. An example is spatial information: an animal can navigate familiar environments with reference to internally-held information that maps an environment's features and tracks its own location. Categories of cell discovered in the brain, whose activity patterns correlate with aspects of the animal's position, are believed to underpin this "cognitive map". By studying these cells we can see how the brain encodes and processes information about high-level concepts while correlating them to measurable real-world quantities (an animal's location or direction).

Grid cells are one such cell type. A grid cell fires at a series of locations at the corners of a repeating pattern of equilateral triangles tiling the environment. Each grid cell has a different pattern, so as an ensemble, the set of grid cells in a brain could encode location finely over a large environment. An animal's particular set of grid-patterns therefore determines how it could encode information about space.

This project developed a biologically-inspired computational model that can simulate differently configured grid cell ensembles, and test how accurately and precisely they can encode an animal's location under different conditions – in particular, how well they perform with different degrees of uncertainty in the information available for the animal to work out its location.

Using this model, I tested hypotheses based on experimental observations of animals' grid cell systems. I showed that the grid cell system can flexibly adapt some aspects of its configuration to optimise encoding in different conditions caused by uncertainty. I also showed that optimising other aspects of its configuration is implausible given the irregularities constraining real biological systems.

This advanced our understanding of how the grid cell system encodes information about space, and this modelling framework could be applied to many more questions in this area. Given recent research demonstrating that grid cells can also encode “maps” of non-spatial concepts, and because principles discovered in this brain area may potentially be generalizable to others, it could help us understand how the brain encodes a wider range of high-level concepts, in particular given uncertain information about the world, and how it can adapt its coding schemes to changing conditions.

Though this was basic research, understanding in this area could inform other applications. Understanding how animals encode and process information to map and navigate environments could be used in developing autonomous robots able to do the same. Brain tissue changes in Alzheimer’s disease first arise in the part of the brain where grid cells are found, and the signals of grid cell orientation were recently found to be weaker in young adults at genetic risk of AD. Understanding cognitive functions associated with this area could contribute to diagnosis and monitoring the progress of the disease, and to therapies compensating for cognitive symptoms.

The project generated one published open access journal article and one preprint manuscript published on bioRxiv. This manuscript and a further article are currently being prepared for submission to journals.

PUBLICATIONS ARISING

The following publications were generated from work conducted as part of this thesis. Some text and figures are shared between these publications and this thesis. A further publication is in preparation, based on the work reported in Chapter 5.

Towse, B. W., Barry, C., Bush, D. & Burgess, N. (2014) 'Optimal configurations of spatial scale for grid cell firing under noise and uncertainty.', *Philosophical transactions of the Royal Society B*, 369(1635). The following figures in this thesis are reproduced or adapted from this article, which is available under the terms of the CC BY 3.0 Licence: Figure 3.2 & Figure 4.1.

Navarro Schroeder, T., Towse, B. W., Burgess, N., Barry, C. & Doeller, C. F. (2017) 'Optimal decision making using grid cells under spatial uncertainty', *bioRxiv*. (A revised version of this preprint has subsequently been submitted to a journal.) The following figures in this thesis are reproduced or adapted from this article, which is available under the terms of the CC BY 4.0 Licence: Figure 6.2, Figure 6.3, Figure 6.4 & Figure 6.5.

ACKNOWLEDGEMENTS

This work was undertaken with the support of a studentship from the Wellcome Trust.

I am indebted to a lot of people who have helped me through the past few years, including some difficult times – I would not have got through the other side of this without all of you. Thank you.

To Neil and Caswell, for your advice, training, support and encouragement, for challenging my habitual pessimism, and for countless sessions of bouncing ideas around.

To Christian and Tobias, for the opportunity to collaborate and for the satisfaction of the moment when model and experiment connect.

To my colleagues past and present, on Gower Street, Bedford Way and Queen Square, for the tips, the training and the company.

To my friends, for holding me up when I needed it, listening to me complain, and cheering me up.

To my comrades, for giving me hope, inspiration, and a chance to change the world with you.

And to my family, for your love and unconditional support, no matter how difficult I got.

TABLE OF CONTENTS

1. INTRODUCTION

1.1. Preamble

In order to support the advanced behaviours exhibited by many animals, their brains must mediate deeply complex relationships between stimuli and responses. This requires representing and storing information about high-level concepts derived from multiple strands of sensory information, and manipulating this information for learning, memory, planning and imagination.

The study of spatial cognition is an important potential avenue to developing our as-yet rudimentary understanding of this, since the high-level concepts that must be represented and processed in the brain nevertheless correspond to easily, reliably and quantitatively measurable variables in the world. With the discovery of cells whose activity reflects information about an animal's location, it became possible to conduct a whole field of experiments in which cell- and circuit-level activity can be compared to real-world correlates. Exploration of this area might be the most accessible way in to understanding potentially more general principles about how the brain encodes and processes high-level information.

In the major part of this work, I report investigations which aimed to use computational approaches to develop our understanding of precisely how the configuration of the entorhinal grid cell ensemble – part of the neural system believed to mediate spatial cognition – can determine the quality of self-location representations, and to investigate to what degree that configuration may or may not be adapted to optimise performance in particular environmental conditions. I also report a related investigation into the possible role of this same ensemble in supporting "non-local" representations of location, which are implicated in processes of learning, memory, planning and imagination.

1.2. Establishing the cognitive map: place & head direction cells

The theory that, at least in the rat, spatial problems can be solved with reference to internal allocentric representations of environments dates to Tolman (1948), who coined the term "cognitive map". This cognitivist view superseded behaviourist theories holding that routes through environments were merely series of simplistic stimulus-response or action-outcome associations (an account of the experiments and theories of the behaviourists and cognitivists can be found in Dudchenko, 2010).

But it was not until over 2 decades later that the neuronal basis of this map began to be uncovered. Place cells – pyramidal cells with spatially restricted firing (O'Keefe & Dostrovsky, 1971) – were discovered in the rat hippocampus. These cells typically had a unique single restricted spatial firing field (**Figure 1.1A**), which was relatively stable across time and across visits, and relatively invariant to variables other than spatial location, leading O'Keefe & Nadel (1978) to identify these cells and this structure with the cognitive map. Wilson & McNaughton (1993) confirmed that place cell activity could be an ensemble code for location, by recording from multiple rat place cells simultaneously and decoding this data to accurately predict the location of the subjects.

Subsequently head direction cells, which fire when the rat faces in a particular direction (**Figure 1.1B**), have been found in a number of areas: in particular within the classic Papez circuit (Ranck Jr, 1984; Taube et al., 1990; Chen et al., 1994; Stackman & Taube, 1998; Sargolini et al., 2006) but also in a number of other areas (overview in Taube, 2007).

Animals are capable of performing "vector navigation" – travelling directly from a current location to a goal location, including via previously unexplored short-cuts

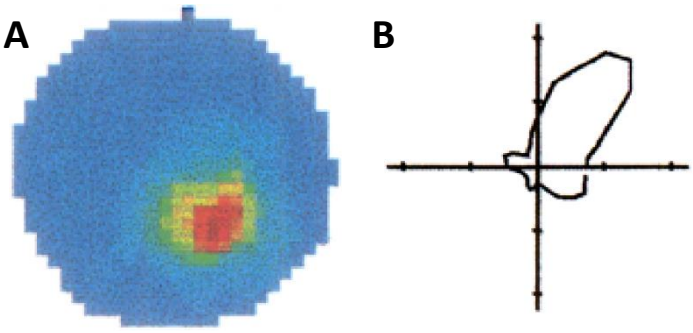

Figure 1.1 – Firing patterns of place and head direction cells

(A) Firing rate map of a CA1 place cell. Colour indicates firing rate at each location, from blue (low firing rate) to red (high firing rate). (B) Directional plot of firing rates of a thalamic head direction cell. Reproduced from Knierim et al. (1995) with permission from Society for Neuroscience.

(Lashley, 1929; Tolman, 1948; Morris, 1981). Place and head direction cell firing signal the animal's current location and heading. But these signals are not enough to complete a cognitive map. This requires the ability to learn the spatial relations between locations, and to use this knowledge to calculate vectors in order to navigate through the environment. Some cognitive map models devised before the discovery of grid cells relied on the plasticity of connections between place cells to encode such spatial relations (e.g. Muller et al.'s [1991] hippocampal "cognitive graph"). This meant that before an animal could navigate efficiently over distances longer than the diameter of the largest place fields (Bush et al., 2015), it would have to conduct relatively meticulous exploration of each new environment in order to learn all the associations between adjacent place fields – a somewhat implausible requirement.

1.3. Grid cells as a potential spatial metric

The discovery and subsequent investigation of grid cells in the rat medial entorhinal cortex (mEC) (Hafting et al., 2005) suggests possible answers to this issue. A grid cell exhibits stable, spatially localised activity rather like a place cell, but in multiple place

fields repeating in a regular triangular grid (**Figure 1.2A-B**). This grid regularly measures out horizontal space with apparently unlimited extent.

Since their discovery, grid cells have also been identified in the mEC of bats (Yartsev et al., 2011) and humans (Doeller et al., 2010; Jacobs et al., 2013), as well as pre- and para-subiculum and plausibly human medial prefrontal cortex (Boccara et al., 2010; Doeller et al., 2010; Constantinescu et al., 2016). In rats, they are present in all principal cell layers of mEC (II, III, V and VI) but they are most densely present in layer II, while many in the deeper layers are conjunctive cells – their firing is determined spatially by a grid-pattern, but also by head direction (Sargolini et al., 2006).

mEC grid cells are organised into discrete modules, within each of which cells display coherent spatial activity patterns with similar grid scale (distance between grid nodes), orientation and distortions but different offsets (**Figure 1.2B-C**). The grid scale common to each module increases in discrete steps. Though smaller scales dominate at the dorsal end of the mEC dorso-ventral axis, the modules are overlapping and interspersed (**Figure 1.2D**; Barry et al., 2007; Stensola et al., 2012; Yoon et al., 2013).

Between different cells in one module whose grid-patterns are offset from one another, all locations in the environment fall within the firing fields of some cells in each module. The firing of one grid cell, or one module of grid cells sharing one grid scale, cannot uniquely define position as their pattern periodically repeats. However, by combining information from multiple modules of grid cells with different grid-pattern scales, the ensemble can, at least in theory, uniquely encode locations over a larger distance (**Figure 1.2E**).

Moreover, as will be discussed in more detail later, the identities of the subpopulation of grid cells active at a particular location can, in theory, code that location's

position vector similarly to a residue number system (Fiete et al., 2008). That is, a system of grid cells could signal, not merely that an animal is at a unique identifiable place, but the relative spatial location of that place within an environment (Barry & Bush, 2012) – presumably (if the grid-pattern is automatically generated across previously unexplored terrain) without the need for the exhaustive prior exploration required in many theories pre-dating the discovery of grid cells (see above). Various researchers have begun to speculate on trajectory-planning algorithms involving grid cells, which could perform vector navigation over much larger distances than

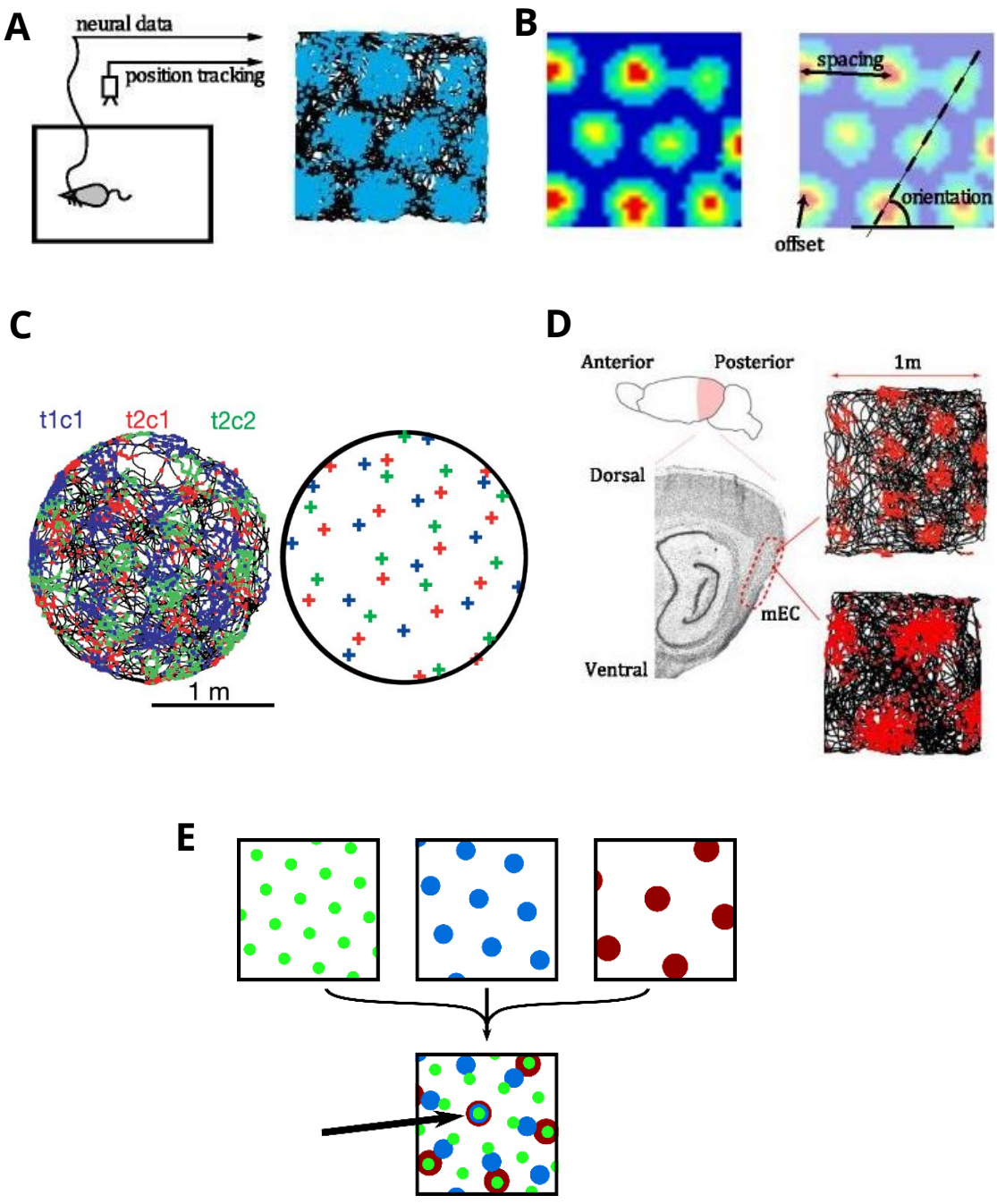

Figure 1.2 – Grid cell patterns

(A) Spikes from individual cells and the animal's position are simultaneously recorded (left) in order to map the locations at which spikes occur (right; black line indicates the animal's path; blue squares indicate its location at each spike. (B) This data is used to create a rate map modelling the cell's firing pattern (by calculating firing rate according to time spent within location bins, and smoothing), scaling from red for high firing rates to blue for low rates (left). Parameters of the grid-pattern are indicated (right). (C) Grid-patterns of different cells in the same module share similar scale and orientation but are offset from one another. Spike locations of three different cells in the same environment are indicated in red, blue and green (left), and the centres of their firing fields compared (right). (D) Grid cells are grouped in modules, with grid scale increasing in discrete steps along the dorso-ventral axis of the mEC. (E) Position information from 3 grid modules with different scales are indicated in green, blue and dark red. In isolation, none can uniquely identify a location. By comparing all 3, the ambiguity can be resolved to identify the location, highlighted by the black arrow. (A), (B) and (D) reproduced from (Bush et al., 2015) under a CC BY 4.0 licence; (C) from (Hafting et al., 2005) with permission from Springer Nature.

approaches using place cells alone (Kubie et al., 2009; Erdem & Hasselmo, 2012; Kubie & Fenton, 2012; Bush et al., 2015).

1.4. Neural representations of boundary location

Border cells in the rat medial entorhinal cortex fire directly adjacent to some or all of the boundaries of enclosures (Savelli et al., 2008; Solstad et al., 2008), and subicular "boundary vector cells" (BVCs) respond more specifically to the presence of a boundary at a particular distance and allocentric direction from the animal. The distance is variable: while some BVCs' firing fields are directly adjacent to a boundary, others are further away (**Figure 1.3**; Barry et al. 2006; Lever et al. 2009; Stewart et al. 2014). Subicular "boundary-off" cells – with firing fields that appear to be the inverse of short-range BVCs – are also found (Stewart et al., 2014).

BVCs' similar responses to both drop-off boundaries (like cliff edges) and wall boundaries implies that they code for boundaries – impediments to movement – regardless of their specific sensory properties (Lever et al., 2009; Stewart et al., 2014).

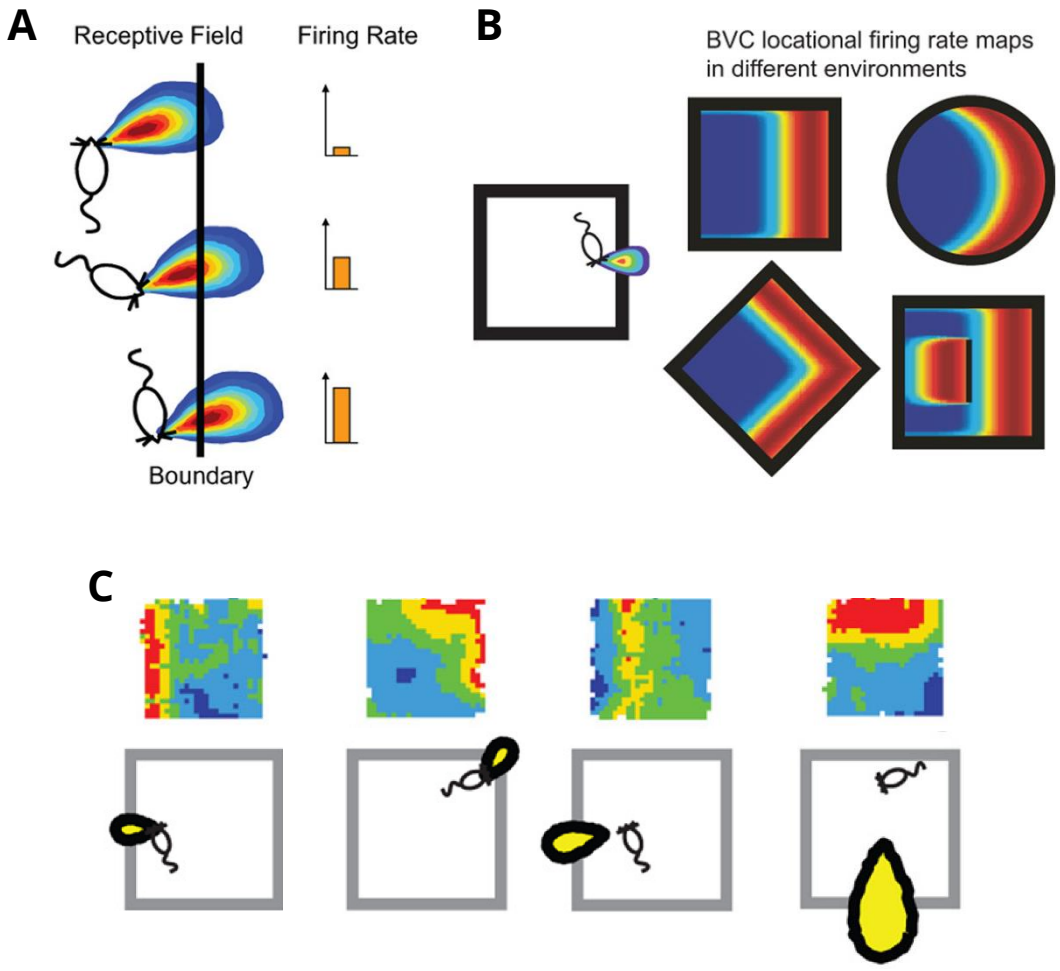

Figure 1.3 – Boundary vector cell firing fields

(A) The modelled receptive field of a BVC. (B) The responses of a BVC modelled in different shaped environments, including the firing field duplication resulting from the insertion of a barrier. (C) The responses of putative BVCs recorded from rat dorsal subiculum (top row), along with inferred receptive fields (bottom row). Note that longer vectors can result in firing in areas not directly adjacent to the boundary that is eliciting the response. Adapted from (Lever et al., 2009) with permission from Society for Neuroscience.

1.5. Connectivity in the hippocampal formation

The main sites where these various types of spatially-tuned cells have been identified are in the hippocampal formation, a group of brain areas in the medial temporal lobe. Following Amaral and Lavenex (2006), which gives a much fuller account of its anatomy, I include within this the hippocampus (narrowly defined as the CA fields CA1, CA2 and CA3) and associated structures: dentate gyrus, subiculum, presubiculum, parasubiculum and entorhinal cortex.

The hippocampal formation is strikingly defined by the serial and parallel connections between its component brain areas, which are organised in a processing loop around which information flows mainly, though not exclusively, in one direction.

Historically, particular emphasis was placed on the idea of a "trisynaptic circuit": information would enter the hippocampal formation at the entorhinal cortex, which projected to the dentate gyrus. The dentate gyrus projected to CA3, which in turn projected to CA1. CA1 was believed to generate the main output of the hippocampus, directed to subcortical areas (Andersen et al., 1971; Amaral & Lavenex, 2006).

We now know that CA1 has strong projections to the subiculum and entorhinal cortex and that these two areas are in fact the main sources of outgoing projections from the hippocampal formation, targeting subcortical and neocortical areas respectively. This has led to a reduction of emphasis on the trisynaptic circuit in favour of a model emphasising a loop in which both serial and parallel connections are significant (Amaral & Lavenex, 2006). The most significant known connections are illustrated in **Figure 1.4**.

The implication of this loop is that place cells in CA1 and CA3, and grid cells in the medial entorhinal cortex (as well as head direction, border and boundary vector cells across various parts of the hippocampal formation), would all be in a position to

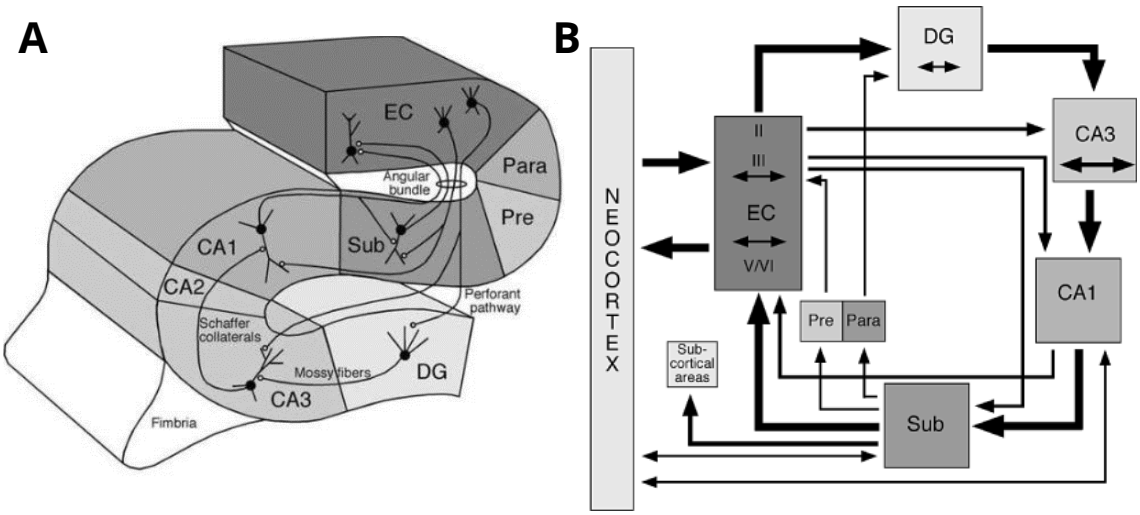

Figure 1.4 – Connections in the hippocampal formation

(A) Major hippocampal formation connections. Entorhinal cortex neurons project to the dentate gyrus, CA3, CA1 and subiculum via the perforant and alveolar pathways. Mossy fibres originate in the dentate gyrus and project to CA3, which in turn gives rise to the Schaffer collaterals that project to CA1. CA1 cells project to the subiculum, and both CA1 and subiculum cells project to the entorhinal cortex, closing the loop. (B) Schematic of hippocampal formation areas and their inter-connections with additional detail of more minor connections including those of the pre- and parasubiculum ("Pre" and "Para"). Note the parallel connectivity – for instance, information from the entorhinal cortex reaches CA3 both directly and via the dentate gyrus – and that the main outputs from the entorhinal cortex to the rest of the hippocampal formation arise in its superficial layers (II and III) but the loop returns to the entorhinal cortex primarily in its deep layers (V and VI). Double-ended arrows indicate substantial recurrent connections within an area. Reproduced from Amaral & Lavenex (2006) by permission of Oxford University Press, USA.

influence one another's activity, however directly or indirectly – the relationships between their different spatial representations will be discussed later.

Since grid cells are the main focus of this work, here I will examine more closely the main site where they are found, the entorhinal cortex.

The entorhinal cortex can be broadly subdivided into lateral and medial areas (lEC and mEC) – grid cells can be found in the mEC. The structure of the EC is laminar,

with numerals I to VI labelling the sequence of layers from “superficial” to “deep”. II, III, V and VI are the principal cellular layers, while I and IV are cell-poor. Grid cells predominate in layer II but can be found in all four principal cellular layers – in the deeper layers, many display conjunctive grid × head direction tuning (Sargolini et al., 2006).

The EC deep layers receive the main inputs from the hippocampal formation (from subiculum and CA1) and send projections in turn to the EC superficial layers. The perforant pathway, which projects to the dentate gyrus, CA fields and subiculum, mainly arises from the superficial layers II and III, though there is a smaller component from layers V and VI (Witter et al., 2000). These connections close the loop discussed above. Conversely, the neocortex’s major connections with the EC mainly come from neocortical areas to the EC superficial layers, and from the EC deep layers out to the neocortex (**Figure 1.4**).

1.6. Anchoring the components of the spatial code to each other and the environment

How are spatial signals maintained, updated and anchored to the environment? Evidence demonstrates that animals use a combination of environmental cues and self-motion inputs. Self-motion inputs allow a representation to be maintained during locomotion without constant reference to cues, or even in their absence: path integration. However, errors in path integration will accumulate over time, leading to an increasing divergence between representation and reality, so it is necessary, at least periodically, to reset the representation using environmental cues in order to keep it anchored to the environment.

1.6.1. Boundary vector cells may mediate environmental cue input to place cells

The existence of BVCs had been hypothesised before their discovery, in a model that proposed inputs with boundary vector receptive fields as substantially determining the location of place cells (Hartley et al., 2000). This was a potential mechanism for anchoring place cell activity to environmental geometry.

O'Keefe & Burgess (1996) had examined the firing fields of place cells across multiple different environmental geometries. They found that place fields could be modelled as the thresholded sum of multiple inputs, each reflecting a tuning curve based on the distance to a boundary in a particular allocentric direction. The BVC model proposed the existence of BVCs to account for these inputs (Hartley et al., 2000; Barry et al., 2006). The BVC model accurately predicted the appearance of additional place fields after the introduction of an extra boundary within an environment; predicted human subjects' search attempts after stretching or squashing of a familiar virtual reality environment; and by inferring the putative BVC inputs to a place cell based on its firing field in one environment, could predict its firing field in a new one. A model in which BVCs are randomly connected as inputs to place cells could account for various statistical properties of place cell populations. Elaborating the BVC model with a learning rule could also account for changes in place fields over time (Barry et al., 2006).

Subicular BVCs matching these predictions were found and characterised some years later (Barry et al., 2006; Lever et al., 2009). This discovery thus supported the theory that place cell firing fields are substantially determined by sensory input about environmental geometry. However, this cannot be the sole factor, because an acknowledged limitation is that this input cannot account for the remapping of place cell fields in response to non-geometric changes to the environment such as colour

(Bostock et al., 1991) since BVCs' receptive fields remain stable through such changes (Lever et al., 2009).

1.6.2. Orientation of spatial representations and the head direction system

To generate a head direction signal, vestibular input is required, while landmarks and motor/proprioceptive systems update the signal (reviewed by Taube 2007). Significant visual landmarks can strongly control the preferred direction of a head direction cell (Taube et al., 1990; Goodridge et al., 1998), and odour cues can influence it at least to a limited degree (Goodridge et al., 1998). The preferred direction will shift to follow visual cues, and in at least some examples, rotation follows cues even if they are moved in sight of the animal, albeit falling slightly short (Taube et al., 1990). This demonstrates how key landmarks can reset the system, largely overriding path integration. Removing cues, blindfolding the animal or turning off the lights does not abolish or change the signal, but the cell's preferred direction drifts over time, presumably reflecting the accumulating errors in path integration. Simultaneously recorded cells' preferred directions drift together, and are shifted by cues together, implying that they are networked together and behave as an ensemble, at least within each brain area where they are found.

Most place cell fields persist in darkness, but without landmarks their spatial firing fields become coarser and less reliable (Markus et al., 1994). According to the BVC model, a key correcting input would be the proximity of boundaries, mediated via BVCs. Place fields appear to be anchored within rotationally symmetrical environments by the same cues as, and rotate coherently with, head direction cells (Muller & Kubie, 1987; Knierim et al., 1995). It is assumed (Stewart et al., 2014) that head direction cells orient boundary vector cells' receptive fields, so it is possible that BVCs in turn mediate the place fields' coherence with the head direction system. Grid-

patterns, too, rotate coherently with each other and with directional cells co-localised in medial entorhinal cortex (Sargolini et al., 2006).

1.6.3. Grid cells, path integration and anchoring to boundaries

Upon their discovery, it was proposed, and became widely accepted, that translation of the grid cell representation was driven substantially by self-motion inputs (Hafting et al., 2005), although there remained disagreement over the precise mechanism by which this is achieved (Fuhs & Touretzky, 2006; McNaughton et al., 2006; Burgess et al., 2007). They were thought to form a "path integration" input into place cells, which had been predicted by O'Keefe & Nadel (1978). The unique subpopulation of grid cells firing at a particular location in an environment was thought to determine and drive the firing field of a particular place cell.

O'Keefe & Burgess (2005) added to this model by suggesting that place cells, gaining associations with particular environmental landmarks, most specifically boundaries, might deliver feedback to their determining grid cells, in order to correct drift resulting from accumulated path integration errors.

More recently, the hierarchical model of the relationship between place cells and grid cells has been challenged. Place cell firing patterns have been shown to appear in rat pups before grid cell firing patterns and to persist in their absence (Langston et al., 2010; Wills et al., 2010; Koenig et al., 2011). In fact, hippocampal inactivation gradually and selectively extinguishes the grid-pattern (Bonnevie et al., 2013) and inverse models have even been suggested in which place cells are the primary input providing the basic building block of grid cells (Kropff & Treves, 2008; Krupic et al., 2014). However, in subsequent recent work the authors of the latter proposal showed that altering an environment's geometry can distort grid and place cell firing patterns differently, showing that their interactions must be more complex (Krupic

et al., 2018). In addition, while place cell firing may persist in the absence of grid cell activity, altering the firing patterns of grid cells does influence those of place cells (Mallory et al., 2018).

Bush, Barry and Burgess (2014) argue that rather than place cell firing fields being determined by grid cells, they are determined by environmental sensory inputs (including boundary vector cells) and can be thought of as forming a separate, but complementary and interacting, representation alongside a path integration-determined grid cell representation. This is consistent with the looping hippocampal formation circuit described earlier that should allow two-way interaction between entorhinal grid cells and CA1 (and CA3) place cells. Note that this interacting, rather than hierarchical, model would still allow for correction of grid cell representations by BVCs, either via place cells or directly.

Subsequently, Hardcastle, Ganguli and Giocomo (2015) showed that error in the grid cell representation accumulates specifically relative to time and distance travelled since the last approach to or near a boundary. As might be expected, encounters with boundaries reduce the error in the represented location most strongly in the direction perpendicular to the boundary. Boundary-related cells, either directly or via place cells, would be likely candidates to mediate this relationship.

1.6.3.1. Environmental geometry influences grid-patterns

In a familiar square environment, the axis of the grid-pattern closest to parallel with one of the walls tends to be at an angle of around 7.5° (**Figure 1.5A**) (Krupic et al., 2015; Stensola et al., 2015). This has been replicated in humans – in a visual search task with a bounded search space, the orientation of grid cell firing patterns (inferred from the hexadirectional modulation of entorhinal fMRI responses) is at 7.5° to the boundaries of a square space, and with a rectangular space the grid-pattern

orientation is anchored to the orientation of the space and follows it through rotations (Julian et al., 2018). It is not yet clear why this should be (though there are hypotheses; see below) but it demonstrates that environmental geometry not only stabilises the grid-pattern but influences its orientation too.

Stensola et al. (2015) attribute the 7.5° wall alignment of the grid-pattern to a shear transformation that also makes the grid-pattern more elliptical (**Figure 1.5B**), and that occurs over time with increasing environmental familiarity. In a larger environment they found discontinuity, with the distortion most apparent in the corners

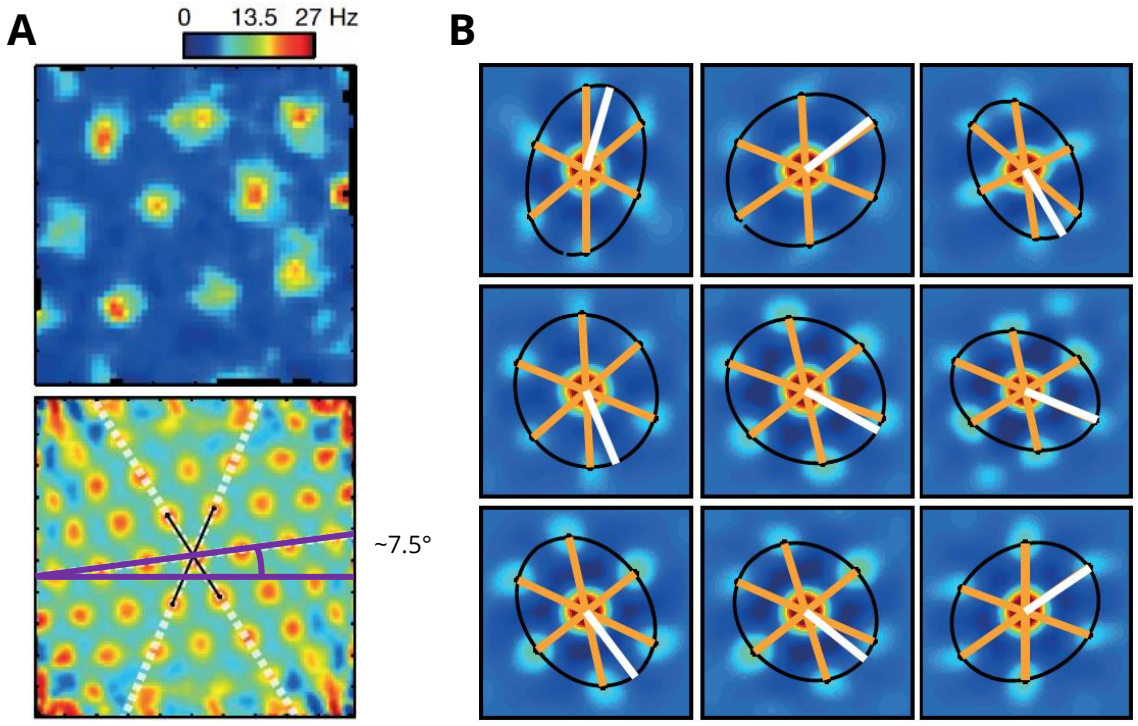

Figure 1.5 – Grid-patterns are oriented to, and shaped by, boundaries

(A) Firing rate map (top) and spatial auto-correlogram (bottom) for a grid cell in a 1.5m×1.5m square arena. White dotted lines indicate grid axes. Purple overlaid lines indicate angle of axis to boundary. (B) Mean spatial auto-correlogram of the firing rate maps for all the grid cells recorded in a module, calculated separately for each of the 3×3 subdivisions in a larger, 2.2m×2.2m square arena. Grid axes in orange. The ellipticity of the pattern (black, with white line indicating ellipse semi-major axis) demonstrates the shear transformation of the grids. Distortions are greater in the corners of the arena. Adapted from Stensola et al. (2015) with permission from Springer Nature.

compared to the centre of the open field. They refer to Krupic et al.'s (2014) model, in which grid-patterns are produced by a distance-related interaction between place-cell-like firing fields and a repulsive force on grid firing fields exerted by boundaries, mediated by boundary cells. They also point out that the 7.5° alignment minimises symmetry between the environment and the grid-pattern, which might serve to disambiguate grid cell firing patterns at geometrically equivalent locations.

This and other recent evidence of grid-pattern distortion from experiments in rats has also called into question the idea that grid-patterns form a completely invariant spatial code. Grid-patterns are temporarily stretched and contracted by deformations of the geometry of a familiar environment (Barry et al., 2007) and grid scale expands in novel environments (Barry, Ginzberg, et al., 2012). Grid-patterns fragment into discontinuous, discrete submaps across connected but walled compartments (Derdikman et al., 2009), though over time with increased experience the patterns do align into a continuous grid spanning multiple compartments (Carpenter et al., 2015). The grid-pattern is heterogeneous in a trapezoid enclosure, with distortion occurring toward the narrower end that appeared to be persistent, not transient (Krupic et al., 2015). Making local changes to environmental geometry by moving the angle of one wall of an enclosure distorts the grid-pattern, with individual grid fields shifting by distances inversely proportional to their distance from the moving wall. In this latter experiment, simultaneously recorded grid cells' patterns tended to distort coherently both within and between modules, so that in principle read-out systems could compensate – however, the authors admit that it is perhaps more likely that the result is distorted spatial perception. This question, which can be asked of all distortions of the grid-pattern, will be discussed more fully in a later section (Chapter 1.9.1).

1.7. Grid cells also organise representations in non-spatial domains

In recent years, the firing patterns of grid cells have also been found to encode continuous variables other than the animal's position in space.

First, entorhinal cells in monkeys performing a visual task were observed to fire in grid-like patterns that mapped the animal's gaze in the visual field, analogously to how grid cells have been observed to map self-location in a two-dimensional environment (Killian et al., 2012). This finding has since been replicated in humans via the detection of hexadirectionally modulated BOLD signals in entorhinal cortex (Julian et al., 2018; Nau et al., 2018).

In a more dramatic departure from the context of their original discovery, grid cells also appear to encode at least some non-spatial variables. It is common to hear spatial metaphors used to talk about things defined by quantitative variables or parameters, with spatial dimensions standing in for the range of the variable(s) and a "parameter space" reflecting the possible set of combinations of values. This is often explicitly visualised in the form of graphs where the ranges of each of the variables are drawn out spatially along different dimensions, as the axes. Evidence arising in recent years indicates a connection between such verbal/graphical metaphors and the way that parameter spaces are actually represented in the brain. Grid cells appear to encode some non-spatial conceptual knowledge in the same way that they encode location in local space!

Human subjects performed a task involving visual stimuli that varied in two continuous parameter dimensions – cartoon pictures of birds with variable neck and leg lengths. "Navigating" the conceptual "bird space" with trajectories in different "directions" resulted in a hexadirectionally-modulated fMRI signal in the entorhinal cortex

and the ventromedial prefrontal cortex – the same brain areas in which similar signals can be detected in virtually-navigating humans (Constantinescu et al., 2016). Entorhinal and hippocampal activity has even been shown to reflect a map-like structure for knowledge about discrete (rather than continuous), non-spatial relationships between stimuli (Garvert et al., 2017). Such findings are not limited to humans either: in rats performing a task that required them to change the frequency of a sound stimulus along a continuous scale, mEC cells were recorded firing in multiple fields at different "locations" along the scale (Aronov et al., 2017).

These findings open up the possibility that the grid cell system may be a more flexible tool with which the brain can represent and manipulate one- and multi-dimensional conceptual knowledge in a general way across different domains. Thus, by studying the ways that grid cells encode information, we may be uncovering not just a component of the basis of spatial cognition, but a component of the fundamentals of cognition as a general, flexible ability of the brain.

1.8. Grid code precision, ambiguity and capacity

1.8.1. Accuracy and precision: aspects of grid code fidelity

In the science of measurement, we can characterise two components of fidelity in a system measuring and representing information about the world. *Accuracy* refers to the closeness between a measurement and the true value, while *precision* refers to the similarity between repeated measurements of the same true value (Joint Committee for Guides in Metrology, 2012).

In the context of representing location by grid cell activity, one can imagine two types of error. I will borrow the above terms from metrology to describe them, but note that for the purposes of this thesis, their meaning is related by analogy but slightly different (since we are considering the values indicated by individual measurements

rather than the population of measurements resulting from repeated representations of the same true value).

Errors of *precision* would be small relative to the scale of a single unit of the repeating grid-pattern, clustering close to the true value, and would be determined by the level of noise in neural firing, the shape and size of fields, and the density of coverage of grids offset from one another within a module. These may also be understood as relating to the *resolution* of the representation.

Errors of *accuracy*, or "*ambiguity* errors" as I will also refer to them, would result from the ambiguity or failure of a code based on periodic patterns. These errors would be larger, nonlocal errors, corresponding to the distances between locations where the set of phases across the modules is similar enough to be indistinguishable (**Figure 1.6**), or resulting from noise perturbing the phase signal in a subset of the modules that causes the modular arithmetic code to indicate a very different location (see below) (Fiete et al., 2008; Sreenivasan & Fiete, 2011).

1.8.2. Grid code capacity and the configuration of grid scales

As described previously (**Figure 1.2**), information from multiple grid modules with different scales can be combined to resolve the intrinsic ambiguity of each module's periodic pattern. In this model, location is represented by a modular arithmetic (MA) code, or residue number system (RNS). This is a system in which a quantity is represented by the set of remainders left after division by each of a set of fixed values, or moduli – here, the moduli are the grid scales and the remainder is the phase of each module (Fiete et al., 2008).

However, while such a system can represent locations over a range greater than any one of the modules, there remains a finite limit on the locations that can be uniquely encoded in this way: the spatial capacity of the grid code. The capacity of an RNS is

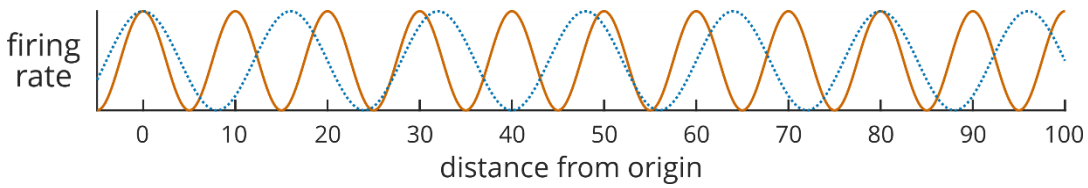

Figure 1.6 – A modular arithmetic grid code's capacity depends on the similarity of module phases at different locations

In the approach proposed by (Fiete et al., 2008), the idealised spatial capacity of a grid cell system is the lowest common multiple of the set of scales present. At two points separated by this distance, the phases of the grid modules will take the same values. Thus, in this example two 1D sinusoid grid-patterns with scales of 10 units (solid orange line) and 16 units (dotted blue line) have the same phases at the origin and 80 units from the origin. However in a more realistic scenario, affected by limited resolution for encoding and read-out, and noise, the capacity to uniquely identify locations is reached when the environment is large enough to encompass locations where the values taken by the phases are sufficiently similar that the signals cannot be reliably distinguished. In this example, the phases at approximately 31 and 49 units away are very similar to those at the origin.

the lowest common multiple of the moduli and Fiete et al. (2008) showed how this would be the maximum range of an idealised grid cell system considered with integer grid scales and distances. At two locations separated by this distance, the phases of the grid modules will take the same values (**Figure 1.6**). The encoding system essentially runs out of labels (or at least runs out of *valid* labels – see below).

In an RNS a coprime set of moduli – having no common factors greater than 1 – maximises the range, as the LCM of a coprime set of integers is equal to their product. So in an idealised system, a coprime set of grid scales would maximise capacity. Such a system would be able to represent distinct locations uniquely across a range many times larger than the largest grid scale and capacity would scale combinatorially with the number of grid modules (Fiete et al., 2008).

More realistically, given noise in the system, finite resolution of read-out systems, and grid scales being not idealised integers but real values, to which concepts of

coprimeness and LCM do not strictly apply, the capacity is instead reached when the environment is large enough to encompass locations at which the sets of grid module phases are so similar they cannot be reliably distinguished. Nevertheless, with grid scales in the right ranges the capacity can still scale combinatorially (Fiete et al., 2008).

The MA code is susceptible to errors. A small error in the phase represented by a single module can result in a disproportionally large change in the position represented by the population. However, the large capacity of such a system might facilitate a form of error correction. Such erroneous decoded locations might easily be identified by comparison to knowledge of recent locations or the extent of the current environment or of the animal's usual behavioural range (Fiete et al., 2008; Sreenivasan & Fiete, 2011). Stemmler et al. (2015) also point out that if the scales are not an integer coprime set, certain labels (combinations of phases) do not correspond to valid locations – if error resulted in such a signal, it might also be easily identified. A read-out system could thus reject these different types of identified errors in favour of plausible alternatives.

The research groups of Andreas Herz and Vijay Balasubramanian have taken a different approach (Mathis et al., 2012; Stemmler et al., 2015; Wei et al., 2015). Rather than this MA code, they model the grid cell system as providing a "nested" representation limited in capacity to the largest grid scale present. Herz et al., and others, argue that error correction mechanisms like those discussed above are nontrivial, and read-out from an MA code would be profoundly disrupted by changes in regularity or scale of grid-patterns (Mathis et al., 2012; Carpenter & Barry, 2016), which have been observed experimentally (Barry et al., 2007; Barry, Ginzberg, et al., 2012; Stensola et al., 2012, 2015; Krupic et al., 2015). Wei et al. (2015) cite estimates that a rat's home range is as small as ~$(10\ m)^2$ (Davis et al., 1948), and it is quite plausible

that grid cells exist with scales around this size, plausibly less than the largest grid scales (Brun et al., 2008) – though this is disputed, as discussed below.

On the basis of a nested representation and using a hypothetical model to read out navigation vectors from the grid cell system via population vectors (which performs as well as an ideal observer), Stemmler et al. (2015) predicted that a ratio of ~1.5 between the scales of successive modules is ideal. On the other hand, using an approach that aimed to minimise the number of grid cells needed for the system to achieve a biologically useful resolution, Wei et al. (2015) predicted a geometric sequence of grid scales with a ratio of either √e (~1.65) or ~1.44 (depending on the read-out mechanism).

However, a recent response defended the MA code hypothesis over the nested code (Vágó & Ujfalussy, 2018). These authors argue that a nested code is much less robust to error or knockout of an intermediate module, and to insufficient input from one module. And they argue, contrary to Wei et al., that the distances typically travelled by rats are actually substantially larger than the largest detected grid scales. Fiete et al. (2008) suggested the same, citing research estimating behavioural foraging ranges, of 0.1 – 1 km per linear dimension (Recht, 1988; Russell et al., 2005). This evidence is more recent than Davis et al. (1948), and includes observations of rats in more natural and open environments than the urban areas in that study.

These authors' analysis concluded that given a small number of modules, while the scale ratio between modules does strongly affect the spatial capacity of the population, the relationship between scale ratio and capacity is extremely irregular and discontinuous. Since even a small deviation in scale can result in a dramatic change in capacity and because observed grid scales are known to be variable (Barry, Ginzberg, et al., 2012; Stensola et al., 2012; Krupic et al., 2015), this implies optimisation is biologically implausible. Further, in systems with more modules and with

neuronal noise accounted for, capacity varies much less with module scales, even when module scales are selected at random. This would make optimisation marginal or unnecessary in any case (Vágó & Ujfalussy, 2018).

1.9. Are grid code parameters optimised?

The fidelity with which the brain can represent information about self-location (like information about any aspect of the environment) is necessarily limited. Maximising it is key to optimal decision-making. The parameters of the grid code – the pattern's orientation; the number of cells in each module and the distribution of their offsets; the scale (spacing between fields) of each module's pattern; the relation between different modules' scales; the number of modules; the profile of the fields (shape, symmetry, width); distortions; and discontinuities – whether varying or unvarying across time and different situations, must affect the fidelity with which the system can represent information. It is therefore reasonable to speculate that these parameters, and any variation in them in response to environmental conditions, would be subject to evolutionary pressures. For instance, as discussed in the previous section, various theoretical work has attempted to work out what particular sequence of scales for the grid cell modules would maximise resolution or capacity (Fiete et al., 2008; Sreenivasan & Fiete, 2011; Mathis et al., 2012; Stemmler et al., 2015; Wei et al., 2015; Vágó & Ujfalussy, 2018).

1.9.1. Optimisation and varying parameters

Where parameters are observed to vary within an animal over time or between contexts, this raises the additional question of how the varying code is read out by downstream systems. Initial discussion of the role of grid cells generally proceeded from the premise that their regular firing patterns were invariant over time and across different environments, and considered this invariance key to their role as a

spatial metric. This implies that the grid-pattern distortions, discontinuities and variability over time that have subsequently been observed would have a negative impact on the fidelity of self-location representations. If downstream read-out systems do not account for changes and irregularities in the relation of grid cell activity to self-location (i.e. grid cell firing patterns), the estimates of location that they derive from the grid cells' activity will be wrong and spatial perception will be distorted.

However, it has been shown that as long as distortions are common to all grid cells within a module, the code can still act as a universal metric (Stemmler et al., 2015) – though note that with limited knowledge of how downstream systems actually "read out" information from grid cell activity, we cannot say with confidence how far this theoretical possibility is borne out by biological systems, and what types and magnitudes of distortion are tolerable to real downstream systems. Nevertheless, it is conceivable that downstream systems account for some or all of these discontinuities and variability, and perform read-out correctly. In this case, we might ask whether said variability is in fact an adaptive, fidelity-optimising response to particular conditions – this question forms the basis of much of this thesis.

For instance, after finding that when an animal is placed in a novel environment, grid scales start out larger, and progressively contract with increasing experience of the environment until they reach a stable baseline size, Barry, Ginzberg, et al. (2012) hypothesised that this might be an adaptive response, maximising the fidelity of self-location representations under conditions of spatial uncertainty. In Chapter 4, I will describe an investigation to test this hypothesis.

1.10. Non-local activity of place cells

Since the initial characterisation of place cells as firing within a specific place field, a variety of phenomena have been discovered in which place cells appear to fire outside those ordinary fields. Here, I term this activity "non-local" firing – and its speculated role in coding representations of remembered or imagined locations and routes "non-local representation".

1.10.1. Sharp-wave ripples and place cell replay in sleep

During eating, grooming, drinking, quiet sitting and slow-wave sleep (SWS), the "large amplitude irregular activity" (LIA) pattern dominates the hippocampal EEG. LIA is more random than the 6-12Hz theta rhythm dominant during translational movement, with a flatter power spectrum, increased power at sub-theta frequencies and transient (50-100ms) sharp-wave ripples (SWRs) of high frequency (~200Hz) activity. Before grid cells were discovered, SWRs were also detected in entorhinal cortex 5-30ms after those in CA1 (Chrobak & Buzsáki 1996).

O'Keefe & Nadel (1978) described LIA and SWRs, noting that place cells would fire together at some SWRs, but argued it was unlikely that much information was conveyed in such events and characterised LIA as little more than the absence of theta. However, Buzsáki (1989) pointed out that synchronised pyramidal cell activity during SWRs could plausibly promote long-term potentiation (LTP) and proposed a role in memory consolidation. The position that LIA and SWRs have an active functional role has since been strengthened by two decades of research on the associated place cell activity. Wilson & McNaughton (1994) showed that place cells coactive during behaviour because of their overlapping place fields fired together more during sleep afterwards than sleep before, and that these correlations were significantly higher during SWRs. These experience-dependent changes were taken to reflect learning, and it was suggested that SWRs are involved in "replay" of this learned information

about past experiences to drive systems-level consolidation (from the hippocampus to the neocortex).

Skaggs & McNaughton (1996), Louie & Wilson (2001) and Lee & Wilson (2002) reinforced the evidence that these events represented replay of past experience by showing that temporal order information was preserved – the sequence in which place cells fired during behaviour was accurately reproduced during SWRs in subsequent SWS (slow-wave sleep), but compressed in time approximately 20-fold, and at a real-time speed during REM (rapid eye movement) sleep. Skaggs & McNaughton (1996) hypothesised that LTP had strengthened the synapses from preceding to succeeding place cells, and in support of the consolidation hypothesis Lee & Wilson (2002) pointed out that the precise ordering and short timescale of replay lent itself to LTP induction.

Monitoring the activity of a place cell during sleep, and delivering a rewarding stimulation to the medial forebrain bundle whenever it fired, causes a rat to disproportionately visit and remain in the location of that cell's place field upon waking (de Lavilléon et al., 2015). By inducing an association that influences spatial behaviour, this provides powerful evidence that place cell activation during sleep genuinely does relate to spatial representation (and that place cells play an active role in spatial behaviour).

1.10.2. SWR-associated place cell replay during waking states

Firing of place cells outside their place fields is not limited to sleep. Kudrimoti et al. (1999) found similar events to those described in SWS, during SWRs in rats kept sitting quietly but awake. More recently, non-local firing even during the same behavioural session has been identified. Foster & Wilson (2006) trained rats to run back

and forth along a linear track for rewards at the ends, and described, while the animals paused at each end, SWR-associated *reverse* sequential replay of recently active place cells. Foster and Wilson contrasted this phenomenon with forward replay in sleep and speculated that it was involved in reinforcement learning of sequential actions, by allowing propagation of value information from the final reinforcement backwards. Csicsvari et al. (2007) replicated reverse replay in SWRs apparently occurring, not at rest, but during exploration in an open field, even alongside continued place-specific firing. Diba & Buzsáki (2007) demonstrated SWR-associated forward play during immobility before a journey on a linear track, as well as replicating the finding of reverse replay at the end. Davidson et al. (2009) found extended forward as well as reverse replay associated with SWRs during open-field exploration. The trajectories represented were not limited to beginning or ending at the rat's present location.

It was initially thought that the reactivation of stored sequences from other contexts was limited to sleep, and awake replay would be limited to sequences representing locations and routes within the current environment. However, this was subsequently disproven by the detection of awake replay in one environment of sequences stored from experience in another environment, indicating that the hippocampus reviews past experiences constantly, not just during rest (Karlsson & Frank, 2009).

1.10.3. SWR-associated non-local place cell firing supports learning

Evidence supports a role in learning and memory for these phenomena. In a spatial learning task, the number of SWRs occurring at reward locations during exploration, and the proportion of subsequent SWRs in sleep during which goal locations were represented, both correlate with later performance (Dupret et al., 2010).

Beyond simply observing correlation, performance on spatial learning tasks can be degraded by using triggered electrical stimulation to suppress SWRs during sleep immediately after training (Girardeau et al., 2009; Ego-Stengel & Wilson, 2010).

The precise role of these events in learning and memory processes is still being explored. Wilson & McNaughton (1994) were the first to propose that replay facilitates systems consolidation, "writing" engrams from the hippocampus into neocortical memory. However, it remains possible that it may merely be stabilising the newly-formed engram within the hippocampus: this question is discussed further in (Ólafsdóttir et al., 2018).

1.10.4. Forward-directed theta sequences during waking behaviour

By decoding the ensemble place cell code to determine the sequences of locations seemingly represented through time, Johnson & Redish (2007) were able to reconstruct the paths in a T-maze described by rapid sequential place cell activations both at the maze junction, and when a cue indicated that the rat had entered the wrong arm. The represented point began at the rat's actual location and swept ahead. When the rewarded arm varied and was cued each time, it went down each arm of the maze in turn. However, when the rewarded arm was kept constant, forward sweeps down the unrewarded arm decreased with increasing experience, as did time spent at the choice point. These forward sweeps apparently occurred independently of SWRs, during the theta rhythm state (though this study's approach to SWR identification has been criticised by Carr et al. 2011), resulting in the term "theta sequences".

Compressed forward sweeps of represented location like this might be explained as epiphenomenal: a simple result of a tendency of individual place cells to precess their firing through phases of the theta cycle: firing later in the theta cycle as the

animal enters the field, and progressively earlier as it moves through the field. Such "phase precession" was first observed in place cells (O'Keefe & Recce, 1993) and was subsequently detected in grid cells (Hafting et al., 2008). However, it is possible to shuffle spike phase data in such a way as to dissociate the occurrence of theta sequences from phase precession (Foster & Wilson, 2007). Wikenheiser & Redish (2015) argue that these sequences are more than just the sum of individual cells' phase precession: that spikes are more precisely and richly patterned and coordinated than would be expected from phase precession alone, and that theta sequences play an active role in information processing, potentially in planning and decision-making.

More recent evidence strengthens the hypothesis that events of this type genuinely do replay a role in planning and/or selecting prospective routes. Activation of path sequences never previously experienced has been observed (Gupta et al., 2010). On a trial-by-trial basis in a spatial alternation task, SWRs were monitored in the immediate run-up to the choice point, and correct selections were preceded by more frequent non-local co-activations of place cells associated with locations on each of the possible route (Singer et al., 2013).

In another study, rats were shown a reward being placed in a visible but unvisited location. A rest period in another location followed before the animal was later allowed access to the location. During this period, place cell sequences corresponding to the prospective route to the reward were activated, but not sequences to an unrewarded but otherwise equivalent location. In this case, sequences leading both to and from the goal were activated, both forwards and in reverse, and these events correlated with periods of higher power in the frequency spectrum corresponding to SWRs (Ólafsdóttir et al., 2015).

The task-dependence of the specific content of non-local activity provides particularly suggestive evidence for a role in navigational planning and decision-making. In rats navigating in an open arena, non-local place cell activity tended to project in the direction the animal was about to travel when they were travelling to a specific hidden goal, but not when foraging randomly (Pfeiffer & Foster, 2013). In a decision task, non-local activity detected immediately around arrival and departure from a choice point was more focussed on the current location, and projected forward trajectories. Such activity correlated with correct choices. But during longer rest at the choice point, trajectories distributed around the environment were represented (Ólafsdóttir et al., 2017).

In what could be interpreted as representing a deliberative process, preliminary unpublished work by Frank and colleagues appears to show non-local place cell activity during a decision-making task concurrently representing two alternative routes in alternating theta cycles[*].

There is also evidence that normal SWRs are necessary for correct spatial decision-making: disruption of SWRs by electrical stimulation during an alternation task decreased performance (Jadhav et al., 2012).

1.10.5. Replay, declarative memory and imagination

The ability to preserve temporal order in encodings of past experiences, as in place cell replay, is obviously a prerequisite for episodic memory, and some researchers have suggested that spatial memory is the very foundation of episodic memory (O'Keefe & Nadel 1978). Johnson & Redish (2007) conceptualised declarative

[*] Reported in a seminar at UCL by Loren Frank, Dec 2017, which was the subject of a UCL website news report (Cashin-Garbutt, 2017)

memory use as “the use of learned information outside the place or context of its initial presentation,” suggesting that non-local firing of otherwise spatially specific cells might correspond to “the use of declarative-like memory in rats.” Since to be useful to inform future behaviour, memories have to be both created and then re-activated, roles for non-local activity of spatial cells in both consolidation and planning are consistent with a general involvement in declarative-like memory.

Knierim (2009) drew a tantalising speculative link between representation of non-local trajectories in the rat hippocampal formation and the apparently impaired ability of hippocampal amnesiacs to imagine spatially coherent novel experiences (Hassabis et al., 2007). Byrne et al. (2007) proposed a model in which internally simulated movement signals to the hippocampus could drive mental exploration. Subsequently, fMRI has revealed the same grid-like activity in the human entorhinal cortex during both virtual and imagined navigation (Horner et al., 2016), as well as while imagining facing in different directions without movement (Bellmund et al., 2016) – the latter is detectable because the fMRI approach is believed to reflect specifically the activity of conjunctive grid × head direction cells (discussed in more detail in Chapter 6.4.1).

The investigation of non-local spatial representations in the hippocampal formation could thus shed light on the physiological basis of complex cognitive processes such as declarative memory formation, consolidation and recall, navigational planning, decision-making, and potentially even imagination.

2. THE ROLE OF GRID CELLS IN NON-LOCAL SPATIAL REPRESENTATION

This project sought to explore whether non-local representations – replay or forward sweeps – also occur in grid cells, and if so to characterise them and their relationship to such representations in place cells. As discussed above, examining the relationship between mEC grid cell and hippocampal place cell activity during non-local representation events might have yielded insights into the neural basis of advanced cognitive processes. This research stream was set aside after the first part of my PhD in order to pursue a more productive project.

2.1. Methods

2.1.1. Data collection

The data used were collected by Hafting et al. (2008) via extracellular recordings of layer II dorsocaudal medial entorhinal cortex grid cells in rats. These data are publicly available[†]. Full methods are in their report (Hafting et al., 2008) and will be summarised here.

Animals were implanted with microdrives connected to tetrodes and recorded while running back and forth on a 320cm linear track. Food was available at the turning points and the position of the animal was simultaneously recorded by tracking an LED attached to the headstage at 50Hz. The position record was later smoothed by

[†] The data were originally accessed in 2011 via http://www.ntnu.no/cbm/gridcell but, as of 23 March 2018, are instead to be found at https://doi.org/10.11582/2017.00020. They have been made available for use under a CC BY 4.0 licence.

Hafting et al. with a moving mean filter. Triggered spikes were stored at 48 kHz during recordings, and sorted offline using graphical cluster-cutting software (*TINT*; Neil Burgess & Axona Ltd.).

I downloaded this processed data and performed further analysis in MATLAB 7 (MathWorks). Only sessions including spikes recorded from at least 4 units in layer II were used: 6 sessions qualified, of durations 5-20 minutes with 4-8 units simultaneously recorded in each. Tracked position data in the axis perpendicular to the track was discarded, leaving a one dimensional record of the rat's position along the track length. Smoothed rate maps were created for each unit by grouping spikes by location of occurrence into 2cm-long bins, normalising spike rate by the total time spent in each bin location, and smoothing using a 5-bin-long boxcar filter. Only spikes which occurred when the animal was moving at least 5 $cm.s^{-1}$ were used to construct ratemaps (**Figure 2.1**). The animal's speed and direction of movement in the track axis dimension was calculated by comparison of position at successive time-points.

2.1.2. Spiking events

Spiking events were identified as candidates for further analysis, using a definition adapted from Dragoi and Tonegawa (2011). Spiking events were defined as epochs separated by at least 50ms, during which spikes occurred at less than 50ms intervals. Spiking events had to include spikes from at least 4 units (**Figure 2.2A**). To ensure that real-time local representations of the rat's movement along the track were not mistakenly interpreted as candidate non-local representations, spiking events lasting longer than 500ms were excluded, as were events during which the rat's mean speed equalled or exceeded $5cm.s^{-1}$. This speed threshold was selected in order to separate the data used to characterise events from that used to construct ratemaps.

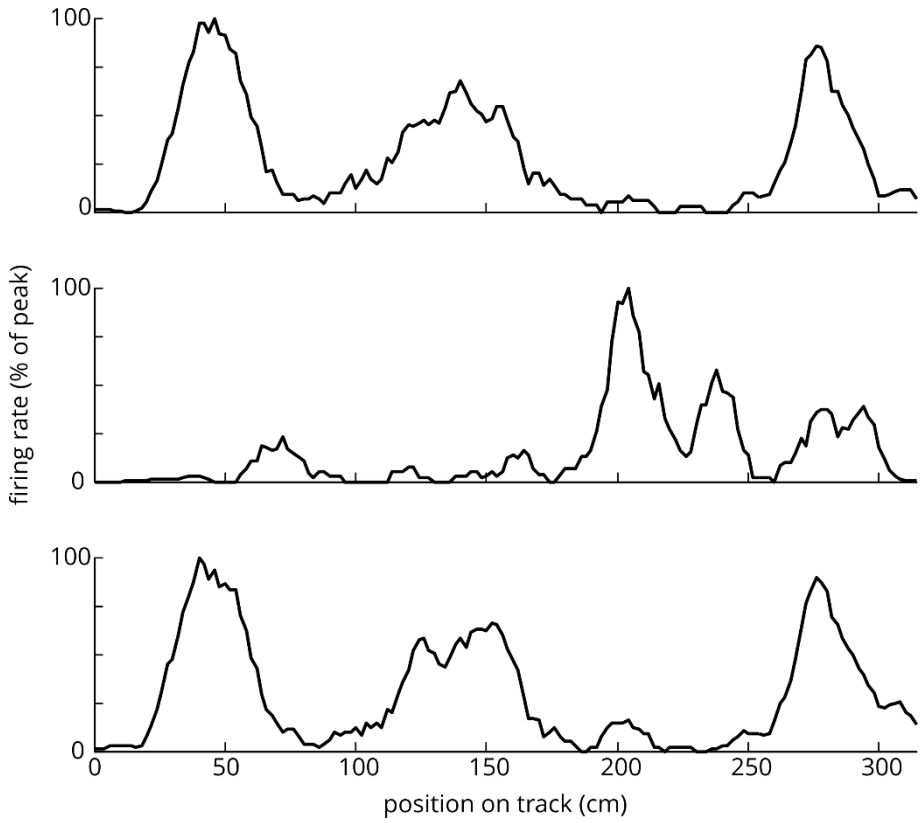

Figure 2.1 – Firing rate maps of layer II mEC neurons along the track

Smoothed, one dimensional rate maps showed multi-peak spatially restricted firing on the track. (Examples shown are from session LT-16030611. Cells are t1c1, t2c2, t4c2).

A timeline of each active unit's spiking activity, analogous to a spatial ratemap, was created for each event by binning spikes in 2ms intervals, and smoothing using a Gaussian filter (standard deviation 5 bins) (**Figure 2.2B**).

2.1.3. Comparison of event temporal structure to spatial map structure

A cross-correlation procedure was used to compare the ratemaps of all cells to one another and the timelines of all cells within an event to one another, thus characterising the overall structure of the spatial representation of the track and the temporal activity during each event. All possible pairings of active units were compared using unbiased cross-correlation (MATLAB *xcorr* function) and the absolute lag/distance to the nearest peak in the cross-correlogram from zero (whether left or right/before or after) was calculated. Only peaks in the cross-correlation which fell within the upper

two-thirds of the range of values within that cross-correlation were considered (**Figure 2.2C-E**).

Each spiking event's temporal structure was compared to the spatial structure of the recorded units' activity on the track. For the cell pairs active in the event, the absolute cross-correlation lags in the event were compared to the absolute cross-correlation

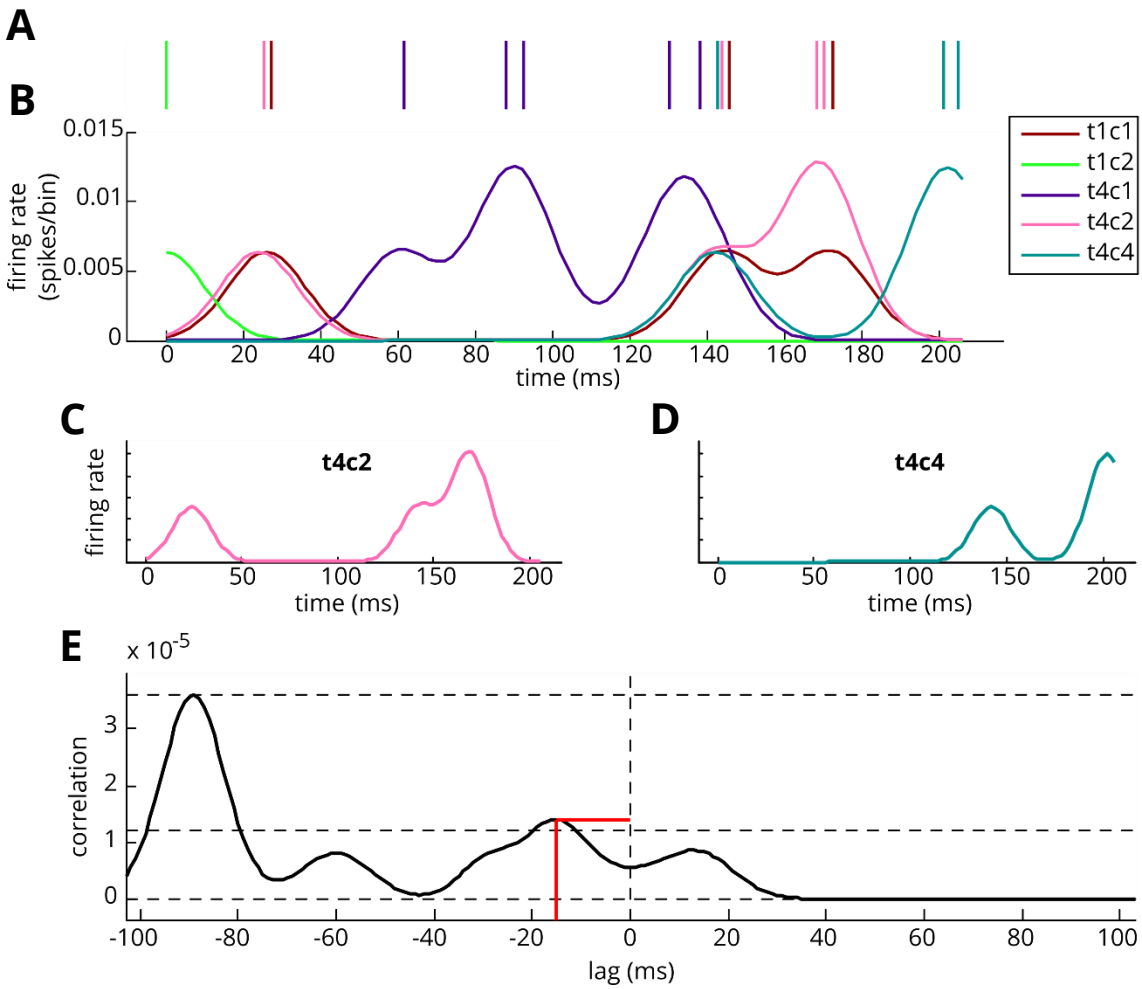

Figure 2.2 – Timeline and cross-correlation of a spiking event

Spike rasters (A) and smoothed firing rate timelines (B) illustrate the sequence of spikes recorded from 5 units participating in a spiking event. Pairs of cells (C and D) are cross-correlated (E). The suprathreshold peak nearest to zero lag is selected and its absolute lag taken as a measure of the temporal proximity of the two cells' firing. (Event 21, detected approx. 286s into session LT-16030611. Unit IDs as indicated in legend. Horizontal dashed lines in E indicate maximum, minimum and threshold. Threshold includes upper two-thirds of range. Red lines in E indicate peak identification and lag measurement.)

distances on the map using one-tailed Spearman's rank correlation – it was decided *a priori* to test specifically whether cells that fired close together in space, also fired close together within an event.

An event was defined as significantly structurally correlated to the spatial ratemaps if this Spearman's rank test returned a significant ($p<0.05$) result. The proportion of events that were correlated was itself tested for significance using a one-tailed binomial test, with the null hypothesis that 5% or less of events would pass the significance threshold (i.e. the number of significantly correlated events was compared to the binomial distribution expected by chance given that a randomly ordered event would have a 5% chance of passing the significance threshold).

2.2. Results

Analysis of Hafting et al.'s publicly available data indicated that layer II cells in medial entorhinal cortex that fired close together during locomotion on a linear track also fired close together in time during spiking events detected during periods of immobility. This suggests that, indeed, these cells could be participating in non-local representations of imagined or remembered routes.

2.2.1. The temporal structure of layer II mEC unit firing during spiking events is similar to the spatial structure of those units' activity on the track

51 qualifying spiking events were detected in the 6 recording sessions. Their durations ranged from 13 to 352 ms (mean = 101 ms) and they included 4 to 42 spikes (mean = 11) recorded from 4 to 6 individual units (mean = 4.3). Of these 51 events, 9 showed significant ($p<0.05$) structural correlation to the spatial distribution of unit activity on the track – that is, cells that fired close together spatially also fired close together in time during events (**Figure 2.3**). This was more than would be expected purely by chance (Binomial test; $p = 8.78\times10^{-4}$ for 9 or more significant events out of

51 if each had a 5% chance of being a false positive). Thus, the spatial structure of cell activity during locomotion was recapitulated in spiking events during relative immobility, in the sense that the ranked temporal proximity of cells firing during potential replay events correlated with the ranked spatial proximity of their firing fields.

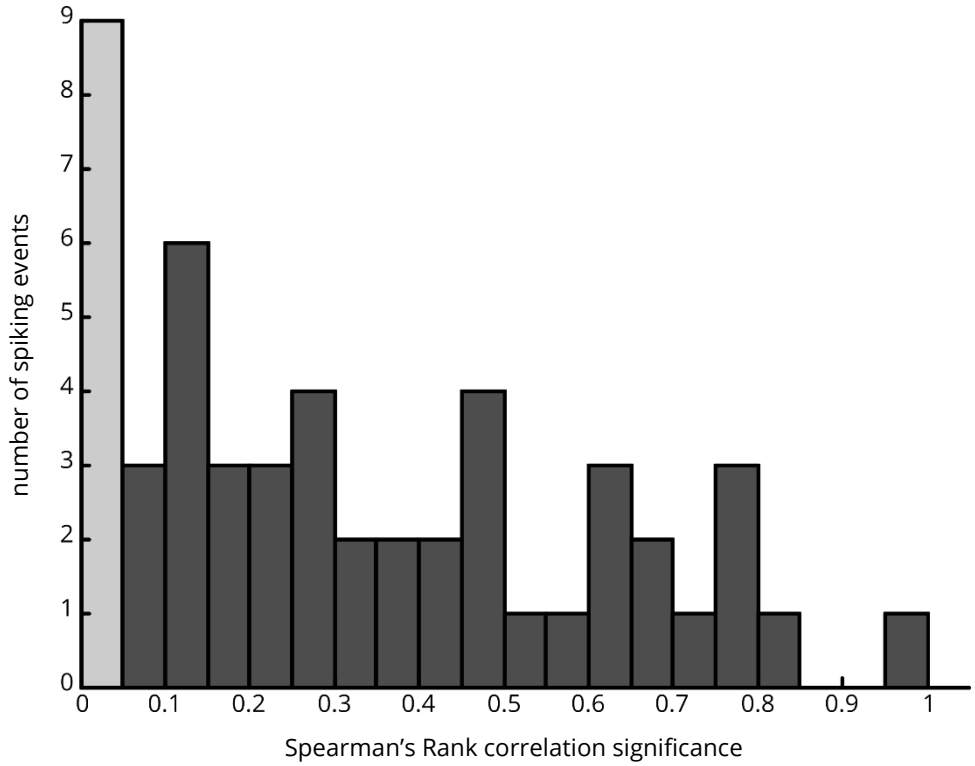

Figure 2.3 – Significance of individual events' similarities to spatial activity structure

During a large proportion of detected spiking events (9/51), cells whose spatial firing fields were near each other also fired close together in time ($p<0.05$ indicated in lighter grey; 1-tailed Spearman's Rank Correlation).

2.3. Discussion

2.3.1. Temporal organisation of grid cell activity during relative immobility reflects spatial proximity of cell firing fields characterised during locomotion

This analysis of electrophysiological recordings indicates that layer II dorsocaudal mEC grid cells that show spatial firing close to one another during locomotion on a linear track, also fire in close temporal proximity during clustered spiking events

during relative immobility on the same track. This is a preliminary indicator that cells in this area may participate in non-local representations of remembered, planned or imagined routes. Hippocampal place cells are well-known to participate in such events, which have been shown to reflect the temporal firing sequences observed during actual navigation, and have been observed during slow-wave sleep (Skaggs & McNaughton, 1996; Lee & Wilson, 2002), REM sleep (Louie & Wilson, 2001), pauses between locomotion (Foster & Wilson, 2006), during active navigation (Csicsvari et al., 2007) and at maze choice points (Johnson & Redish, 2007), in many but not all cases associated with short-wave SWRs.

2.3.2. Limitations

It remains unclear whether cells are actually firing in the same sequence that their fields appear on the track. In fact, it is challenging to design an algorithm to assess this, since unlike most place cells, grid cells have multiple fields. Therefore, representation of a route may well include repeated activations of a particular cell at different parts of the spike sequence, and since grid cells will not necessarily share equal scale or be perfectly regular, the pattern will not necessarily be entirely cyclic even for one-directional travel on a straight track. An extension to the above method could assess the relative lags between activations of different cell pairs at the closest next peak in a cross-correlation. That is, compare how long after cell A, cells B, C, D... first tend to fire, and cells A, C, D after cell B, etc. However, even that approach could only capture the most proximal following activity, and does not consider the full repetitive pattern that characterises a grid cell.

Attempting to actually decode ensemble cell activity to indicate the represented location might be the best route, but would likely require simultaneous recordings of a much larger number of cells (including cells with multiple grid scales, to avoid the the intrinsic to periodic firing patterns). It is also difficult to decode a

representation which may very well “play” at a different, but unknown, speed from the “real-time” representations on which a decoding algorithm must be based, since the expected absolute firing rates of cells corresponding to represented locations is unpredictable. A Bayesian approach could constrain reconstruction by relating each decoded position to the previous decoded position, but would employ circular logic by assuming the continuous route representation whose existence it is supposed to test!

The search for replay events could be further constrained in terms of the direction of play – looking specifically for either backwards or forwards play of trajectories. However, as place cells show both forward and backward replay when the rat is waiting at the end of the track, it is not clear which should be expected. Trettel & Colgin (2014) were able to present preliminary evidence of grid cell replay by examining REM sleep (as opposed to waking behavioural data as I did) and constraining their search using the premise that grid cell replay might follow place cell replay in that condition – i.e. it would run forwards in real-time (Louie & Wilson, 2001). Below, I will discuss more complete evidence published more recently.

Additionally, a search could be limited only to events coinciding with SWRs. However it was not possible to reliably identify SWRs in the dataset I was using, because the EEG recording had no reference, making it impossible to distinguish SWRs from the very similar artefacts produced by jaw muscle activity.

A further point for consideration is the aforementioned question of distinguishing between “forward sweeps” of cells firing in sequence and straightforward local phase precession during movement (see Introduction). Looking for coordination or task-dependent variation of the phenomenon, as well as detecting non-local sequences during stationary rest, would be important for this question. Alternatively, excluding all such events and focussing a search on events occurring outside periods

of theta state or during SWRs would be possible with appropriate local field potential recordings, as mentioned above.

2.3.3. Training and preparation for experimental investigation was in progress when the project was cut short

Experimental investigation of the non-local grid cell activity was also planned, in three experimental situations: on a one-dimensional track if analysis of the Mosers' public dataset was not deemed conclusive; on a T-maze based on the experiments of Johnson & Redish (2007) so as to look for planning-related activity at the choice point; and in an open 2-dimensional arena, where I hoped to detect unconstrained advance route-planning before travel to a hidden previously learned reward location, and/or replay upon reaching the reward.

While conducting the computational analysis described above, in parallel I trained in the surgical and electrophysiological techniques this would require. I conducted hippocampal electrode implants in two male Lister Hooded rats (an intermediate training step, short of the complex mEC surgery), and successfully identified and recorded a number of place cells (an example is shown in **Figure 2.4**).

I also began piloting behavioural training to inform final experimental design. I used a square arena with start boxes outside each of the 4 corners, and wells below the surface in which food rewards could be placed. Wells and rewards were concealed by a layer of sand. One well was baited at a time for a set of trials. I began training rats on a trial protocol in which they were placed in a pseudorandomly selected start box, a visual cue was then revealed to indicate which corner they were at, and after a set period during which I speculated it might be possible to detect non-local activity corresponding to route-planning, the door was opened and the animal was expected to learn to navigate to the baited well and dig to collect the reward.

2.3.4. Outlook

While performing the above computational and experimental project, personal communications with Josef Csicsivari's group in 2012 indicated that the presence or absence of sequential replay events in entorhinal cortex remained ambiguous, even

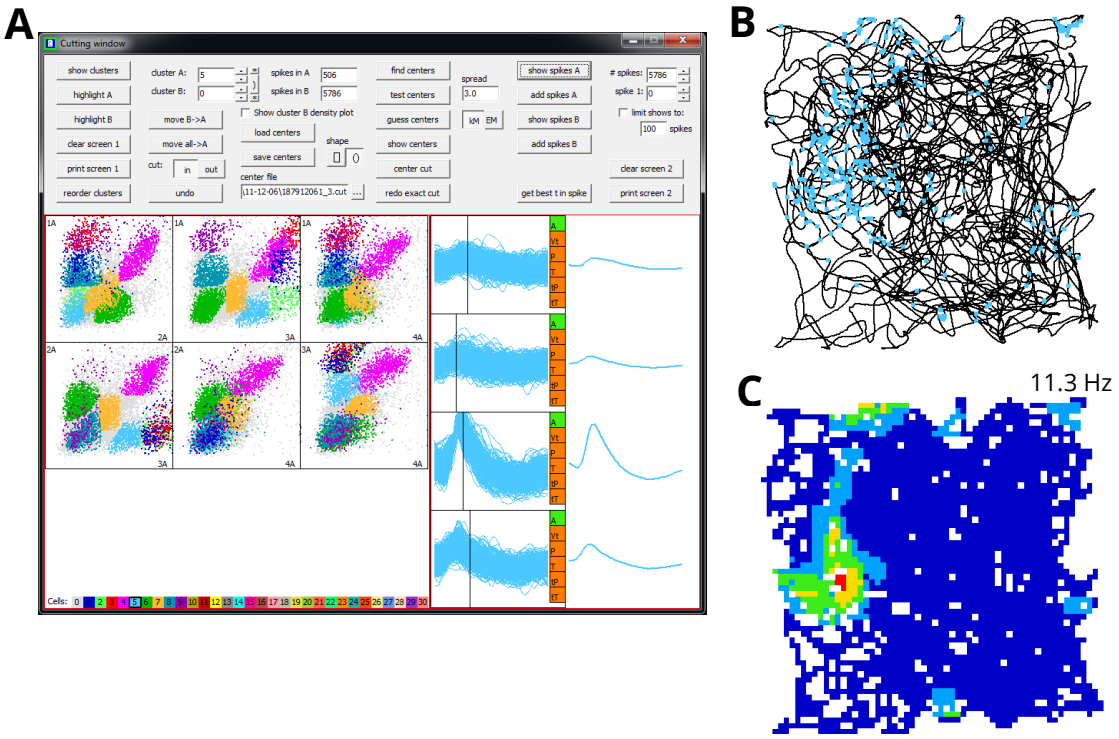

Figure 2.4 – Place cell tetrode recording by the author

Tetrode recordings were taken from a right hippocampal implant in a male Lister hooded rat as it foraged for scattered food in a 1m square environment. Clusters of spikes from separate units were manually identified by their differing amplitudes on separate electrodes within a tetrode, as well as temporal properties. (A) The *TINT* (Neil Burgess & Axona Ltd.) interface: on the left are the compared amplitudes on pairs of electrodes of each spike recorded. Different colours indicate manually identified spike clusters. Right of this are the overlaid traces of all spikes from unit t3c5 (tetrode 3, cell 5) as recorded on each of the four electrodes, and on the far right are the averages of all these traces. Note the characteristic spike shape of a pyramidal cell, most clearly visible on the third electrode. (B) The locations of the spikes from unit t3c5 (light blue) overlaid on the tracked path of the rat (black line). (C) A rate-map constructed from this data: note the spatially restricted firing typical of a place cell (Peak firing specified on figure. The range from 0 Hz to peak firing is divided into bands of 20% indicated by colour, hot colours indicating higher firing rate.)

with access to larger numbers of recordings of entorhinal neuronal firing and local field potential. Thus, to overcome the limitations in the conclusions I could draw from the Moser's public dataset would probably require gathering more grid cell data than present in the Moser or Csicsivari datasets, specifically simultaneous recordings from multiple modules. Together with my supervisor, we decided that this course of action would likely be both time consuming and over-ambitious. Accordingly, we decided to halt this project, and to take a purely computational approach, given the risks and slow progress associated with continued experimental approaches.

At the time, I considered that a promising alternative approach might target simultaneous recordings from the hippocampus and entorhinal cortex of dually implanted rats. This approach would be even more technically challenging, but would enable identification of non-local representations in place cells (based on the existing characterisation of these events) so as to specifically examine grid cell activity at the same time, to detect whether grid cells show the same non-local representations at the same time (and to characterise the relationship, or absence thereof, between the hippocampal and entorhinal processes).

Indeed, this has since been done by other researchers, and consistent with my preliminary findings, replay has been observed in grid cells. Simultaneous recordings in CA1 and mEC deep layers (the main entorhinal recipients of hippocampal inputs) showed grid cells replaying coherently with place cells, the location encoded by the former exhibiting an average delay of 11ms delay relative to the latter (Ólafsdóttir et al., 2016). Conversely, grid cells in superficial mEC have been recorded replaying independently of place cells, more during performance of a task than during rest (O'Neill et al., 2017). This suggests a tentative model in which hippocampal-initiated replay, transmitted to the mEC deep layers, is involved in memory consolidation,

while independent replay in mEC superficial layers may be more relevant to planning navigation. Indeed, comparing activity during periods of immobility interspersed throughout performance of a spatial decision task revealed that in the former, place cells and mEC deep layer grid cells replay together and represent more remote locations, but while the animal was engaged in the task, replay is more associated with the task and the hippocampus and mEC exhibited less coherence (Ólafsdóttir et al., 2017). However, note that this distinction is contested, with one group arguing that the detection of coordinated grid and place cell replay may have been spurious and could be excluded by assessment with more rigorous criteria (Trimper et al., 2017) – in turn, the original authors have criticised the methodology of this response (Caswell Barry, personal communication, March 2018).

3. A MODEL TO ASSESS GRID CODE FIDELITY UNDER SPATIAL UNCERTAINTY

I built upon an existing model in order to investigate grid cell systems' performance in various new conditions. This existing model simulates a modularly-organised ensemble of grid cells firing in response to a position signal, decodes their firing to estimate position, and allows investigators to assess the performance of the system by comparing these estimates to the original 'true' position. My development of this model incorporated varying degrees of uncertainty into the position signal, allowing exploration of a range of new questions. The work reported in this chapter was published as part of this article: Towse, B. W. et al., (2014) 'Optimal configurations of spatial scale for grid cell firing under noise and uncertainty', *Philosophical transactions of the Royal Society B*, 369(1635).

3.1. Description of the one-dimensional model

3.1.1. Grid cell firing patterns

Spiking activity of a population of grid cells, organised into *L* discrete modules by spatial period size, was modelled in a one-dimensional environment using MATLAB v7 (MathWorks). The spike output of a grid cell, *j*, within a particular module, *i*, was modelled, following (Mathis et al., 2012), as a Poisson process with rate modulated by position on an open interval, $x \in (0, x_{max})$, according to a periodic Gaussian tuning curve $\alpha_{i,j}(x)$:

$$\alpha_{i,j}(x) = f_{max} e^{-\frac{\left(-\frac{r\lambda_i}{2} + mod\left(\frac{r\lambda_i}{2} + x - \varphi_j,\ r\lambda_i\right)\right)^2}{2\sigma_i^2}} \qquad 3.1$$

where f_{max} is the maximum firing rate (which is constant across the population), λ_i the baseline spatial period defining the module, r the multiplier applied to that spatial period to control grid scale expansion, φ_j the spatial phase offset, σ_i the tuning width of the grid fields, and *mod (a, b)* represents the modulo function.

Within each module with a shared scale λ_i, tuning curves were created for M equidistant spatial phases $\varphi_j = \frac{(\beta_i + j)\lambda_i}{M}$ where $0 \leq j < M$ and β_i is a random additional offset on the interval (0, 1), common to all tuning curves within a module but different between modules. This was added in order to prevent biases that might result

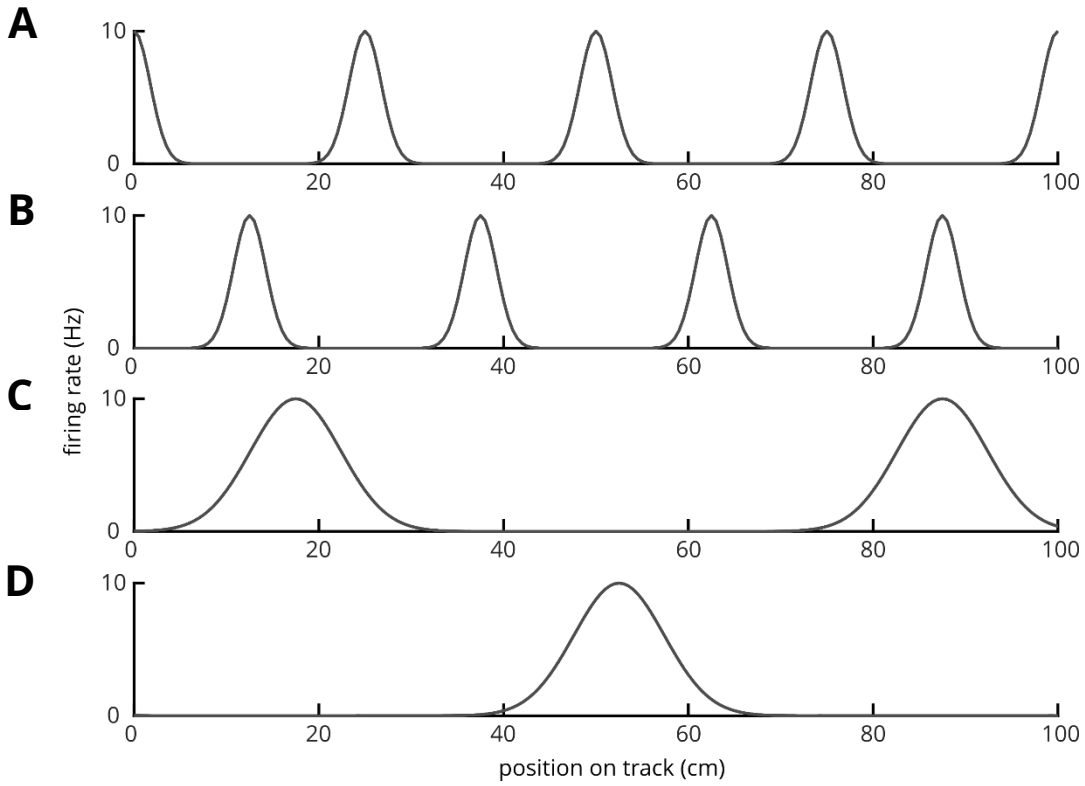

Figure 3.1 – Tuning curves of modelled grid cells

Example tuning curves generated using equation 3.1 are displayed on a 1m track. The grid-patterns are not expanded, i.e. $r = 1$.

(A) Grid scale 25 cm (λ = 25 cm), with 0 cm offset (φ = 0 cm)

(B) λ = 25 cm, φ = 12.5 cm

(C) λ = 68.6 cm, φ = 17.15 cm

(D) λ = 68.6 cm, φ = 51.45 cm

from the alignment of tuning curves across modules. Thus a total of $L \times M = N$ neurons were simulated.

3.1.2. Determining module scales

3 systems for determining relative module scales were used: geometric, co-prime, and random. In a geometric system, a set of modules was created by specifying a spatial period multiplier, p, a smallest scale ($r \times \lambda_1$), and a total number of modules L. The spatial period of each module was determined as $r\lambda_i = r\lambda_1 \, p^{i-1}$ where $0 \leq i \leq L$. In a co-prime system, a set of modules were created with scales in the ratios of prime numbers 2 : 3 : 5 : … (e.g. $\lambda_3 = \frac{5}{2}\lambda_1$). Finally, random systems were constructed to compare to the geometric system with p=1.4 as follows: 1000 systems were created by taking the smallest and largest grid scales occurring in the geometric system and selecting a further $L-2$ scales from a uniform distribution ranging between these scales. Hence yielding L scales with upper and lower scales matched to the p=1.4 system.

3.1.3. Modelling spatial uncertainty

Gaussian noise ε_i was generated separately for each module and added to the actual position, x, to yield a noisy position estimate $x + \varepsilon_i$ (in 2D independent noise was added in both x and y dimensions: $x + \varepsilon_{x,j}$, $y + \varepsilon_{y,j}$). The degree of uncertainty was varied by modifying the standard deviation of ε_i. All cells within a module therefore received the same noisy position input, but cells in different modules received different input (the rationale for this is discussed in section 3.2.2). Thus, cell firing rate was now modulated according to $\alpha_{i,j}(x + \varepsilon_i)$.

3.1.4. Decoding

The signal extracted from the grid cell system was the number of spikes, k, generated by each neuron during a finite read-out period, T – i.e. a population response $\boldsymbol{K}$

= $(k_1, \ldots, k_N)$. We assume the decoding cannot take the added noise into account in any way, so that given a position x the probability of observing the response $\boldsymbol{K}$ in time T, following (Mathis et al., 2012), is taken to be:

$$P(\boldsymbol{K}|x) = \prod Poisson\big(k_i, T\alpha_i(x)\big) = \prod \frac{\big(T\times\alpha_{i,j}(x)\big)^k}{k!} \times e^{-T\alpha_{i,j}(x)} \qquad \textbf{3.2}$$

From the population response $\boldsymbol{K}$, we can decode position as the maximum likelihood estimate of x, that is $\hat{x}(\boldsymbol{K})$. Given the initial assumption that all values of x within the environment are uniformly likely,

$$\hat{x}(\boldsymbol{K}) = \max_{x\in[0,x_{max}]} P(x|\boldsymbol{K}) = \max_{x\in[0,x_{max}]} P(\boldsymbol{K}|x) \qquad \textbf{3.3}$$

Thus $\hat{x}(\boldsymbol{K})$ may be closely approximated by calculating $P(\boldsymbol{K}|x)$ for a sufficiently finely spaced uniform sample of x values on the interval $[0, x_{max}]$, and selecting the value of x which yields the greatest $P(\boldsymbol{K}|x)$. I used a spatial bin size of Δx = 0.5 cm. Where two or more values of x yielded the same maximal $P(\boldsymbol{K}|x)$ (i.e. decoding was ambiguous), one was randomly selected.

3.1.5. Measuring error

The mean maximum likelihood estimate square error, or MMLE, assesses the accuracy of decoding possible with a particular grid system, based on the square error of position decoding. Exact MMLE is defined (Salinas & Abbott, 1994; Bethge et al., 2002) as:

$$\chi^2 = \mathbb{E}((x-\hat{x})^2) = \sum_{K\in\mathbb{N}^N} \int_0^1 \big(x-\hat{x}(\boldsymbol{K})\big)^2 P(\boldsymbol{K}|x)p(x)\mathrm{dx} \qquad \textbf{3.4}$$

where $\mathbb{E}(b)$ is the expected value of a random variable b. MMLE values for each set of grid cell network parameters were estimated using the Monte Carlo method. For each iteration c, a sample position x_c was selected, and with the introduction of noise

ε to the modelled grid cells, a population spike response K_c was generated, then decoded to yield $\hat{x}(\boldsymbol{K}_c)$. With a large number of iterations MMLE can be approximated (Mathis et al., 2012). 1000 iterations were performed per experiment (i.e. $1 \leq c \leq 1000$):

$$\chi^2 \approx \frac{1}{1000}\sum_{c=1}^{1000}\left(x_c - \hat{x}(\boldsymbol{K}_c)\right)^2 \qquad \textbf{3.5}$$

For a given set of parameters in a geometric or coprime grid system 10 experiments of 1000 iterations each were performed, to calculate 10 independent estimates of MMLE, unless specified. MMLE figures are therefore reported as the mean of the 10 independent estimates ± standard error of the mean (N.B. this applies in chapters 3 and 4, while later investigations used a different approach). For the random grid scales, a single 1000 iteration experiment was performed for each of the 1000 generated systems.

3.1.6. Comparison of decoding performance to chance levels

For the purposes of comparison, chance performance levels were calculated for each track size (i.e. corresponding to a uniform distribution of decoded locations). For a one-dimensional environment, this was $d^2/6$.

3.1.7. Parameters

In all simulations in this chapter, and subsequently except where otherwise indicated, the following parameters were used, following Mathis et al. (2012):

- Read-out time period, T = 0.1s. This is the approximate length of a theta cycle.
- Maximum grid cell firing rate f_{max} = 10Hz. The peak firing rates recorded from individual cells vary, and 10Hz is a representative value consistent with experimental findings (Hafting et al., 2005).

- Smallest baseline spatial period, λ_1 = 25cm. This is consistent with experimental findings (Barry et al., 2007). Additionally, with grid periods smaller than approximately this distance, at top speed a rat would cross more than one unit of the grid-pattern during a single theta cycle, making it difficult to see how useful information could be read out from such grid cells (Mathis et al., 2012).
- Total number of modules, L = 8. Recordings from dorsal to intermediate/ventral rat mEC have so far detected 5 or 6 modules, leading to estimates that there may be 5-10 modules in total (Brun et al., 2008; Stensola et al., 2012).
- Tuning width of grid-pattern bumps, $\sigma_i = r\lambda_i \frac{3}{20\sqrt{\log_e 100}}$. This is consistent with experimental findings (Brun et al., 2008).
- The number of equidistant phase offsets represented within a module of grid cells, M = 20 or M = 100, thus the total number of cells, $N = L \times M$ = 160 or 800. Note that this is much smaller than the estimated 6.6×10^4 cells in layer II of the rat mEC (Mulders et al., 1997).

3.2. Aspects of the model

3.2.1. Cell spiking

Mathis et al.'s model modelled the output of each cell as a Poisson process, taking the spike count from each cell within a theta cycle time window. I have retained this. Poisson processes are widely used to approximate neuron firing. The fine firing pattern of a grid cell is more complex than this due to phase precession (O'Keefe & Recce, 1993; Hafting et al., 2008), but the overall spike count is generally close to Poisson (Kluger et al., 2010). Examining the additional information that could be read out from phase precession was beyond the scope of my investigation.

I also retain Mathis et al.'s read-out time period for spike count, set at 100ms. This is the average period of the theta oscillation, which is thought to coordinate hippocampal processing and segment it into chunks (Buzsáki, 2002).

3.2.2. Uncertainty

The spatial firing patterns of grid cells within a single module appear to be coherent, consistent with attractor dynamics playing a role (Fyhn et al., 2007; Yoon et al., 2013), while there is a greater degree of independence between modules (Stensola et al., 2012). This independence implies that beyond intrinsic neuronal noise, different modules could signal slightly different values given the reality of noisy inputs from multiple cues and sensory modalities. Therefore, uncertainty is modelled by providing slightly different inputs to each of the grid system modules. The different inputs are determined by randomly selecting from a Gaussian distribution around the actual value, enabling variation of the degree of uncertainty by varying the standard deviation of this distribution.

3.2.3. Decoding

In order to assess how faithfully the grid cell system represents the input location, it is necessary to decode their output. "Optimal" decoding refers to methods that, by some measure, extract as much information as possible from a neural signal to reconstruct the encoded stimulus, and there are two broad categories.

In *Bayesian inference*, a "loss function" describes the expected cost to the organism of estimating $x_{estimate}$ when the true stimulus value is x_{actual}, and a function is found that minimises the average result of the loss function across possible outcomes. *Maximum a posteriori (MAP) inference* simply selects the estimate $x_{estimate}$ at the maximum of $p[x_{actual} | \boldsymbol{K}]$, the probability density of that actual stimulus value given the observed output ($\boldsymbol{K}$, the spike count vector). When all the possible stimulus values

are *a priori* considered uniformly equal, this becomes equivalent to selecting $x_{estimate}$ at the maximum of p[$\boldsymbol{K}|x_{actual}$]. This special case of MAP inference is called *maximum likelihood inference* (Dayan & Abbott, 2001).

Choosing a reasonable loss function for use in Bayesian inference would require making many weakly-justified assumptions about the organism's behaviour, so I rule this out. This model considers the independent encoding and decoding of a set of discrete independent inputs, so assuming uniform prior probability is a reasonable starting point for investigation of the system. Therefore, like Mathis et al., I use maximum likelihood inference. In Chapter 7, I will discuss further the possibility of using different approaches to decoding.

3.2.4. Mean square error as a measure of performance

Mathis et al. use mean square error (MSE) as a measure of the fidelity of grid coding. MSE is a common, if somewhat arbitrary, measure for the performance of estimators, as it comprises both an estimator's variance (assessing precision) and its squared bias (assessing accuracy) (SAS Institute, 2009).

3.3. Results

I used this model to explore some factors determining the performance of the grid cell code. For this initial exploration of the code's basic properties, the component of the model simulating spatial uncertainty was not used (i.e. the standard deviation for this was set to zero).

First, I examined decoding error in grid cell systems with geometric ratios between adjacent grid module scales that ranged from 1.1 to 2.0, including factors √2 (1.41) and √3 (1.73), simulated in a 1m-long 1D environment (the simulations for square root ratios were run by Caswell Barry). **Figure 3.2A** shows that decoding error is very

low overall (squared error generally being less than 1 cm^2), with an improvement in encoding accuracy for 100 cells per module compared with 20 cells per module – presumably because Poisson firing noise is averaged across a larger cell population. In addition, there is a moderate effect of the geometric ratio on encoding accuracy, such that the smaller ratios, which have more small-scale grids, are more accurate. The performance of the system with ratio 2 and 20 cells per module is particularly poor, with a high variance indicating the presence of two types of error, reflecting failures of precision and accuracy respectively.

The presence of two types of error is illustrated by **Figure 3.2B**, where the frequency of large amplitude errors (defined here as instances of decoding with squared error greater than 10 cm^2) generated by systems with different geometric ratios is quantified. These errors are larger than would be expected if they were owing to imprecision in the smallest grid scale, and therefore presumably reflect errors of accuracy: large errors caused by ambiguity in the periodic code or by modular coding translating small perturbations in one or some modules' phase signal into a very different position signal (as discussed in Section 1.8.1). **Figure 3.2B** shows that these "ambiguity errors" begin to appear in grid systems with 20 cells per module as the ratio approaches 2. Although these occur very infrequently (in less than 0.5% of decoding trials), the errors are large and contribute disproportionately to the mean squared error. For example, in the 1.9 ratio system with 20 cells per module, 0.31% of trials produced large errors and these have a mean square size of 38.1 cm^2, whereas the remaining trials have a mean squared error of 0.75 cm^2. In the grid systems with 100 cells per module, no ambiguity errors occurred in any of the trials. **Figure 3.2C** replots the data from **Figure 3.2A** with the large errors removed – as expected, the performance of systems with 20 cells per module and larger geometric ratios (1.7 and greater) is improved, and variability reduced.

The presence of ambiguity errors in grid systems with 20 cells per module is clearer in 18 m linear environments (**Figure 3.2D**). The mean squared decoding error is dominated by the infrequent but very large decoding ambiguity errors, which also cause large variance. Note the decoding accuracy allowed by geometric ratio 2, and to a lesser extent √2, is particularly poor. The former exceeds the limits of the *y*-axis (mean squared decoding error 8979 and 2687 cm^2, respectively). The proportion of trials showing decoding ambiguity errors is shown in **Figure 3.2E**. These errors occur for all grid systems with 20 cells per module and their amplitudes are increased relative to the 1 m track (because the 18 m track provides greater scope for larger errors). Taking the 1.9 scale ratio, again these errors account for 0.32% of the trials,

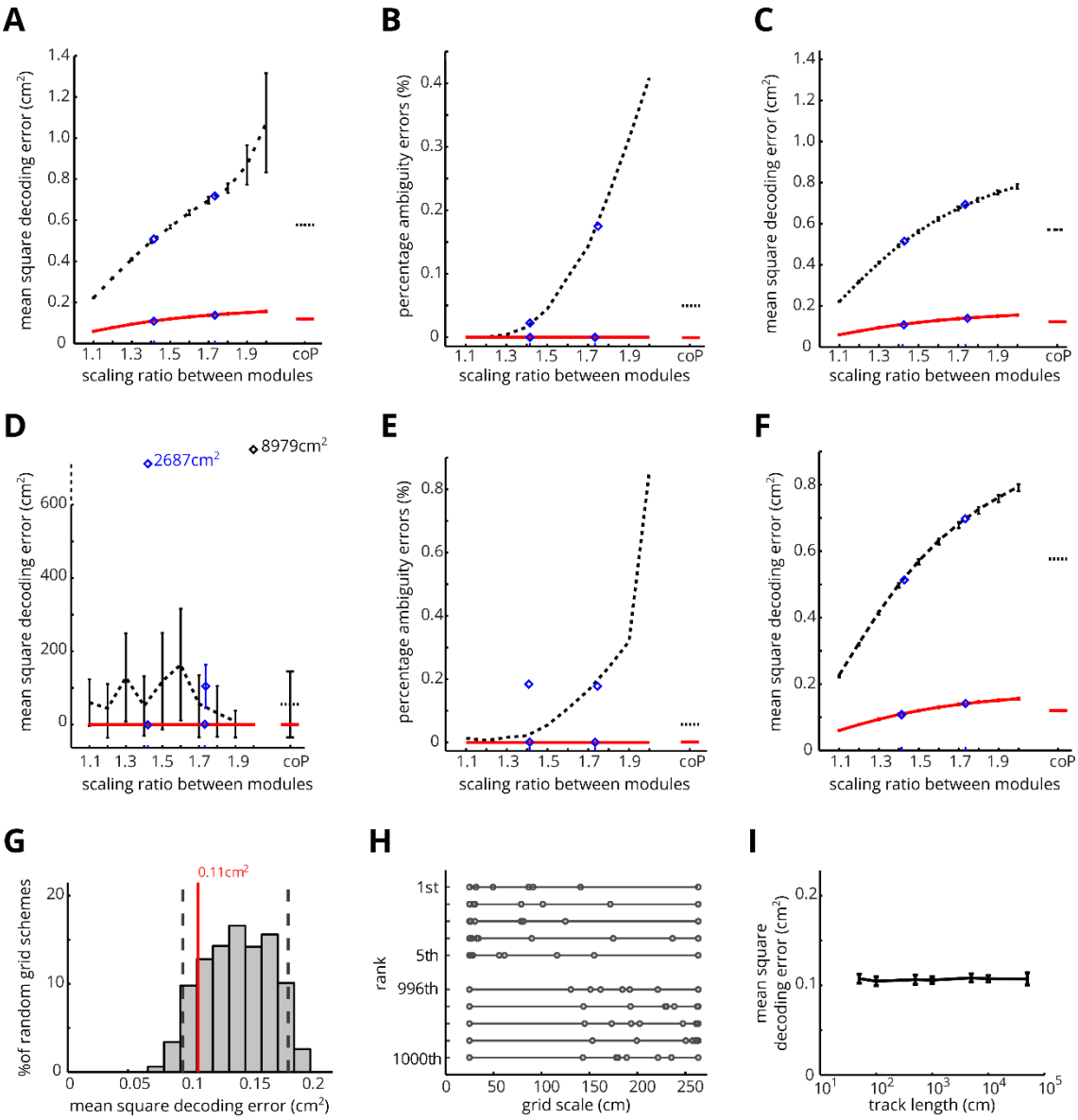

Figure 3.2 – Decoding error in systems with different grid scale configurations

(A-C) Simulations in 1 m environment. (A) Mean squared decoding error (MSE) for geometric grid systems with ratios 1.1–2.0, including √2 and √3 (blue diamonds). Errors for coprime system (labelled "coP") shown on right of axis. Systems have 20 (black dashed line) and 100 grid cells per module (red solid line). Error bars indicate SEM of 10 simulations each consisting of 1000 decodings of locations from grid cell activity. (B) Frequency of large (> 10 cm^2) errors. (C) MSE (as in A) with large errors excluded. (D–G) Simulations in 18 m environment (again, blue diamonds indicate ratios √2 and √3). (D) MSE for geometric systems (points for ratios √2 and 2.0 are off the scale). (E) Frequency of large errors. (F) MSE with large errors excluded. (G) Decoding errors for 1000 grid systems with random scales matched to a ratio 1.4 geometric system (100 cells per module; a single 1000-iteration experiment per system). 5th and 95th percentile of the random population shown as grey dashed lines. Matched geometric system lies at the 15.4th percentile (solid red line). (H) Module scales in the best and worst performing random systems. (I) MSE for a ratio 1.4 geometric system (100 cells per module) in 1D environments 0.5–500m.

but their mean square size was 2500 cm^2, while the size of the errors in the remaining trials was effectively unchanged at 0.76 cm^2. The geometric ratio 2 coding scheme in particular suffers from a large number of decoding ambiguity errors on 0.86% of trials, indicating the inefficacy of integer scale ratios. The geometric ratio √2 scheme also exhibits a disproportionate number of ambiguity errors when compared with the similarly scaled 1.4 and 1.5 schemes—this appears to reflect the fact that under the √2 scheme alternate grid modules follow a geometric progression with ratio 2. Again the grid system with 100 cells per module does not generate ambiguity errors. Decoding error for the same grid systems is shown without the infrequent, but very large, decoding ambiguity errors in **Figure 3.2F**. As with **Figure 3.2G**, this shows that the remaining (precision) errors increase with increasing scale ratio, as would be expected from the concomitant increases in the breadths of tuning of the grid firing fields in all but the smallest scale module.

The performance of configurations of grid modules with a co-prime sequence of scales (i.e. a 2 : 3 : 5 : 7 : 11 : 13 : 17 : 19 ratio of scales, starting from 25 cm and ending at 237.5 cm) is similar to a geometric series with ratio approximately 1.5 (range 25–427 cm) for both the 1 and 18 m environments, and in systems with 20 and 100 cells per module (see the rightmost points in **Figure 3.2A-F**). It performs slightly worse than the ratio 1.4 geometric series, whose overall range (25–264 cm) is best matched to it. Thus, there seems to be no specific advantage for a co-prime series of grid scales over a geometric series in these conditions. Grid systems with geometric ratio 1, i.e. where all grids are 25 cm in scale, were also simulated, but the data are not shown because they give such large errors, being unable to disambiguate locations more than 25 cm apart (e.g. mean squared error with 20 cells per module on a 1 m track is 1669 cm^2).

Figure 3.2G examines the decoding error for grid systems with a random distribution of grid scales between 25 and 264 cm, for comparison with a geometric series with scale ratio 1.4 (which has the same range of scales and is investigated further below). (The simulations of these random grid systems were run by Caswell Barry.) The mean error in the geometric system lies at the 15.4th percentile of the distribution of random scales, showing that on average a geometric series performs somewhat better than a random series with a similar range of scales but that this advantage is slight and all systems exhibit only precision errors. The five randomly generated grid systems that gave the lowest decoding errors (rank first to fifth) as well as the five yielding the highest errors (rank 996th to 1000th) are shown in **Figure 3.2H**. The best performing random systems include more small-scale grid modules than the poorly performing systems, which are dominated by larger scale grids, and so somewhat resemble the geometric series of scales. This reflects the fact that, on the 18 m track with 100 grids per module, ambiguity errors are unlikely to occur,

and so the maximum decoding accuracy is obtained by minimizing precision errors—hence small grid scales are favoured.

Figure 3.2I provides an indication of the actual capacity of the grid system and how this compares to the 18 m track used in the previous simulations. Specifically, decoding error of a ratio 1.4 geometric system with 100 grids per module is examined on tracks of increasing length. In all cases, the decoding errors are small, consisting mainly of precision errors even on the largest track (500 m), suggesting that the maximum range of this system is considerably larger than this value, as suggested by Fiete et al. (2008).

These initial simulations demonstrated several points. The presence of two types of error is clearly shown: precision errors which are common but relatively small in magnitude and ambiguity errors which are infrequent but potentially very large. The small decoding errors resulting from precision errors are reduced further in grid systems with more small-scale grid modules and also in systems with more cells per module. Although ambiguity errors are infrequent, typically occurring in less than 1% of iterations, their large size was shown to disproportionally degrade the system's performance. Ambiguity errors were found to be more prevalent in systems with fewer cells per module (20 versus 100) as well as in the larger environment (18 versus 1 m) where their magnitude was also increased. There was no specific advantage for the co-prime system over a similarly scaled geometric system. However, the geometric system following a ratio of 2 between modules performed poorly owing to a disproportionate number of ambiguity errors on the 18 m track, and to a lesser extent this was also true for the ratio √2 system.

3.4. Discussion

3.4.1. Trade-offs between precision and accuracy

This initial exploration demonstrated trade-offs between precision and accuracy in variously configured grid cell systems, encoding position without spatial uncertainty in one-dimensional environments.

Localised precision errors reflect small errors in the decoded location, while larger ambiguity errors result from decoding location to the wrong part of the environment. There were two sources of noise in the system – the variable spatial uncertainty, and Poisson noise inherent in the cell spiking dynamics. In the absence of the former, the larger ambiguity errors are relatively rare.

In fact, with enough cells included per module, ambiguity errors became completely absent: with information from more cells, Poisson noise in individual cells is unlikely to result in confusing the grid code labels for two different locations. This means the system can correctly disambiguate more states, enhancing both precision and range: the combinatorial power of the system was demonstrated by the low errors even in a 500m environment. Thus, as predicted by theoretical work (Fiete et al., 2008), systems with incommensurate scales can unambiguously encode location in environments much larger than the largest grid scale.

Increasing the number of cells per module decreased the size of precision errors as well as ambiguity errors, because the impact of the Poisson noise can be averaged out across a larger number of cells, and the larger population gives a better approximation to the idealised population vector for a given position.

In the absence of ambiguity errors, grid codes with smaller scales (whether geometrically progressing scales with a smaller ratio, or random systems which

happened to have more small scales) experienced smaller precision errors: they can represent space more finely.

Unlike precision errors, where ambiguity errors do occur they scale with the size of the environment relative to the grid scales. In even a moderately-sized environment, therefore, ambiguity can introduce significant errors orders of magnitude larger than the precision errors. With 20 cells per module in an 18m environment, the slight reduction in precision errors conferred by smaller geometric scaling ratios is overridden by the ambiguity errors. For ratios between 1.1 and 1.9 there is no simple relationship apparent between ratio and errors.

No particular advantage for a coprime sequence of scales was observed compared to similar geometric schemes. As discussed in the Introduction, the particular theoretical advantage of the coprime scheme in maximising the LCM of the scales is specific to an idealised model – once realistic noise is introduced, ambiguity errors can occur in environments smaller than the LCM but large enough to encompass locations at which the sets of grid module phases are too similar to be reliably distinguished.

3.4.1. Nested grid codes fail in larger environments

Geometric systems with scaling ratios of 1 and 2 perform particularly poorly. With a "nested" grid code (one with an integer module scale), all combinatorial power is lost and it becomes impossible to distinguish locations further apart than the largest grid scale. This was to be expected and follows simply from first principles discussed in the Introduction. The lowest common multiple and thus the theoretical maximum capacity of a nested set of scales is, of course, equal to the largest scale. To a lesser extent, systems with factor √2 suffer from a similar problem as alternate modules are nested.

Noteworthy was the fact that a nested system (with scaling factor 2) began to show very large failures even before the environment exceeded the scale of its largest grid. This is likely because the system lacks redundancy. If there is an error in the output of the largest module, the output of the other modules, which are smaller than the environment, cannot help to disambiguate. This corroborates the lack of robustness in nested codes that was predicted.

However, it was clear at this point that more in-depth exploration of different scale configurations, including at the limits of the systems' ranges, might shed more light. Such an investigation was conducted later and is reported in Chapter 5.

4. GRID-PATTERN SCALE EXPANSION IS ADAPTIVE FOR CODING IN CONDITIONS OF SPATIAL UNCERTAINTY

4.1. Background

When an animal is placed in a novel environment, grid scales have been observed to start out larger, and progressively contract with increasing experience of the environment until they reach a stable scale similar to that measurable beforehand in an already-familiar environment (Barry, Ginzberg, et al., 2012). This was a surprising finding, as spatial representations would be expected to remain stable in order to facilitate navigation and learning about features of the environment (for instance, associating a particular landmark with a consistent location). A shifting representation would require downstream and associated systems and connections to adapt over time if confusion is to be avoided.

Barry et al. hypothesised that grid expansion in a novel environment may be understood more generally as a response to spatial uncertainty, proposing that expansion may be a compensatory mechanism. Here, I used the model I developed, in simulations of one- and, by adapting the model, two-dimensional environments, to test this hypothesis.

The work reported in this chapter was published as part of this article: Towse, B. W. et al., (2014) 'Optimal configurations of spatial scale for grid cell firing under noise and uncertainty', *Philosophical transactions of the Royal Society B*, 369(1635).

4.2. Methods

4.2.1. Extension of the model for two-dimensional environments

The model described in Chapter 3 was extended to simulate behaviour in two-dimensional environments for part of this investigation. Here, I explain how the 1D version of the model was adapted for 2D simulations.

4.2.1.1. Grid cell firing patterns

Two-dimensional template tuning curves for each grid scale (and expansion thereof) were generated with locations of grid nodes specified as a regular triangular grid with scale $r\lambda_i$ and expected firing rate at each location determined by a Gaussian distribution centred on the nearest node:

$$\alpha_{i,j}(x,y) = f_{max}\, e^{-\frac{d^2}{2\sigma_i^2}} \qquad \textbf{4.1}$$

where d is the distance from (x, y) to the nearest grid node.

Within each module, M = 195 offset tuning curves (yielding a total of 8 × 195 = 1560 cells in the system) were distributed in a 13 × 15 rectangular grid via translations of this original tuning curve, as well as adding a random translation common to all grids in the module. Finally, in a given experiment, all grid tuning curves in all modules were rotated to a common, randomly selected orientation with respect to the environment. All these transformations were fit to the array of sampled locations using cubic interpolation.

4.2.1.2. Modelling spatial uncertainty

In the two-dimensional simulation, independent noise was added in both x-and y-dimensions: $x + \varepsilon_{x,i}$, $y + \varepsilon_{y,i}$. Where position signals altered with noise fell outside the

environment, they were corrected to the closest location at the edge of the environment before being input to the grid cells.

4.2.1.3. Decoding

In two dimensions, the tuning curve only gives expected firing rates at the discrete sampled intervals, rather than being calculated as the continuously-varying result of an equation across the environment. Therefore, in the calculation of $P(\boldsymbol{K}|x)$, $\alpha_{i,j}(x,y)$ is calculated by cubic interpolation from the tuning curve, which gives expected firing rates only at the sampled intervals. As all possible locations are considered independently in the probability calculations, no further adaptation is required to transfer from 1 to 2 dimensions.

4.2.1.4. Measuring error

Equation 3.5, used to estimate mean maximum likelihood estimate square error, was adapted for the 2D model:

$$\chi^2 \approx \frac{1}{1000}\sum_{c=1}^{1000}\left(x_c - \hat{x}(\boldsymbol{K}_c)\right)^2 + \left(y_c - \hat{y}(\boldsymbol{K}_c)\right)^2 \qquad \textbf{4.2}$$

4.2.1.5. Comparison of decoding performance to chance levels

For comparison to the performance of the grid cell systems, the performance of decoding via blind chance was calculated in square 2D environments as $d^2/3$.

4.2.2. Model parameters

I conducted this part of the investigation in a grid system configured in a geometric series of scales (the evidence in Chapter 3 indicates this performs as well as any other) with a ratio of 1.4. Such a scaling ratio is indicated (on average) by the work of Stensola et al. (2012), although note that a larger ratio would be required to produce a range comparable with the smallest and the largest grid scales that have

been reported (i.e. 25–500 cm; Brun et al., 2008) with only eight modules, more consistent with the average ratio of 1.7 found by Barry et al. (2007). I used 100 cells per module, because this minimizes the effect of decoding ambiguity errors arising from Poisson firing.

For one-dimensional simulations, I used the larger 18m environment, in which the system has to navigate environments larger than the largest grid scale by exploiting the combinatorial power of the grid code.

In the subsequent two-dimensional simulations, the environment size was restricted to $1m^2$ due to the heavy computational burden of running the model in large 2D environments.

Note that the uniformity of grid-pattern orientations across modules is a simplification – at least a minor one. The issue is discussed further in a later chapter (Section 6.5.2). To summarise, grid-pattern orientation does vary between modules more than within them (Stensola et al., 2012), though the modules' orientations do tend to cluster (Krupic et al., 2015) and clustering does appear to be stronger in square environments than unpolarised circular environments (Stensola et al., 2012; Krupic et al., 2015). In this work, I considered grid cell populations with uniformly oriented grid-patterns as a simplified starting point – a future extension could be to examine the effect of non-uniformity of orientations.

4.3. Results

Figure 4.1A shows the decoding error for the grid system, for two levels of uncertainty, as a function of the grid scale expansion factor in the range 0.125–7. For both levels of uncertainty, small expansion factors lead to large decoding errors, reflecting the occurrence of ambiguity errors caused by spatial uncertainty (as shown

above, in this grid system and environment Poisson firing alone does not cause ambiguity errors, or at least does so only extremely rarely, owing to population coding). On the other hand, for larger expansion factors, the overall decoding error increases owing to decreasing precision. The scaling factor representing the optimal trade-off

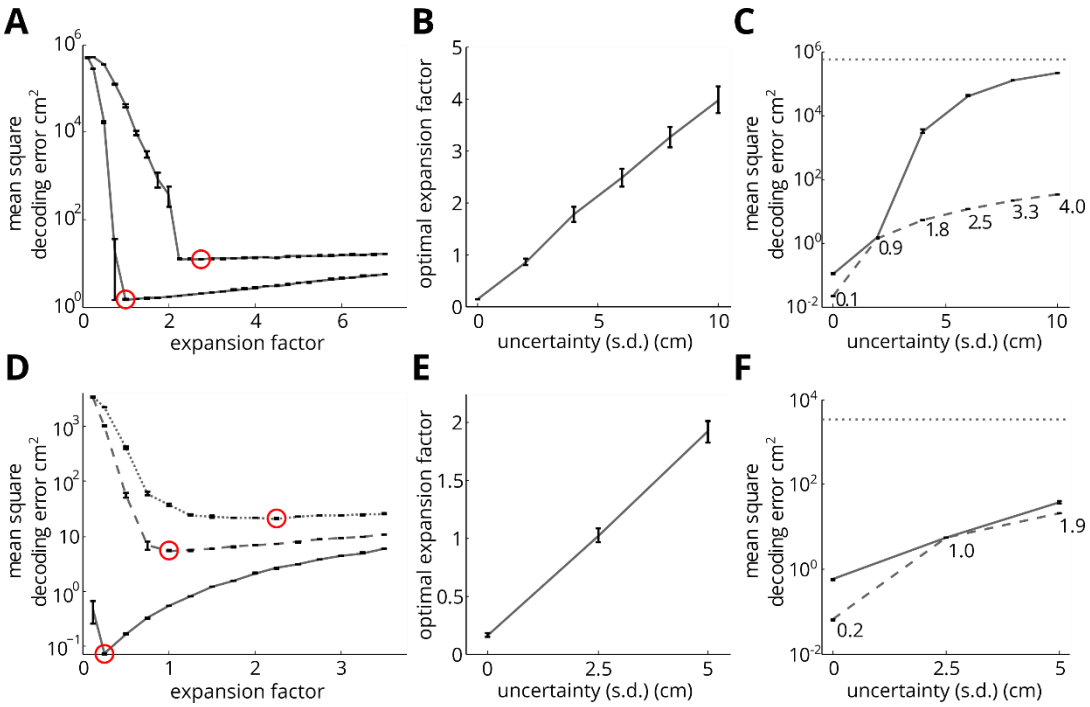

Figure 4.1 – Expansion of a grid system is an optimal response to spatial uncertainty

(A) MSE in an 18 m 1D environment in grid systems subjected to varying expansion, under lower (σ_ε = 2 cm; solid line) and higher uncertainty (σ_ε = 6 cm; dashed line). For each level of uncertainty, there is an optimal expansion factor that minimizes decoding error (circled in red), and grid scale expansions smaller or larger than this will result in greater errors. (B) The mean optimal expansion factor is greater for higher levels of uncertainty; this relationship appears linear. (C) MSE for baseline (solid line) and optimally expanded (dashed line) grid systems, and for performance at chance (dotted line). Numerical labels in (C) indicate mean optimal expansion.

(D-F) show simulations in a 2D 1m^2 environment and are equivalent to (A-C) respectively. In (D), the uncertainty levels represented are σ_ε = 0 cm (solid line), 2.5 cm (dashed line) and 5 cm (dotted line)

Error bars are the SEM of 10 experiments per set of conditions, each experiment consisting of 1000 decodes of random locations.

between these two factors depends on the level of uncertainty. In fact, the optimal expansion factor, which minimizes decoding error in this situation, increases linearly with the level of spatial uncertainty, as illustrated in **Figure 4.1B**. The differences in decoding error generated by the optimally expanded and initial (unexpanded) grid systems are shown in **Figure 4.1C**.

A similar pattern of results is generated by the grid system in a two-dimensional, 1 m^2 environment (see **Figure 4.1D-F**, where expansion factors ranging from 0.125 to 3.5 were assessed). Note that at low uncertainty (σ_ε = 2.5 cm) the optimal grid expansion is 1.0 (i.e. comparable to 'baseline' scales measured empirically), and with an increase in uncertainty (to 5 cm) the optimal expansion is 1.9, which is of a similar order of magnitude to the expansion recorded empirically in exposure to a novel environment (Barry, Ginzberg, et al., 2012).

At zero spatial uncertainty, the estimated optimal expansion factor is less than one and represents shrinkage of the grid firing pattern. In fact, the true optimum is likely to be even smaller than that observed here. This estimate was limited by the range examined, and expansion factors smaller than 0.125 were not examined. However, the fact that these shrunken grids can code location with so little error is further evidence of the power of grid systems to encode unique locations over ranges much larger than their scales.

4.4. Discussion

4.4.1. Grid expansion in novelty as a compensatory response to spatial uncertainty

This investigation showed that increasing spatial uncertainty increases errors in the grid cell system's representation of location, and that expansion of the grid scales can partially mitigate this deterioration of performance. This provides a plausible

context for the experimental finding that grid cell firing patterns expand in novel environments – where greater spatial uncertainty would be expected – and then gradually contract back with experience of that environment (Barry, Ginzberg, et al., 2012).

The effect of grid scale expansion can be understood in terms of precision and ambiguity errors.

With low spatial uncertainty, ambiguity errors are less likely. Increasing grid scale increases the magnitudes of precision errors, and so smaller grid scales are favoured. Higher spatial uncertainty the increases incidence of ambiguity errors. Expanding the grid-patterns seems to mitigate for this for two reasons.

First, increasing the scale of the grid-pattern reduces the size of the spatial uncertainty relative to the pattern. This would ensure that the noisy position estimates input to the grid cell modules more frequently remain close within the same unit of the repeating grid-pattern as the actual position. This should reduce the likelihood of decoding to an entirely different position. The optimal expansion appeared to approximately maintain the standard deviation of the uncertainty noise below 10% of the smallest grid scale.

Second, expanding the grid cell pattern also increases the spatial range of the system, so that the limited environment occupies a smaller fraction of the overall capacity. Potentially confounding locations that correspond to similar firing patterns are thus more likely to be outside the boundaries of the environment. In this simulated system, decoding is only permitted to locations within the environment, so those candidate locations are effectively ruled out of consideration and ambiguity errors prevented. This is similar to the mechanisms of error correction in the grid

cell system proposed previously (Fiete et al., 2008; Sreenivasan & Fiete, 2011) and discussed in the Introduction.

4.4.2. Alternative hypotheses

This is not the only hypothesis seeking to contextualise grid expansion in response to novelty. A major alternative hypothesis is that it promotes the 'remapping' of place cell firing, which also co-occurs with the expansion (Barry, Ginzberg, et al., 2012). This would be consistent with models suggesting that remapping reflects a mismatch between path integration-based grid inputs and environmental sensory inputs to place cells (Burgess, 2008; Barry, Ginzberg, et al., 2012). Expanding grid-patterns via a targeted viral knockout of mEC HCN1 channels in mice does make place cells' fields more likely to shift location across days (Mallory et al., 2018). However, increased place field lability as a result of chronically expanded grid-patterns is not necessarily the same thing as acute, temporary expansion acting as a prompt for remapping.

Another possible hypothesis is that expansion and contraction in novelty and familiarity are associated with a need for different behavioural strategies. *A priori*, in a novel environment we might expect animals to travel longer distances to survey for resources and opportunities (food, potential mates, etc.), and once the animal had grown familiar with the locations of these, we might expect its range to contract only to areas of interest and travel to be minimised. However, the question of how locations are learned and stored in a consistently usable way for future behaviour when the representation is shifting, seems particularly troublesome in relation to this explanation.

A key question is whether grid scale varies in relation to other forms of spatial uncertainty apart from novelty. If it does, this supports the hypothesis that grid scale

variation is driven by the need to minimise errors. Of course, the different hypotheses are also not mutually exclusive, and the phenomenon might play multiple roles in the system, potentially including others not yet proposed.

There is indeed some preliminary evidence for this. Grid scale was observed to expand in mice navigating a two-dimensional virtual environment, relative to a real arena. Greater spatial uncertainty would reasonably be expected in a VR environment, due to the multi-modality richness of real cues compared to simpler, visual-only VR cues, and due to conflict between VR cues and uncontrolled real cues in the VR apparatus such as sounds, smells, the edges of the display screen and the running ball. Consistent with this, spatial information in grid and place cell firing patterns was reduced in VR (Chen et al., 2018).

Experiments comparing grid scale in cue-rich and cue-poor real environments also suggest an interaction between cue-richness and grid scale. However, in those experiments this relationship was confounded by multiple other interacting effects, so it is not yet possible to draw clear conclusions from this (Manson, 2017).

Further experimental work, including real and/or virtual reality manipulations of cues to vary their reliability, could shed further light here.

4.4.3. Neuromodulators may signal uncertainty and control grid scale changes

Previous work has demonstrated that grid scale is influenced by the I_h (hyperpolarisation-activated cation) current, which is dependent on the HCN1 (hyperpolarisation-activated cyclic nucleotide-gated 1) channel subunit and varies topographically from dorsal to ventral mEC, the same axis along which grid scale varies (Giocomo et al., 2007, 2011; Mallory et al., 2018). *In vitro* investigation demonstrates that this current in layer II mEC stellate cells may be modulated by cholinergic manipulations (Heys & Hasselmo, 2012). Thus, there is a physiological

mechanism by which acetylcholine release, known to be associated with novelty, could plausibly account for grid scale expansion in novel environments (Barry, Heys, et al., 2012).

A more generalised model of how the brain signals and processes types of uncertainty proposes interacting roles for acetylcholine and noradrenaline (Yu & Dayan, 2005). This model distinguishes between expected uncertainty, due to known unreliability of predictive cues within a context, and unexpected uncertainty, when context itself changes. Acetylcholine is proposed to signal the former, and noradrenaline the latter. The relative levels of each are proposed to determine a subject's Bayesian inferences in environments which are both noisy and changeable. When a subject encounters a novel environment, and must ascertain this and then learn about new cues (which may be unreliable), both types of uncertainty and both neuromodulators may be relevant.

However, recent evidence challenges the proposal that novelty-related grid scale expansion is triggered via aceytlcholine signalling: modulating medial septal cholinergic activity in mice impacted on some aspects of mEC activity and induced behaviours usually seen in novel environments, but did not alter grid-patterns (Carpenter et al., 2017). This could mean that acetylcholine does not play a role in this mechanism, or that it is insufficient and other triggers are also required. Note also that novelty-related grid scale expansion was discovered in rats and has not yet been replicated in mice, so there could be other differences.

Thus, closer examination of the role of noradrenaline – either as a necessary accompaniment to cholinergic signalling or an independent mechanism – could be fruitful. There is a speculative pathway by which noradrenaline might influence grid scale, by possibly causing cAMP upregulation, which is known to affect the I_h current in layer II mEC stellate cells (Heys & Hasselmo, 2012).

In general, further exploration of grid scale changes and neuromodulation in the context of this theoretical framework of uncertainty sources could be extremely interesting. Following the study by Carpenter et al., experiments would include further cholinergic and noradrenergic manipulations in combination with electrophysiological techniques in behaving animals.

5. SPATIAL CAPACITY OF GRID CELL CODING SCHEMES

5.1. Background

Chapter 1.8.2 discussed predictions from various theoretical approaches about the dependency of grid cell system's spatial capacity on the configuration of the different modules' grid-pattern scales. In Chapter 3 I reported that my first experiments with a biologically-inspired model allowed some testing of these predictions. In summary, systems with sufficient numbers of grid cells to compensate for their intrinsic noise, under conditions without spatial uncertainty, were indeed able to represent unique locations across distances much larger than the largest grid scale present in the system. Under such conditions and in the relatively small simulated environments used in most of the experiments, there was little difference in performance between different scale configurations, while when the number of cells was too low to compensate for intrinsic noise some variation in error magnitudes by scale configuration did arise but a monotonic or regular relationship was not apparent.

Here I describe further experiments with the biologically-inspired model to explore this question in more depth. I will show that the distances between locations where different grid periods' phases take the same, or very similar, values are related to the sizes of environments in which the grid code will suffer ambiguity errors, and thus to the spatial capacity of the grid cell system. Exploring the performance of different grid coding schemes, I will demonstrate that grid code capacity does depend on the arrangement of grid scales, but that the relationship is too sharply irregular for optimisation to be plausible in reality: corroborating (Vágó & Ujfalussy, 2018) for systems with small numbers of grid modules, but disputing their claim that this dependence becomes irrelevant with larger numbers of grid modules.

5.2. Methods

This investigation applied the 1- and 2D versions of the model described in Chapter 3 and 4. Here I will set out the particular parameters used and additional analysis methods.

5.2.1. Grid-pattern parameters

Spiking activity of grid cell populations was modelled as described previously. In order to ensure that environments larger than the systems' theoretical maximum capacities (the lowest common multiple of the set of scales in the system) were computationally tractable, the systems were limited to 4 discrete modules, each with 195 cells having tuning curves offset from one another. Thus a total of 4 × 195 = 780 neurons were simulated.

In 2D simulations, every experiment was divided into 10 sets, in each of which a random orientation was selected to which all grid tuning curves in all modules were rotated. The tuning curves were calculated once and then rotated using cubic interpolation.

Coprime and geometric scale configurations were explored. As before, the coprime configuration had scales in the ratios of prime numbers 2 : 3 : 5 : … (e.g. $\lambda_3 = \frac{5}{2}\lambda_1$). In all models, the smallest spatial period, λ_1 was set as 25cm. In the geometric systems, based on previous theoretical predictions and experimental evidence, ratios p = 1.4 (Stensola et al., 2012), 1.5 (Stemmler et al., 2015) and 1.65 (Barry et al., 2007; Wei et al., 2015) were used for the first experiments, with finer variations in the ratio explored later.

5.2.2. Monte Carlo estimates of mean square error

In 2D simulations *N* = 37500 iterations were performed for each experiment (3750 for each set with a different, random orientation of the grid-pattern). In 1D simulations, *N* = 37500 iterations were performed for each experiment in the first section of the investigation (**Figure 5.1**), while *N* = 300000 iterations were performed in all subsequent experiments (**Figure 5.2** and **Figure 5.3**).

Note that for this and the investigations reported in Chapter 6, mean square decoding error was taken across all iterations performed for each set of conditions and parameters, and reported ± 95% confidence interval. This approach was a development from the earlier reporting method – in which the total number of iterations was divided into 10 batches, and results reported as the mean of the resulting 10 MSE estimates ± standard error of the mean – as that approach was unnecessarily arbitrary, especially for the very large number of iterations performed in these later experiments.

5.2.3. Assessing "near miss" grid phase similarity

For any given location *x*, the distance to the nearest point at which the phase of a grid cell module, *i*, is equal to its phase at *x*=0, which I will refer to as phase similarity per module, h_i, is:

$$h_i(x) = {}^{\lambda_i}/_2 - \left|mod(x,\ \lambda_i) - {}^{\lambda_i}/_2\right| \qquad \textbf{5.1}$$

The mean phase similarity, $\hat{h}$, at any location *x* therefore indicates how close the phases are to matching the phases they had at *x*=0:

$$\hat{h}(x) = \tfrac{1}{4}\textstyle\sum_{i=1}^{4} h_i = \tfrac{1}{4}\sum_{i=1}^{4}\left({}^{\lambda_i}/_2 - \left|mod(x,\ \lambda_i) - {}^{\lambda_i}/_2\right|\right) \qquad \textbf{5.2}$$

I sought to devise a measure that would encapsulate the hypothesised effect of grid module similarities on causing ambiguity errors. For example, very near misses (very small h_i) contribute much more to the probability of an error than larger h_i, which is not captured by taking the mean value over modules (**Equation 5.2**). The probability of an ambiguity error given the phase similarities h_i in each module and the degree of spatial uncertainty (i.e. the standard deviation, σ_ε, of the Gaussian noise in locational inputs to each module) can be estimated as the probability that the noise in grid phase exceeds the phase similarity in any of the modules. I made use of the Complementary Error Function *erfc(x)*, to estimate this as:

$$\prod_{i=1}^{4} erfc\left(\frac{h_i(x)}{\sigma_\varepsilon \times \sqrt{2}}\right) = \prod_{i=1}^{4} erfc\left(\frac{{}^{\lambda_i}/_2 - \left|mod(x,\ \lambda_i) - {}^{\lambda_i}/_2\right|}{\sigma_\varepsilon \times \sqrt{2}}\right) \qquad \textbf{5.3}$$

Second, from the premise that ambiguity errors are likely to occur across the distances between locations where the phases of all the grid modules are similar, it follows that the larger the environment than said distance, the more chances there are for ambiguity errors of that size to occur. So I scaled the measure at each location by the difference between that *x* and the environment size, *L*. I sum these, excluding the locations that fall within 12.5 cm (half the smallest grid scale) of the ends of the environment, since errors this small are considered precision, not ambiguity errors (so the range of locations sampled in the environment is *S*: from 12.5cm to *L*-12.5cm, at intervals of 0.5cm).

$$Predicted\ phase\ similarity\ effect\ (L) = \sum_{x \in S}\left\{\left[\prod_{i=1}^{4} erfc\left(\frac{{}^{\lambda_i}/_2 - \left|mod(x,\ \lambda_i) - {}^{\lambda_i}/_2\right|}{\sigma_\varepsilon \times \sqrt{2}}\right)\right] \times (L - x)\right\} \qquad \textbf{5.4}$$

Note that this measure was not intended to predict the actual magnitude of self-localisation error, but merely the varying effect that phase similarity is hypothesised to contribute to the error. The prediction to be tested was, therefore, simply that this measure would positively correlate with mean square error.

5.2.4. Statistical methods

An ANOVA was used to assess the effects of uncertainty, grid code scheme, environment size and the prediction measure, on mean square decoding error (see Results; SPSS v. 24, IBM). Type III Sum of Squares was used in order to obtain the independent effect for each factor with the other factors controlled for. The assessment included the main four grid-scale schemes considered – geometric schemes with ratios 1.4, 1.5 and 1.65, and a coprime scheme – under uncertainty levels, σ_ε, 1cm and 2.5cm, and in a range of 1D environments increasing from 0.4m, in 0.2m increments, up to a maximum of either the lowest common multiple (LCM) of the scheme's grid scales minus 12.5cm (this subtraction excludes simple precision error confusions with the LCM distance), or 27m, whichever was smaller for each grid scheme.

5.3. Results

5.3.1. Performance of grid cell systems in environments of increasing size depends on the scale scheme

I focussed my investigation on modular systems of grid cells with scales arranged in 4 different ratios, each proposed by previous experimental or theoretical work: geometric series with ratios 1.4 (Stensola et al., 2012), 1.5 (Stemmler et al., 2015), and 1.65 (Barry, Ginzberg, et al., 2012; Wei et al., 2015), and a coprime series (Fiete et al., 2008).

Examining simulated grid firing in 2D and 1D environments (**Figure 5.1A-B**) I found that, as shown previously, decoding errors increased with environment size in both

cases. However, the rate of increase varied greatly depending on the grid scale scheme, and exhibited tipping points at which the rate of increase rose sharply.

Theoretical analyses of grid coding schemes indicate that the maximum possible capacity of an idealised system is the lowest common multiple (LCM) of the component grid scales (Fiete et al., 2008). Thus, to validate this method, I first turned to a scenario where spatial uncertainty – modelled as independent noise in the location encoded by each module (see Methods) - was absent (**Figure 5.1A-B**). Large 2D environments are computationally burdensome to simulate, so investigating 1D environments as well allowed exploration of a wider range of environment sizes and parameters.

As expected, in most cases decoding errors remained relatively small until the environment scale approached the LCM of the grid scales, after which performance rapidly deteriorated to chance levels (for geometric ratio 1.4, LCM = 85.75m; ratio 1.5, LCM = 6.75m; coprime scheme, LCM = 26.25m), since in environments larger than the scheme's LCM, it is unable to unambiguously represent all locations. The exception to these observations was the ratio 1.65 geometric scheme, in which the LCM was considerably larger than the maximum environment scale tested and which retained a low error rate for all scales tested (LCM = 8984.25m vs the 100m 1D environment, **Figure 5.1B**).

Next, I explored the impact of spatial uncertainty on the accuracy with which self-location was represented in the grid cell system (**Figure 5.1C-E**). As expected, increased spatial uncertainty degraded decoding accuracy such that, for high levels of uncertainty, performance was close to chance for all schemes and environment sizes (**Figure 5.1E**). Strikingly, for intermediate levels of uncertainty, the relationship between decoding performance and environment size differed markedly from the zero uncertainty condition. Instead of a single tipping point, corresponding to the

capacity of the grid system, performance deteriorated earlier and in stages, with multiple interim tipping points at which the rate of increase in decoding error ticked up.

I hypothesised that these interim tipping points occurred when the environment reached sufficient size that it contains distinct locations with similar but not identical

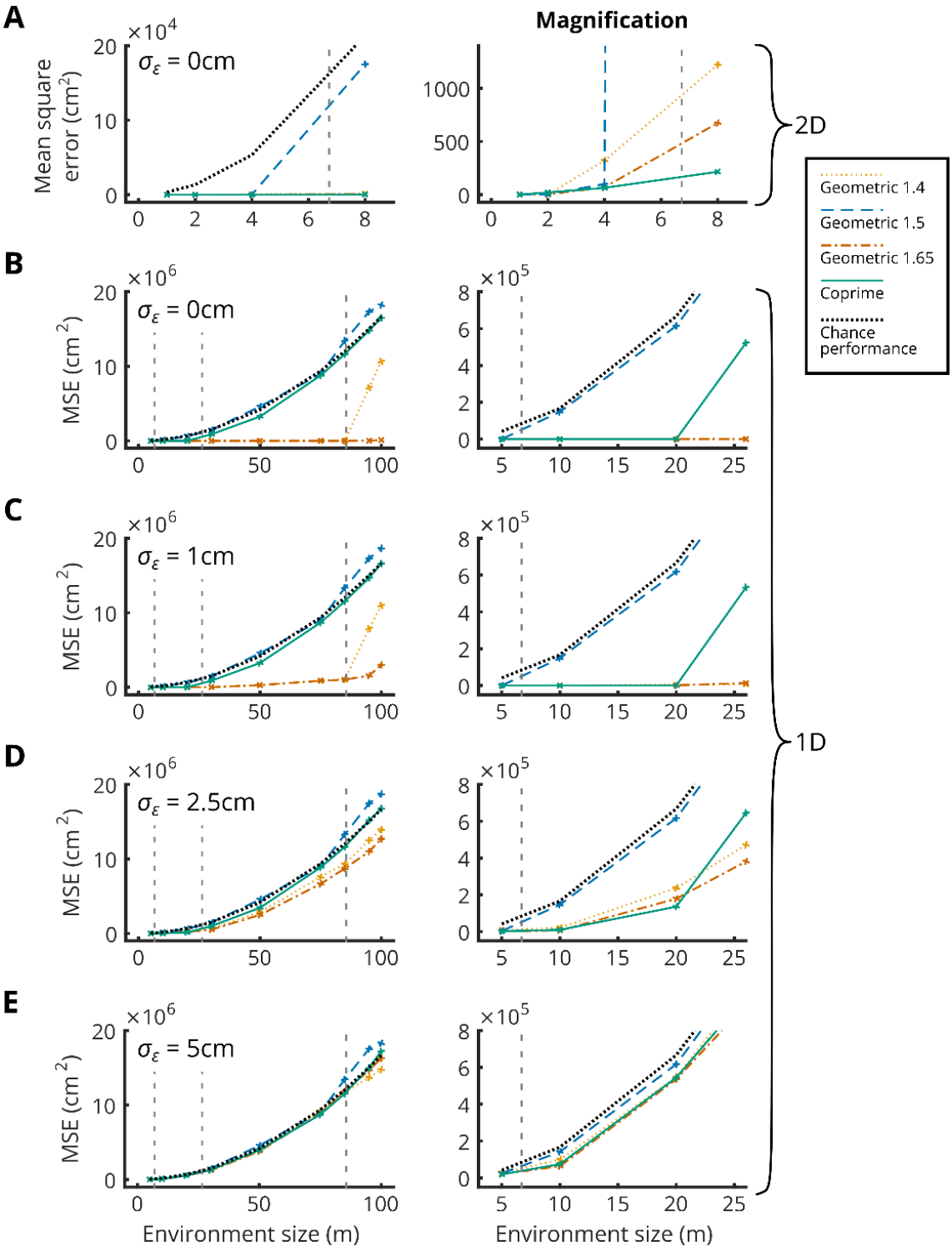

Figure 5.1 – Performance of grid cell systems in environments of increasing size depends on scale scheme

Performance of different grid cell schemes in 1D and 2D environments of varying size is indicated by the mean square decoding error. Grid scale schemes are indicated as follows – geometric ratio 1.4, orange dotted line; geometric ratio 1.5, blue dashed line; geometric ratio 1.65, vermillion dash-dot line; coprime, bluish-green solid line. All schemes have 4 modules, each with 195 cells. Black dotted line indicates chance performance. Vertical dashed grey lines indicates the lowest common multiples of the scales for the coprime (26.25m) and geometric ratios 1.5 (6.75m) and 1.4 (85.75m) schemes (geometric ratio 1.65 not shown as the LCM = 8984.25m). Magnified axes on the right. **(A)** 2D environment with no spatial uncertainty ($\sigma_\varepsilon = 0$). **(B-E)** 1D environments: (B) $\sigma_\varepsilon = 0$cm; (C) $\sigma_\varepsilon = 1$cm; (D) $\sigma_\varepsilon = 2.5$cm; (E) $\sigma_\varepsilon = 5$cm. *N* = 37500 for each data point. Error bars omitted for clarity.

grid representations – i.e. when the environment was large enough to encompass distances across which the phases of the grid modules come close to the same values (**Figure 1.6**). With a relatively small degree of uncertainty in the system, these near-misses would sometimes produce large decoding errors analogous to those seen when the absolute capacity (LCM) is exceeded.

5.3.2. Sharp increases in decoding errors relate to near-misses in grid phase similarity

To test the hypothesis that increases in decoding errors reflect near-misses in grid phase similarity, I incrementally increased the size of a test environment while examining how the performance of the grid coding system, subject to spatial uncertainty, co-varied with grid phase. Specifically, I identified points where decoding error grew rapidly and assessed the similarity of phases in grid modules at locations separated by the distances encompassed by environments of these sizes. Observation of the several coding schemes (illustrative examples in **Figure 5.2A-C**) indicated that increases in the error rate tended to occur in environments slightly larger than

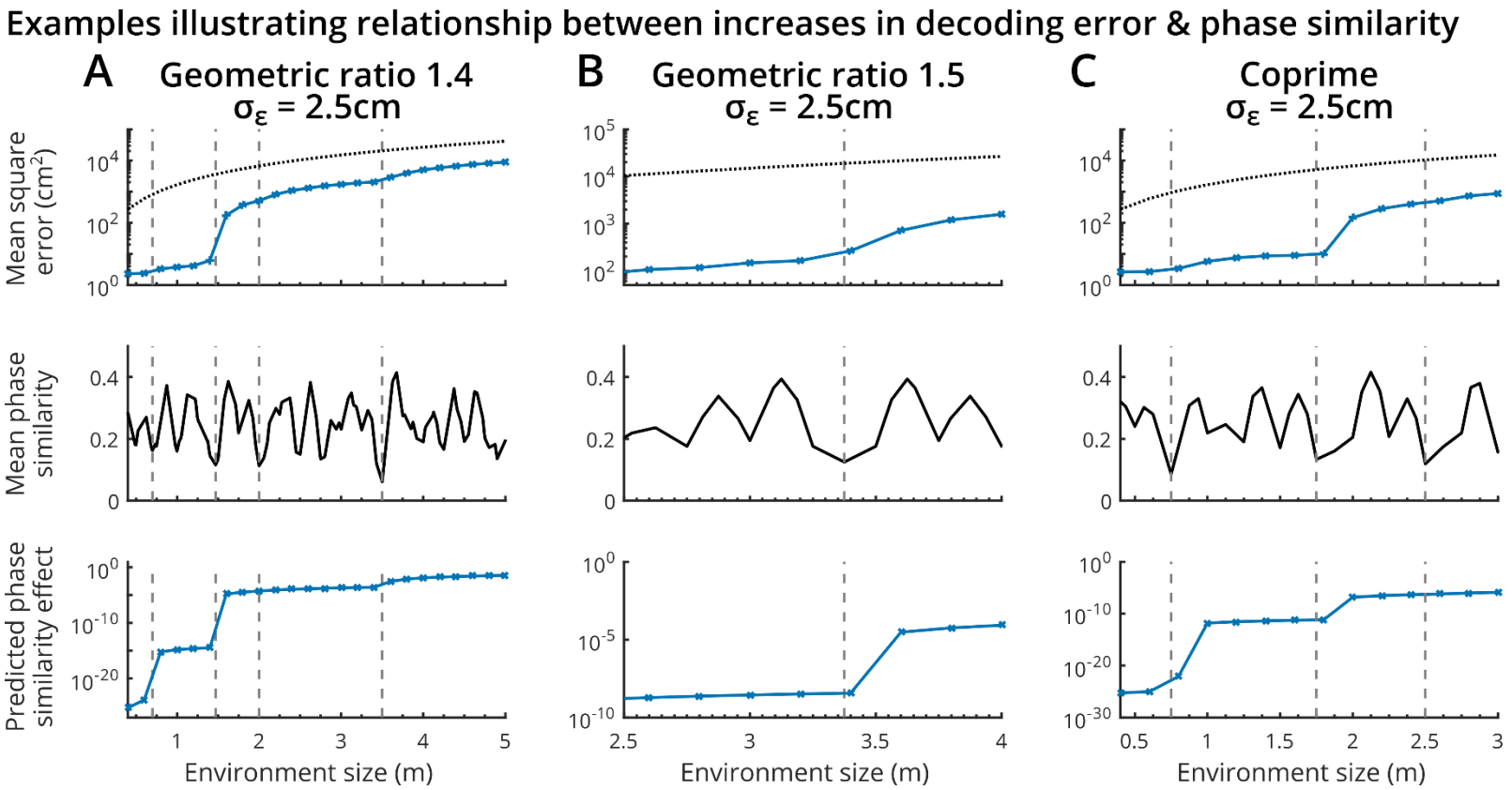
Examples illustrating relationship between increases in decoding error & phase similarity
A
Geometric ratio 1.4
σε = 2.5cm
B
Geometric ratio 1.5
σε = 2.5cm
C
Coprime
σε = 2.5cm
Mean square error (cm²)
Mean phase similarity
Predicted phase similarity effect
Environment size (m)
Environment size (m)
Environment size (m)

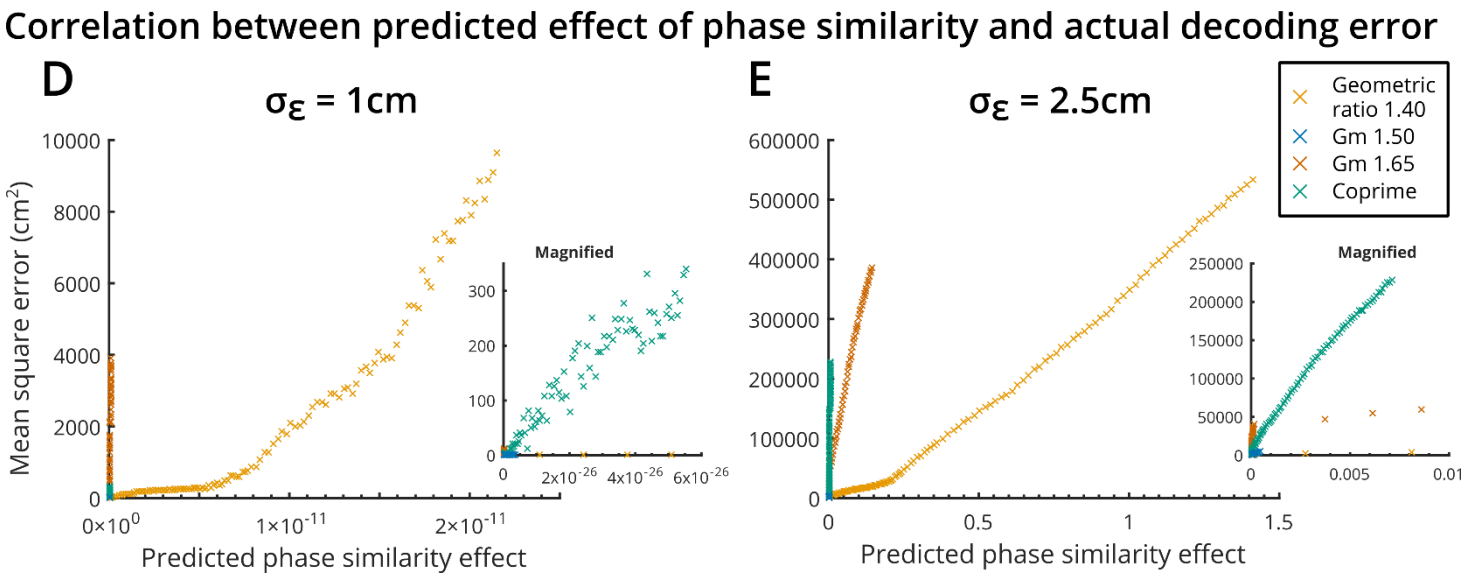

Figure 5.2 - Sharp increases in decoding errors do relate to similarity of grid phases

(**A-C**) Illustrative examples from a subset of the range of simulations showing how, as the environment is increased in size, rapid increases in decoding error tend to be preceded by the environment growing to encompass distances across which the grid modules' phases come closer to matching. Top row: mean square decoding error (blue solid line: σ_ε = 2.5cm; black dotted line: chance performance). Second row: mean phase similarity. Third row: predicted phase similarity effect (see Methods). Grey vertical dashed lines across the rows connect points where the similarity score is particularly low. (A) Geometric scheme, ratio 1.4; (B) geometric ratio 1.5; (C) coprime scheme. (**D-E**) Correlation between the measure of predicted phase similarity effect and the mean square decoding error. Data is shown for the main four grid schemes considered, in a range of 1D environment sizes (see Methods section 5.2.4) for uncertainty levels (D) σ_ε = 1cm and (E) σ_ε = 2.5cm. Inset: magnified portions of the same graphs. N = 300000 iterations per data point. Error bars are omitted for visibility.

distances over which the grid phases took similar values – quantified using a phase similarity score (**Equation 5.2**).

To better assess this effect, I derived a measure to predict the effect of phase similarity and environment size on error rate (**Equation 5.4**) – for each environment size tested, I made predictions based on the cumulative effect of similarity score and environment size (**Figure 5.2A-C** and Methods). By design, the prediction value jumped substantially for distances across which the grid phases take similar values, which as noted, coincided with jumps in the measured decoding error. Indeed, comparing across a wide range of conditions, there was a clearly visible correlation between the predicted effect of phase similarity and the actual decoding error (**Figure 5.2D-E**). This correlation was significant, independently of the effects of uncertainty level, grid code scheme, and environment size [ANOVA Type III Sum of Squares, $F_{(1,851)} = 926.697$; $p = 2.81\times10^{-138}$] (see Methods), corroborating the hypothesis that "near-miss" grid module phase similarities contribute to deteriorating grid coding performance.

5.3.3. Performance across fine variations in grid scheme geometric ratio

Armed with this understanding, I next conducted a fine-grained examination of the performance of different geometric grid schemes with ratios from 1.3 to 1.8.

I first examined the performance of different grid scheme ratios in small environments – from slightly smaller to slightly larger than the largest scales of these grid schemes (**Figure 5.3A-C**; **Figure 5.4** plots the same results as **Figure 5.3**, but with the x-axes indicating the largest scale present in each scheme rather than the ratio between scales, as this seems to be an important factor).

In the absence of spatial uncertainty, all schemes performed similarly in small environments which were similar in size to the largest grid scales - exhibiting a trend in

favour of smaller ratios (**Figure 5.3A**). This is consistent with the work described in Chapter 3 showing that in situations where the main source of decoding error is small precision errors, schemes with lower ratios and hence smaller average grid scales allow for greater resolution to minimise these errors. When uncertainty is introduced, however, performance deteriorates for all schemes but most dramatically for those with small ratios (**Figure 5.3B-C**). A large ratio, and therefore a largest grid scale that comfortably exceeds the environment size, minimises the occurrence of ambiguity errors.

Larger ambiguity errors were not always absent under a zero-uncertainty regime. In larger environments, while performance for most schemes follows a similar smooth trend of low error, this is punctuated by large decoding errors – for example, ratio 1.3 in the 10m environment and ratio 1.5 in 5 and 10m environments, as well as others. (**Figure 5.3D**). These schemes yield points with similar grid phases within environments of those sizes – or in the case of a ratio 1.5 scheme, precisely the same grid phases at the lowest common multiple of the set of grid scales: 6.75m (**Figure 5.5**). These similarities are close enough that even without spatial uncertainty, the intrinsic Poisson noise in the modelled neurons is sufficient to prevent successful disambiguation. This conclusion is supported by the performance of schemes with the same ratios but 10 modules – the large decoding errors are eliminated since the larger set of scales does not come close to reaching similar phases over these distances.

Having established these behaviours of the system, I examined some more realistic scenarios - performance under greater uncertainty and in larger environments.

Consistent with the prediction put forward by Vágó & Ujfalussy (2018), in a grid system with a small number of modules, decoding error in environments significantly

Figure 5.3 - Performance across fine variations in grid scheme geometric ratio

Decoding performance across a range of geometric schemes (ratios 1.3, 1.38, 1.385, 1.39, 1.395, 1.4, 1.405, 1.41, 1.415, 1.42, 1.48, 1.485, 1.49, 1.495, 1.5, 1.505, 1.51, 1.515, 1.52, 1.6, 1.63, 1.635, 1.64, 1.645, 1.65, 1.655, 1.66, 1.665, 1.67, 1.7, 1.8), in different conditions. Red-purple: 0.5m environment; sky blue: 1m; orange: 5m; blue: 10m; vermillion: 50m; blue-green 100m. Solid lines indicate mean square decoding error and correspondingly-coloured dotted lines indicate chance

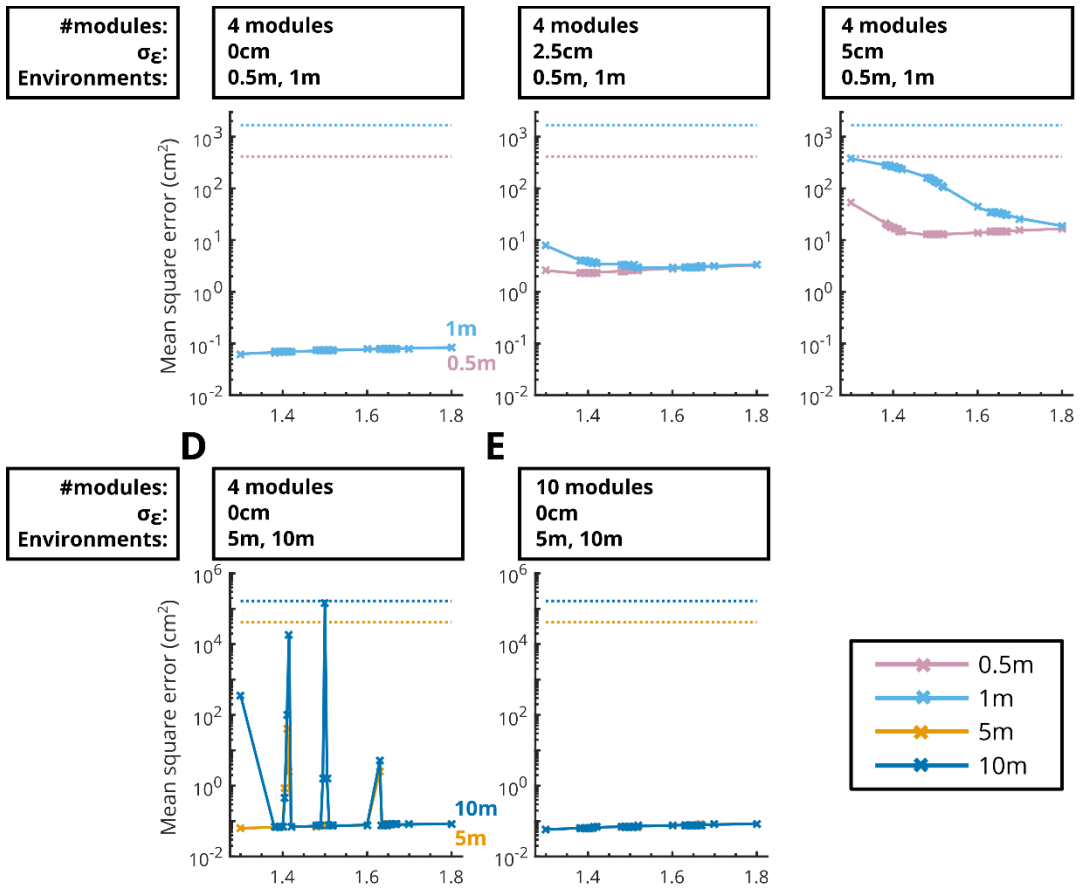

performance level in that size of environment. Module numbers, uncertainty s.d. and environment sizes indicated above each plot. N = 300000 iterations per data point. Error bars omitted for visibility. N.B. in (**D**) the few instances of large decoding errors where scale configurations yield equal or similar grid phases across distances smaller than the 5 and 10m environments: ratios 1.3 and 1.5 in 10m; ratio 1.63 in both, and a number of ratios around 1.41 (in 5m) and 1.415 (in 10m).

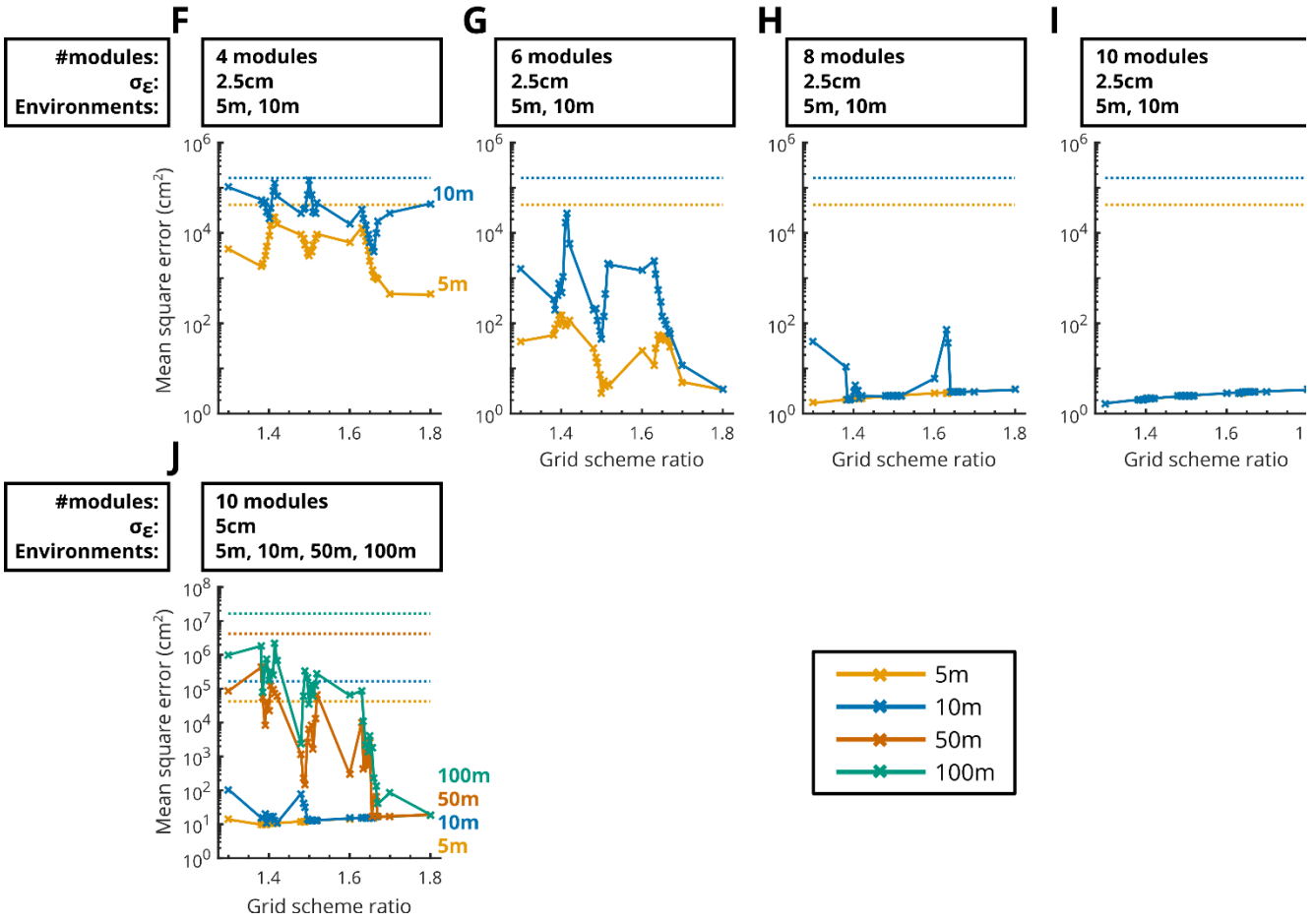

Figure 5.4 - Performance across fine variations in grid scheme geometric ratio, plotted by largest grid scale

This figure displays the same results as **Figure 5.3,** re-plotted with the x-axis showing the largest grid scale present in that grid system, in order to assess performance by whether the environment exceeds the range of the largest grid-pattern period. Note that the range of largest grid scales (i.e. the x-axis range) varies with the number of modules.

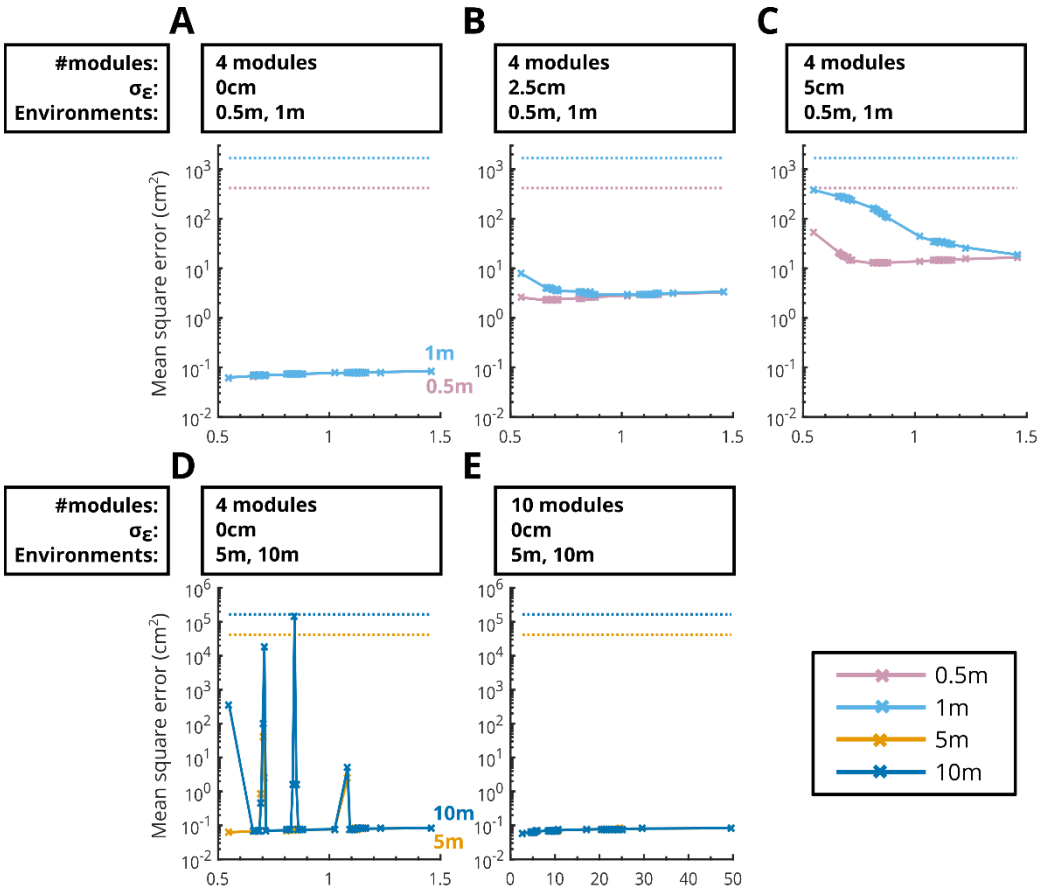

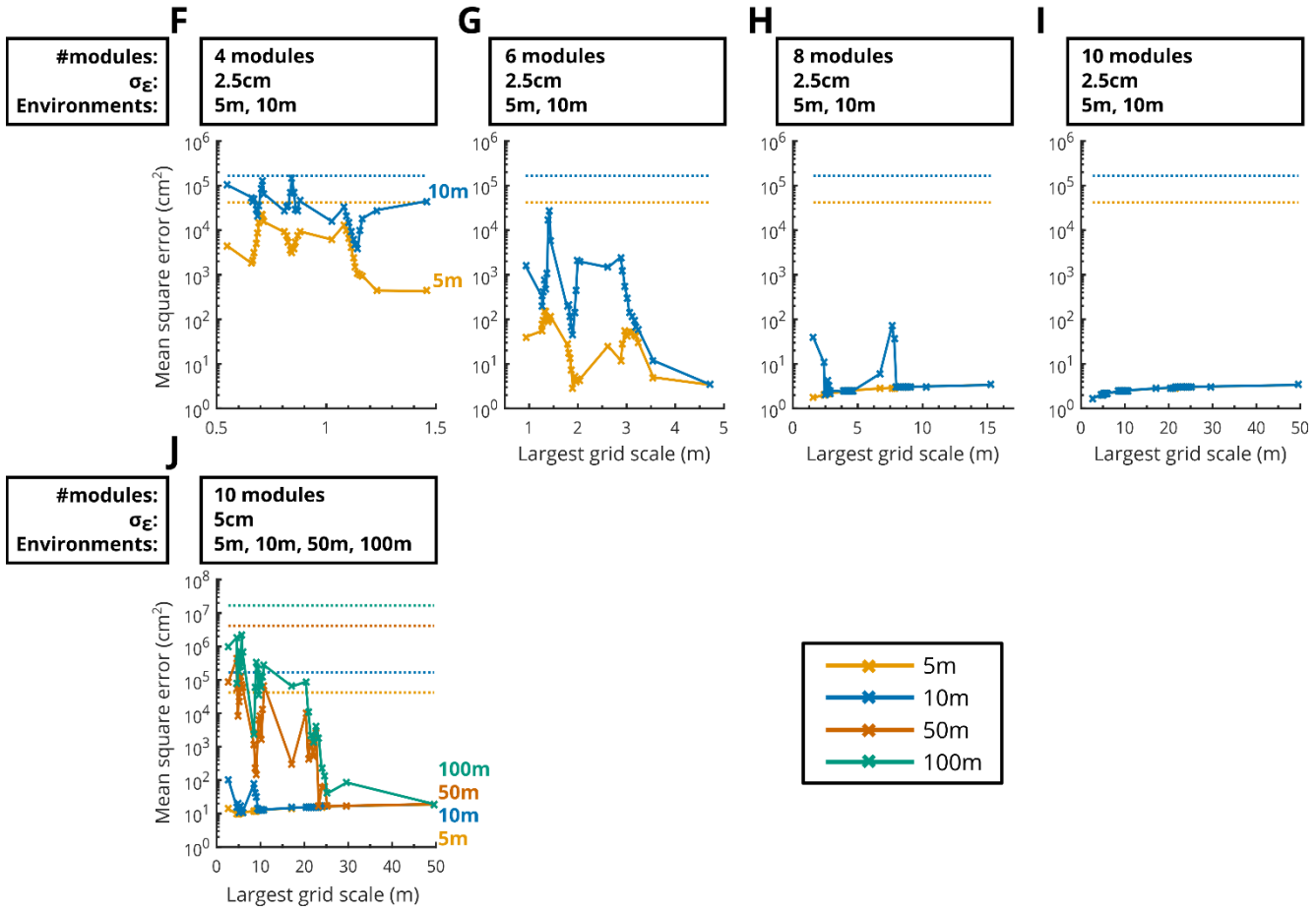
F
#modules:
σε:
Environments:
4 modules
2.5cm
5m, 10m
G
6 modules
2.5cm
5m, 10m
H
8 modules
2.5cm
5m, 10m
I
10 modules
2.5cm
5m, 10m
J
#modules:
σε:
Environments:
10 modules
5cm
5m, 10m, 50m, 100m
Mean square error (cm²)
Largest grid scale (m)
10m
5m
100m
50m
10m
5m
5m
10m
50m
100m

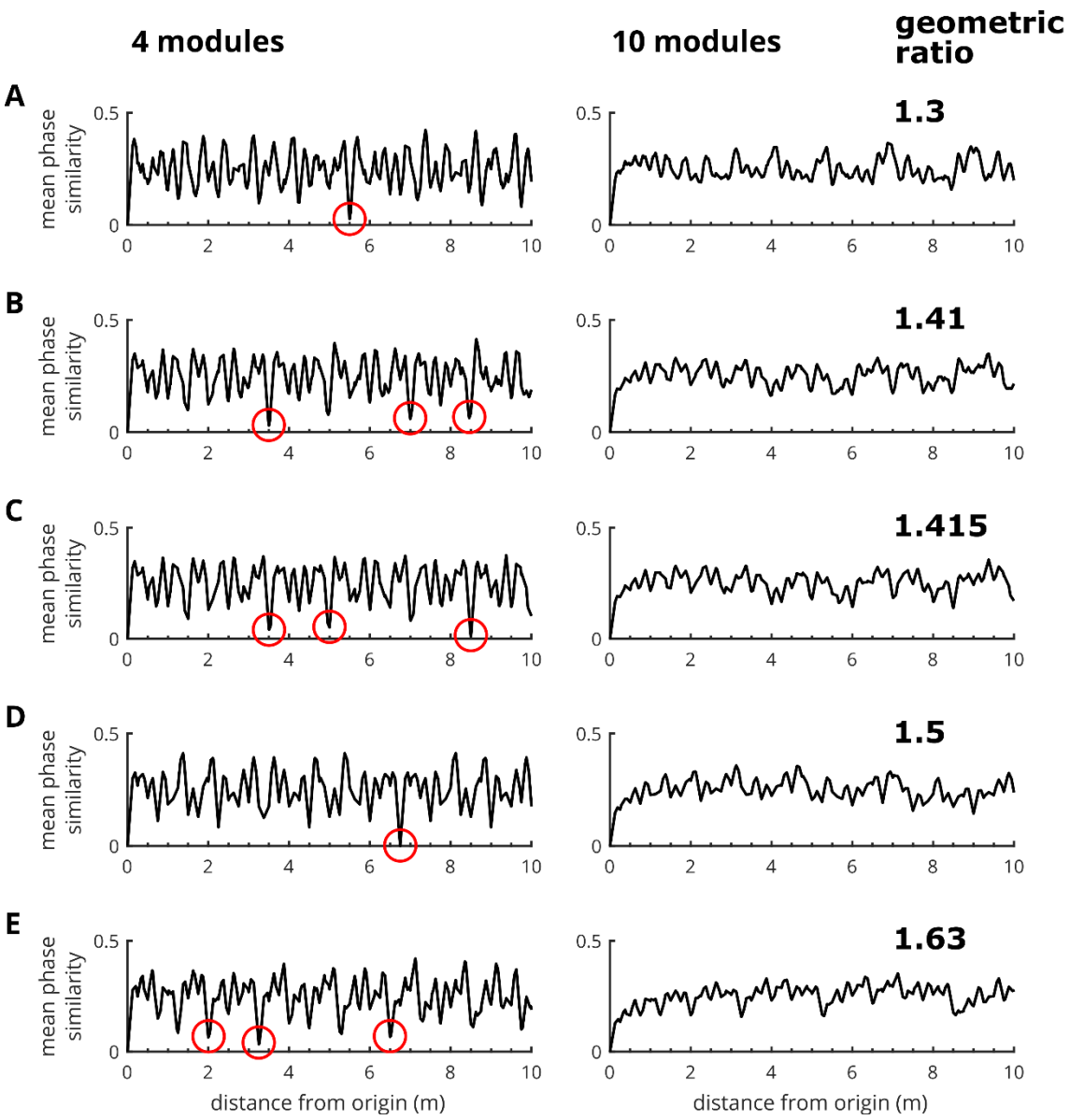

Figure 5.5 - Very similar module phases across short distances given by pathological geometric ratios

The poor performance of 4-module schemes (left column) with these ratios in 10m and, for some, 5m environments (**Figure 5.3D**) can be explained by how, within these distances, they yield points with very similar grid phases. At these distances, the similarity score comes extremely close to zero (indicated by red circles; in the case of ratio 1.5, it reaches zero, since the lowest common multiple of the scales is 6.75m). Systems with ten modules (right column) do not come close the same phase values in this distance range, and correspondingly, decoding error is low (Figure 3E). Geometric ratios: (A) 1.3; (B) 1.41; (C) 1.415; (D) 1.5; (E) 1.63.

larger than the largest grid scale varied substantially with the geometric ratio between the modules – but this variation was non-monotonic, irregular, and sharply discontinuous over even small differences in ratio (**Figure 5.3F**). Ratios that performed better than others in one size of environment were also seen to perform worse in others – for instance, a scheme with a ratio of 1.5 suffered less decoding error than other similar ratios in a 5m linear environment, but much worse than its neighbours in a 10m environment, which exceeds the LCM of the system. As the number of modules increased to 6, 8 and 10 (**Figure 5.3G-I**; this increases the size of the largest grid scale, the LCM and, all else being equal, the expected capacity) performance improved and smoothed out, as predicted by (Vágó & Ujfalussy, 2018) – a smoothly monotonic trend emerges, with smaller ratios giving slightly better performance. However, if the degree of spatial uncertainty is increased and larger environments are examined, non-monotonic, irregular, sharply discontinuous variation re-emerges (**Figure 5.3J**).

5.4. Discussion

I simulated self-localisation by modular grid cell systems with different sequences of grid scales, in different sizes of environment, in order to investigate their spatial capacity. I showed an association between the points at which increasing environment sizes lead to sharply increasing decoding error in a particular grid cell system, and the distances over which the phases of its modules can take very similar values at more than one location within the environment. Equipped with this understanding, I explored the self-localisation performance of different grid code schemes under different amounts of spatial uncertainty. I found that when spatial uncertainty is moderate and the environment is large compared to the largest grid scale, self-localisation performance varies sharply and irregularly with grid scheme ratio, making optimisation of grid scheme ratio biologically implausible.

Thus, using a biologically plausible simulation I have tested and extended previous theoretical investigations. These results corroborate Vágó & Ujfalussy's predictions for systems with a very small number of grid modules, but contradict their prediction that this irregularity would smooth out with a larger number of modules (Vágó & Ujfalussy, 2018).

5.4.1. Capacity as a question of incrementally degrading performance and tolerable levels of error

Fiete et al. showed theoretically that the capacity limit of a grid code would be the distance separating locations where the module phases were sufficiently similar as to produce indistinguishable signals (Fiete et al., 2008). This would in turn depend on the precision with which phase can be signalled and read out. These simulations in a biologically inspired model broadly corroborate this, while emphasising that when both the grid cells' intrinsic noise, and a degree of independent spatial uncertainty across modules, are brought into play, the system's performance degrades incrementally with increasing environment size, as more sets of locations with similar grid phase signals are encompassed.

"Capacity" therefore depends not only on the precision of the module phase signal and read-out, but what degree of error is tolerable. For instance, consider the performance of the grid systems with 6 modules, in a 5m environment, with moderate spatial uncertainty (σ_ε = 2.5cm). Across the set of ratios tested, decoding error was greater than in many other cases tested, with long-range ambiguity errors definitely occurring. Nevertheless, mean square error ranged no higher than 147.3 cm^2 (**Figure 5.3G**) – equivalent to root mean square 12.1 cm, similar to the length of a rat's body without the tail and probably a tolerable degree of error.

This may explain some of the discrepancies between my results and the predictions of other investigators. Previous theoretical approaches have sought the limit of a

spatial coding system's capacity as the largest range over which it can encode location without any ambiguity errors. That is, they take an "all or nothing" approach to performance. However, realistic biological systems may be expected to tolerate errors with at least a limited frequency and magnitude, especially if in a trade-off for optimising other features. This is particularly plausible given the potential of the grid code to facilitate mechanisms in downstream read-out systems for identifying and correcting ambiguity errors (as discussed in the Introduction and below) (Fiete et al., 2008; Sreenivasan & Fiete, 2011). Thus, rather than simply seeking the point at which ambiguity errors first appear, this approach assesses varying degrees of accuracy and precision in fallible coding systems.

A limitation of this approach is that I am not yet in a position to propose realistic loss functions that would indicate the actual behavioural or fitness cost of errors with different frequencies and magnitudes and indicate a realistic limit for tolerable error – future investigations could perhaps examine this question. Behavioural studies, perhaps involving interventions using tools such as optogenetics to introduce erroneous signals to the grid cell system or its inputs, could shed more light.

5.4.2. Optimisation of grid ratio is not plausible

I aimed to examine whether a particular grid scale scheme would allow for optimal performance in large environments. I found different trends under different conditions. With zero uncertainty, decoding error is very low in environments that are small relative to the largest grid scales, across the full set of geometric ratios tested. There is a smooth, slight trend for smaller errors when the geometric ratios between the grid scales are smaller. As shown in Chapter 3, when ambiguity errors are prevented, a set of grid modules with smaller scales improves resolution – but the variation is limited. In environments larger than the biggest grid scale, but still smaller

than the lowest common multiple of the scales, this low-error performance continues smoothly, interrupted only by what have been described as “pathological” ratios (Vágó & Ujfalussy, 2018). These are ratios that yield a set of grid scales with either a very small lowest common multiple (e.g. 1.5, or as shown in Chapter 3, √2), or points with very similar grid phase signals within the environment – sufficiently close that the intrinsic noise of the grid cells is enough to cause ambiguity errors.

When a degree of uncertainty is introduced, error remains low in environments that are smaller than the largest grid scale or of a similar order of magnitude. In larger environments, however, decoding error is increased and much more variable as a function of the geometric ratio determining grid scales. As predicted by Vágó & Ujfalussy (2018), with a small number of modules the variation is sharply irregular and non-monotonic, with very small changes in ratio yielding dramatic changes in performance. When the number of modules is increased, performance smooths out, also as predicted by Vágó & Ujfalussy. However, this appears to be merely a result of the extra grid scales exceeding the environment size: when the environment is increased in size, the irregularity emerges again.

Experimental observation has shown substantial variation in the ratio between module scales, across the range 1.1 to 1.8 (see Figure 5D in (Stensola et al., 2012)), with different investigations identifying averages of 1.42 (Stensola et al., 2012) and 1.7 (Barry et al., 2007), the former value being based on more data. It is unclear how much of this variation is due to limitations in measurements and how much due to actual biological variation, and a geometric sequence may well remain a good approximation for the relationship between real grid scales. However, our simulations show that in a large-environment moderate-uncertainty regime, mean square decoding error can change by nearly two orders of magnitude with an absolute change of just 0.015 in geometric ratio (**Figure 5.3G**). It does not seem biologically plausible

that the parameters of the grid coding scheme could be set and maintained with this level of precision in reality. Additionally, a ratio that gives a peak in performance under one condition can give a trough in another. For instance, with 4 modules and uncertainty σ_ε =2.5cm, a ratio of 1.5 performs better than similar ratios in a 5m 1D environment, but little better than chance in a 10m environment.

This suggests that if the grid code is required to function under such regimes, it is unlikely that grid ratios are adaptively optimised in reality, despite the fact that it is possible to identify optimal ratios in theoretical work. Pressure for optimisation may therefore be more likely to act on other factors, such as the number of modules, the number of cells per module, or the distribution of cells between modules.

If optima cannot be maintained, does this also suggest that the "pathological" ratios noted above, such as 1.5 or √2, which yield extremely poor spatial capacity, cannot be reliably avoided? If not, the possibility of combinatorial capacity for the grid code would, in practice, be ruled out. However, such a collapse in capacity requires that the relative scales of the whole series of grid modules present in an animal precisely land on the same pathological ratio. It seems likely that the same variability that precludes optimisation would also make such pathologically poor performance improbable.

Speculatively, it is also conceivable that as the grid scale scheme develops in an animal, if an arrangement yielding particularly poor performance did arise, a learning system could prompt a small change in any of the modules, which would be enough to shift the scheme out of the narrow trough in performance. It is possible to imagine a mechanism capable of identifying pathological ratios for correction at the point in development when the grid-patterns are being established and prior to any extensive physical navigation testing the capacity limits of the system. It would merely

be necessary for the brain to probe its newly-developing grid cell system with a simulated movement signal that engages it in virtual navigation along a straight-line trajectory – much like the forward-play or replay discussed in the Introduction and Chapter 2 – and see how far it is possible to get before the system's output is indistinguishable from that at the beginning of the process. Theoretically this would be even detectable in infant animals since it would result in periodic repetitive firing of entorhinal cells in development, which could later be identified as grid cells (and retrospectively decoded) by their firing patterns once the animal is old enough to roam beyond the nest.

5.4.3. Capacity and behavioural range

As discussed in the Introduction, the field has seen debate about whether the grid code is likely in fact to represent spatial ranges larger than the largest grid scale present in the animal. Contributing to this disagreement, estimates of the natural range of rats have varied. At the lower end is the suggestion that a rat's home range is as small as ~$(10\ m)^2$ (Davis et al., 1948). The existence of grid cells with 10m periods is quite plausible: the smallest scales detected are less than 50cm, the largest scale detected thus far is 5m (Brun et al., 2008), and the total number of modules has been estimated at less than ten (Stensola et al., 2012). So this might render combinatorial capacity unnecessary for the grid code. However, this work was based in urban areas, and more recent work that has studied rat behaviour in more open, natural environments suggests much larger ranges of ~$(0.1 – 1km)^2$ (Recht, 1988; Russell et al., 2005). Grid scales reaching such sizes are possible but seem less plausible.

If the rat's natural range substantially exceeds the scale of its largest grid-pattern, then either the code would need to attain combinatorial capacity, or it must not be

able to continuously represent the environment over its full roaming range. For instance, it might use a splintered representation that does not continuously cover the range as a whole but remaps between different sub-regions of the range (Fyhn et al., 2007). If, as has been speculated, the grid code is necessary for planning navigation along novel vectors (Kubie et al., 2009; Erdem & Hasselmo, 2012; Kubie & Fenton, 2012; Bush et al., 2015) the animal would have to rely on other strategies to navigate between these sub-regions, such as learning to associate specific sub-regions with specific landmarks or features visible at a distance and simply homing in on them, or only using familiar paths between sub-regions.

It has been proposed that a grid code could maintain combinatorial capacity with error-correcting mechanisms made possible by the properties of the code. The nature of ambiguity errors in this system is that small errors in the signal or read-out of a module's phase can result in decoding to a distant location. It would be possible to easily identify such erroneous location estimates by comparing them to previous estimates of location immediately beforehand (introducing a Bayesian prior to the process of self-localisation; this could be facilitated by combining the grid system with a slow-moving representation of location, such as in the place cell system) or if the estimated location falls outside the known range of the environment (Fiete et al., 2008; Sreenivasan & Fiete, 2011).

In the present model, location is encoded and decoded moment-by-moment, without comparison to any previously-occupied locations, so if this type of error-correction does indeed occur, this work provides only a floor for the performance of the grid code and error could in fact be much smaller. This would suggest that the system's spatial capacity for self-localisation is indeed combinatorially large. Note, however, that these error correction mechanisms have been hypothesised in the context

of continuous self-localisation. If the grid code is also used for non-local representation and planning novel trajectories, the algorithm for this is not yet known, and it would need to be established whether such error correction mechanisms could apply to it too – otherwise the grid code might be able to produce a continuous representation of self-location across a large range, yet be unable to plan navigation across comparable distances.

Ultimately, resolving these questions will require experimentation in much larger environments than spatial cells have yet been recorded in, both to examine whether continuous grid-patterns extend across the full range, and whether animals are capable of planning novel trajectories for vector-based navigation across those same distances.

6. GRID-PATTERNS ORIENT ADAPTIVELY IN POLARISED ENVIRONMENTS

6.1. Background

Up to this point, my investigations have modelled spatial uncertainty as isotropic – the same in all directions, and the same in all parts of the environment. However, this is not the case in most real situations, in which both the environmental and idiothetic spatial information available to an animal varies by axis and location. For instance, when standing a short distance from a long, relatively flat and smooth wall, we can locate ourselves with much more confidence and precision in the axis perpendicular to the wall (e.g. "I am one arm's length away from the wall" or "I have travelled only one footstep since I was one arm's length away from the wall") than parallel to it. Consistent with this, error in the grid cell representation has been observed to accumulate relative to the time and distance travelled since the last visit to an environmental boundary, and specifically a visit to a boundary reduces error more in the axis perpendicular to the boundary (Hardcastle et al., 2015).

In this section, I will describe an experiment in which I adapted the previously-described grid cell model to test whether, when spatial uncertainty is instead modelled as anisotropic – greater in one axis and less in another – the particular orientation of the grid cell pattern relative to those axes affects the fidelity of grid code self-location representations. I will also compare the results of this *in silico* experiment with *in vivo* observations on the same question made by collaborators.

The work reported in this chapter was published as part of this article: Navarro Schroeder, T. et al. (2017) 'Optimal decision making using grid cells under spatial uncertainty', *bioRxiv*. doi: 10.1101/166306.

6.2. Application of the model

6.2.1. Grid cell system and environment

As in Chapter 4, a geometric sequence of grid scales with ratio 1.4 was used, beginning with 25cm as the smallest scale. Each module contained 195 grid cells offset from one another. In order to reduce the computational burden, the system was limited to four modules. In each experiment, the grid-patterns shared the same orientation across all the modules.

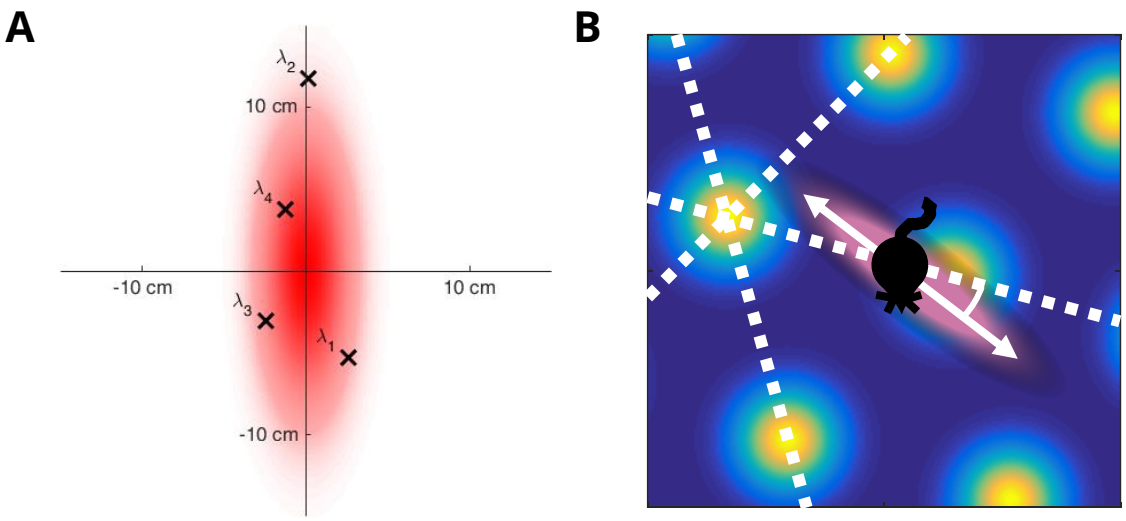

Figure 6.1 – Modelling anisotropic uncertainty

(A) An example of modelled anisotropic uncertainty. The animal's true location is at the origin. Red shading indicates a two-dimensional probability density distribution, produced by combining two one-dimensional Gaussian distributions with different standard deviations in orthogonal axes, from which noisy position estimates (black crosses) are drawn independently and input to each of the grid cell system's four modules. (B) The orientation of the axis of greater uncertainty was varied relative to the grid axes. In this example, the grid cell firing pattern is shown with a rate map (blue indicates low firing rate, yellow high); pink shading around the animal indicates the probability density distribution from which noisy position estimates are drawn; the double-ended white arrow highlights the axis of greatest spatial uncertainty; and the dashed white lines highlight the axes of the grid-pattern are highlighted with dashed orange lines. The orientation of the grid-pattern relative to the axis of greatest uncertainty – i.e. the angle between this axis and the grid-pattern axis – can be seen.

The simulated environment was circular, with radius 50cm. The "true" position in every iteration was the centre of the environment. Gaussian noise was added independently to the position signal fed to each module as previously. To render this modelled uncertainty anisotropic, the standard deviation of the noise was varied independently in the environment's Cartesian x and y axes, as illustrated in **Figure 6.1A**.

6.2.2. Assessing grid system performance

For each combination of levels of uncertainty in x and in y, I assessed the performance of grid systems whose patterns were placed at orientations to these x-y axes from 0° to 30°, at intervals of 2.5° (**Figure 6.1B**; due to the six-fold rotational symmetry of the grid-pattern, 30° is the largest possible angle between any line and the closest of the pattern's axes). For each case, 75,000 iterations of this procedure were performed, split into 5 blocks of 15,000 each. In each of these 5 blocks, the square grid across which the environment was sampled to produce tuning curves was set at a different orientation to the environment's Cartesian axes, in order to control for any effect of uneven sampling (the orientations were 0° and 4 orientations randomly selected and then used across all conditions). The results of equivalent pairs of uncertainty levels (e.g. standard deviation respectively in x & y of 0 & 5 cm, and 5 & 0 cm) were then combined to total 2 × 5 × 15,000 = 150,000 iterations. MSE is reported in this and subsequent investigations as the mean square across the full complement of iterations ± 95% confidence interval (note this is the same practice as used in Chapter 5, in which the change from the experiments in Chapters 3 and 4 was explained).

6.3. Results

Consistent with earlier experiments and as expected, decoding errors were very small in the absence of spatial uncertainty, while increasing levels of uncertainty resulted in significantly degraded decoding performance (**Figure 6.2B**).

Alongside that, this experiment demonstrated a dramatic effect on performance of the orientation of the grid-pattern relative to the distribution of uncertainty. Mean square decoding error was minimised by orienting the grid-pattern so that its axes are maximally misaligned from the axis of greatest spatial uncertainty. Due to the six-fold rotational symmetry of the pattern, this means the pattern axes nearest the axis of greatest uncertainty will be 30° away, and the other pattern axis will be aligned with the axis of least uncertainty (**Figure 6.2**).

With the most anisotropic conditions tested (σ_ε set to 0cm and 5cm in the two axes), this 30° orientation resulted in a 40% decrease in mean square decoding error relative to the opposite case of 0° (**Figure 6.2A**). As anisotropy becomes less extreme, the effect can still be seen but becomes less pronounced, and disappears as the uncertainty in the two axes approaches equality (**Figure 6.2B**).

Control experiments confirmed that the effect remained consistent as other parameters of the grid cell system – grid scale, grid cell firing rate, number of grid cell modules – varied (**Figure 6.3**).

6.4. Comparative human fMRI experiments

In order to test the prediction from this modelling, I and my lab colleagues set up a collaboration with Christian Doeller and Tobias Navarro Schröder (based at the Donders Institute for Brain, Cognition and Behaviour, Radboud University, the Netherlands) who conducted and analysed human fMRI experiments. These experiments

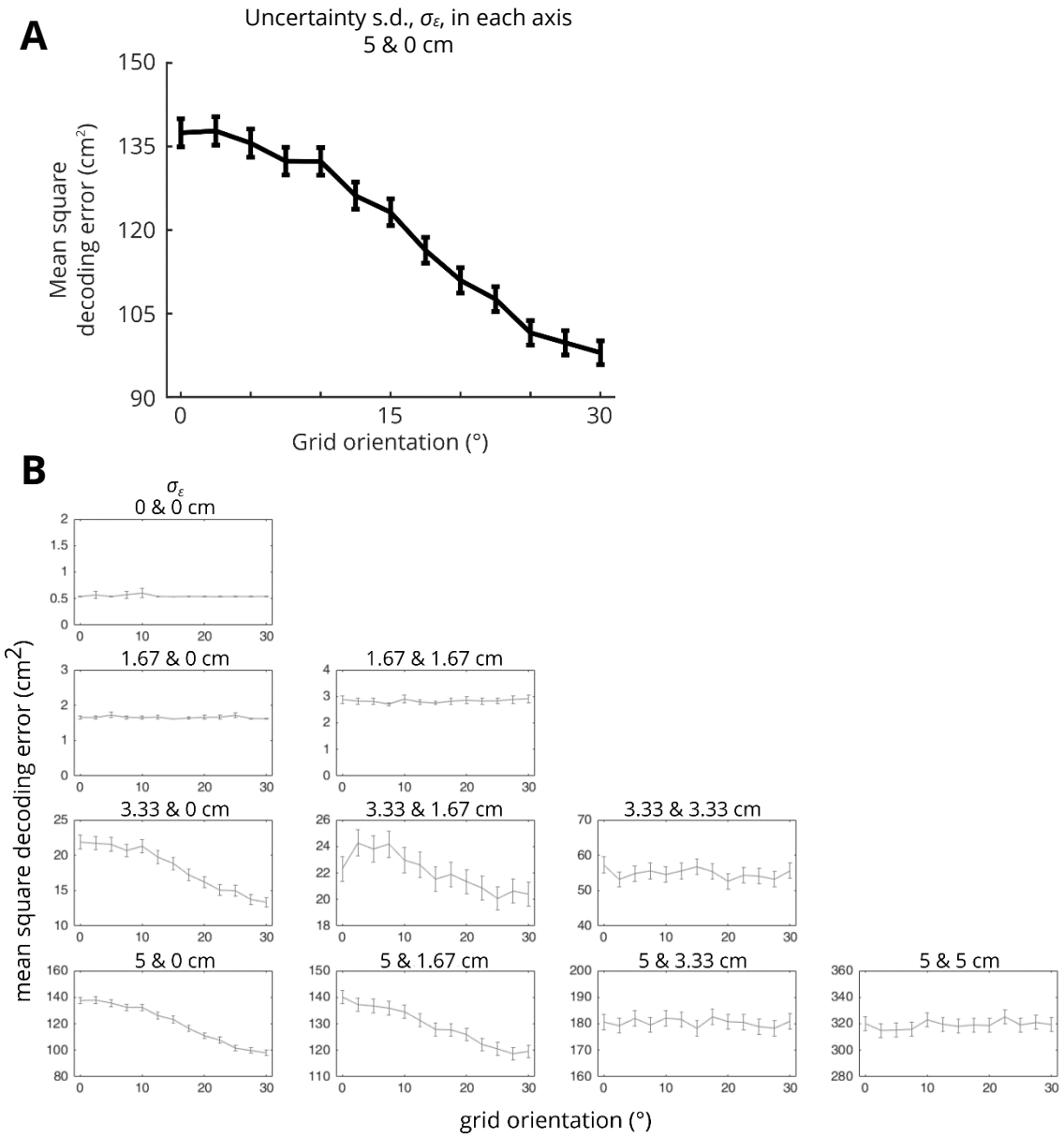

Figure 6.2 – Error in self-localisation under anisotropic uncertainty is minimised by orienting the grid-pattern axes away from the axis of greatest uncertainty

The performance of grid cell systems in environments where spatial uncertainty is anisotropic depends on the orientation of the grid cell pattern to the direction of that anisotropy. Uncertainty s.d. (σ_ε) indicates the standard deviation of spatial uncertainty in two orthogonal axes, and grid orientation indicates the angle between the minimal angular offset of a grid axis from the axis of greater uncertainty. (A) With the most extreme anisotropy tested, a 30° orientation reduced MSE 40% compared to a 0° orientation. (B) As anisotropy becomes less extreme, the effect becomes less pronounced. Error bars indicate 95% confidence interval (n=150,000).

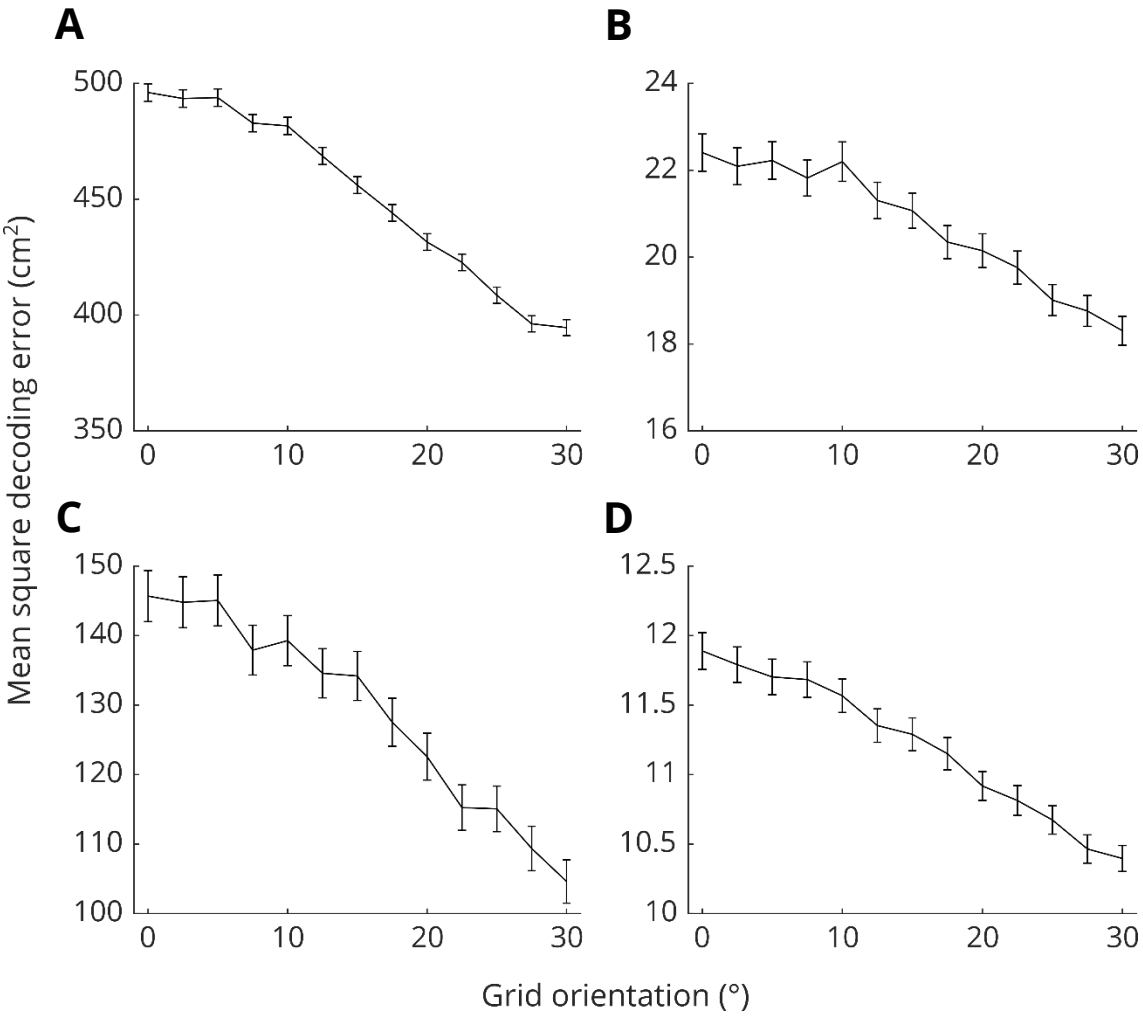

Figure 6.3 – The dependency of self-localisation fidelity on grid orientation is stable within reasonable sets of grid cell system parameters

Performance is consistently best when the grid axes are aligned away from the axis of least spatial uncertainty, across variations in the parameters of the grid cell system. Error bars indicate 95% confidence interval, n = 150,000 unless otherwise specified. (A) Grid period scaling factor reduced to 1.2. (B) Grid period scaling factor increased to 1.65. (C) Grid cell maximum firing rate reduced to 2Hz. (In order to compensate for increased effects of noise in this system, the number of cells per module was quadrupled. Due to the high computational intensity of this simulation n = 75,000.) (D) Number of modules increased to 8, with scales continuing to increase geometrically.

are reported more completely in our joint publication (Navarro Schroeder et al., 2017): since these experiments were not carried out by me, here I will simply summarise the approach and main findings in order to inform comparison with my results.

6.4.1. Background

The particular collective properties of grid cells' firing patterns permit the unusual opportunity to infer details of cell firing patterns from the bulk activity of a large population of cells, measured indirectly via an fMRI BOLD signal, as shown by the original experiment that provided evidence for grid cells in the human brain (Doeller et al., 2010).

Since the offsets of the grid cells in a module appear to tile space evenly, the bulk activity of a population of pure grid cells would not be expected to vary in a macroscopically detectable way. However, a macroscopic signal can be predicted based on two facts: first, many grid cells are conjunctive – that is, their activity at the nodes of a grid-pattern is modulated by head direction – and second, the preferred directions of these conjunctive cells tend to align with the axes of the grid-pattern. Thus, a population of conjunctive grid cells whose grid-patterns share the same orientation would be expected to show greater overall activity when running direction is parallel to grid axes, than when running direction is misaligned from the grid axes. And indeed, these experimenters were able to show that the BOLD signal in the entorhinal cortex of virtually navigating humans varied by running direction with six-fold rotational symmetry (this effect is commonly referred to as "hexadirectional modulation" of the BOLD signal). Additionally, they showed that running speed modulated both the firing of rat conjunctive grid cells and this fMRI signal in humans.

6.4.2. Methods

Our collaborators applied this fMRI approach to determine the orientation of grid cell patterns in human subjects without the need for direct electrophysiological recordings of individual cells. Human subjects performed a navigation task in virtual environments where the spatial information available for self-localisation in one axis was greater than in the other, orthogonal axis, while brain activity was monitored using fMRI.

6.4.2.1. Environments

Experiments were conducted with two virtual arenas. Both were circular and featured extra-maze cues that polarised the arena along one axis crossing the centre. In the first environment, the reference axis was implicit, created by configural cues – 12 triangles surrounded the arena, upright on one half and inverted on the other, so that the points at which the configuration of the triangles switched formed the reference axis. In the second, there were only two extra-maze cues on opposite sides of the arena, creating a more explicit, non-configural reference axis between them (**Figure 6.4**).

Since the cues were out of reach of the subject, the main source of information for self-localisation during navigation was parallax – the change in the direction of a stationary cue from the point of view of a moving observer. In environments like these, where the main cues are beyond the arena and out of reach, the angular movement of cues from the point of view of the subject is greater when moving perpendicular to the reference axis. Thus these environments had an axis of greater spatial information and an axis of greater spatial uncertainty, with which the predictions of my model could be tested.

6.4.2.2. Task

In both arenas, subjects performed an object-location memory task at the start of which they were shown, and navigated to, locations associated with a number of everyday objects (6 in the first environment, 4 in the second). They then proceeded with trials each with a "replace" phase and a "feedback" phase. In the "replace" phase they were cued with an image of one of the objects, randomly selected, and had to navigate to the associated location before pressing a button when they believed they were in the right place. In the "feedback" phase the same object then appeared in the correct location and they would navigate to it and collect it.

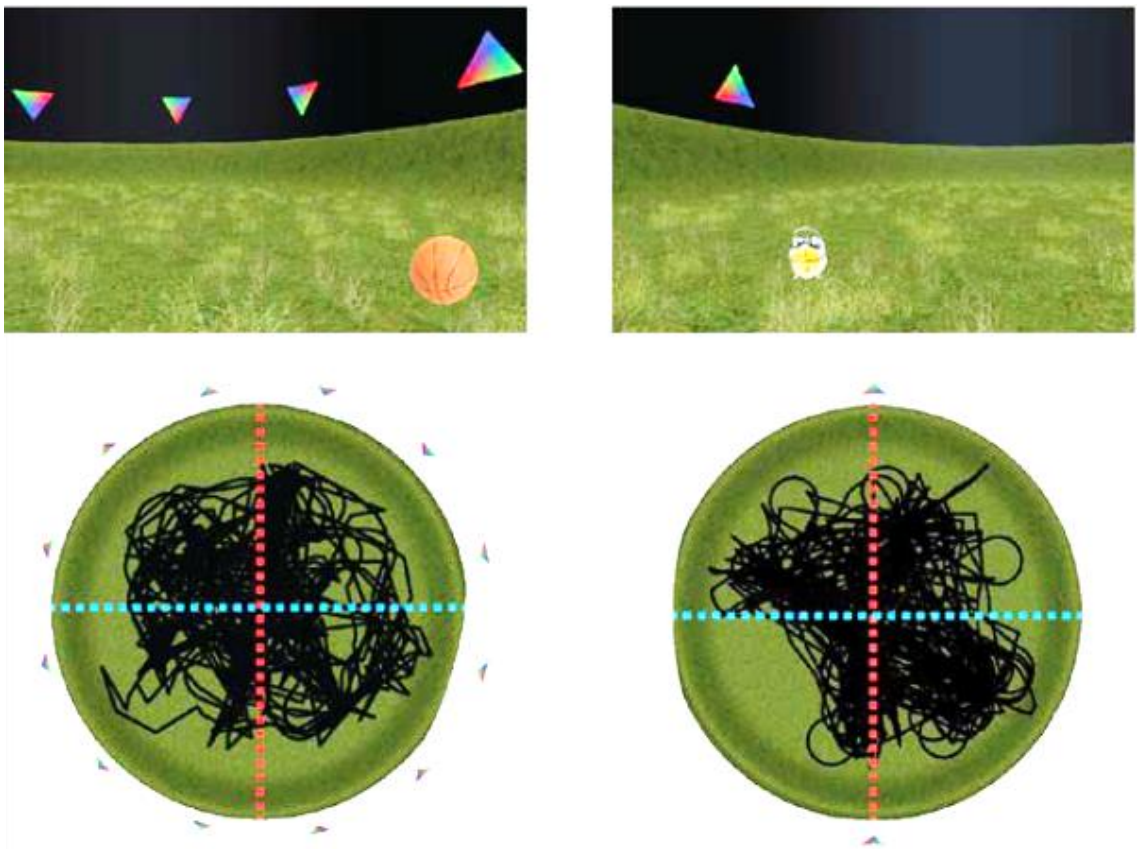

Figure 6.4 – The virtual arenas used in the fMRI experiments

The environments used in the first (left) and second (right) experiments, from a first-person view (top) and from above (bottom). The reference axes are indicated with red dashed lines on the lower images, and the perpendicular axes indicated in blue.

6.4.3. Results

In each experiment, hexadirectional modulation of the fMRI signal was detected in the right entorhinal cortex, indicating the presence of grid-cell-like activity. The inferred orientations of the subjects' grid-patterns were clustered: misaligned from the reference axis – the axis of greater spatial uncertainty – and aligned with the perpendicular axis, as predicted by my modelling results.

More specifically, in both experiments the inferred grid-pattern orientations clustered across subjects close to 30° from the reference axis. The effect was significant in both experiment 1 (N=26, circular V test for deviation from homogeneity perpendicular to the polarisation axis: V=6.68, p=0.032) and experiment 2 (N=24, circular V test: V = 5.95, p=0.043) (**Figure 6.5**).

6.4.4. Do hexadirectional BOLD signals genuinely indicate grid-pattern axes?

Preliminary experimental findings provide evidence supporting the inference of grid-pattern axes from the axes of BOLD modulation (Tobias Navarro Schröder, personal communication, March 2018). Magnetoencephalographic (MEG) recordings were made in human participants performing the same task in the arena from experiment 1. This revealed a hexadirectional modulation in a high-frequency band (60Hz – 120Hz) similar to the modulation of the BOLD signal, clustered on the same axes. Next, grid cell patterns were recorded by direct entorhinal electrophysiological recording in rats simultaneously with local field potential (LFP) recording. There was a hexadirectional modulation of LFP in the same frequency band as the MEG signal in humans, and the axes of this modulation matched the axes of the grid-patterns of the entorhinal cells. Thus, measuring brain oscillation modulation has allowed us to match grid-pattern axes to the axes of the BOLD signal modulation.

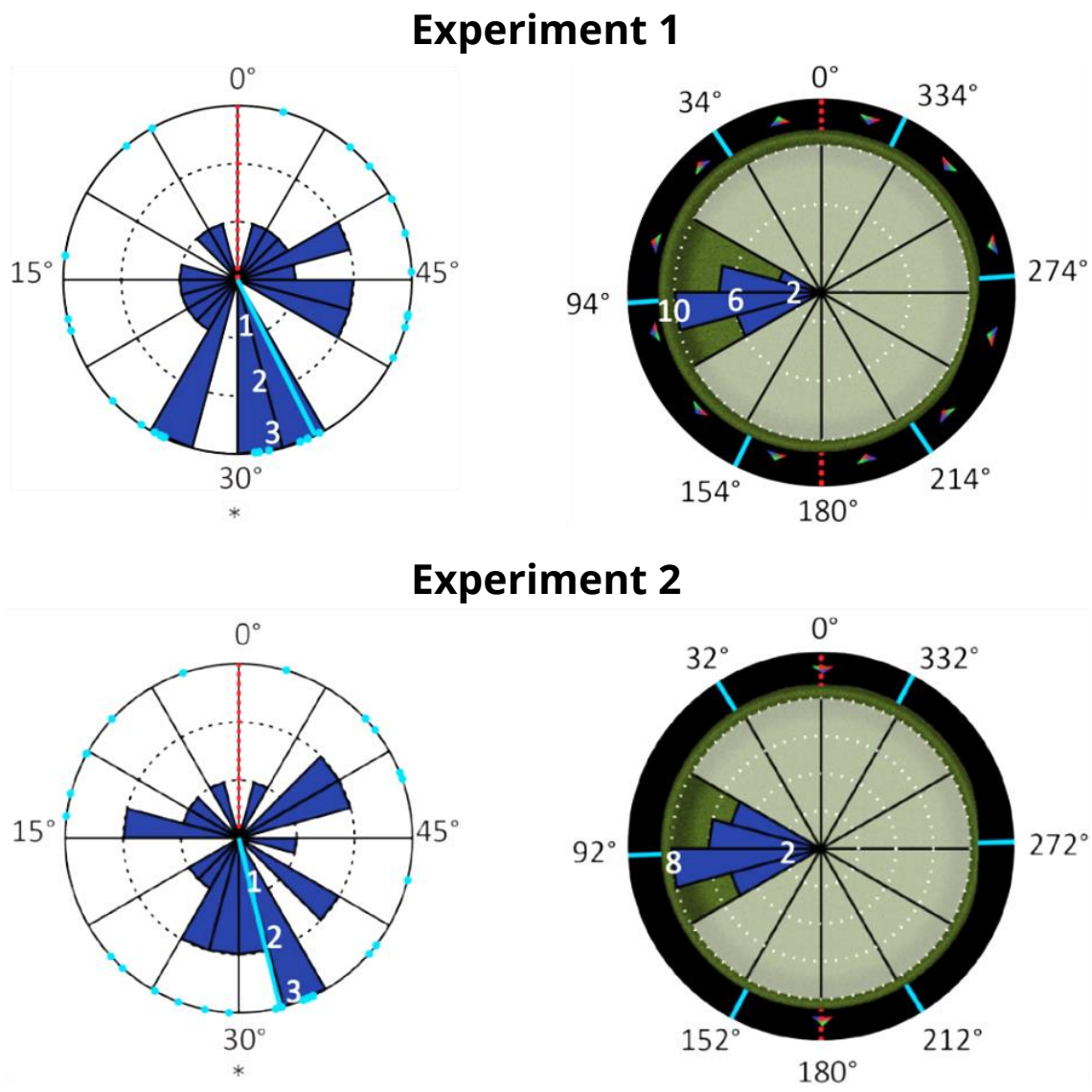

Figure 6.5 – Human grid-patterns in a polarised environment align away from the axis of greater spatial uncertainty

Inferred orientation of subjects' grid-patterns from experiments 1 (top) and 2 (bottom). On the left, grid-pattern orientations in 60°-space are indicated by light blue dots and clustering is demonstrated by the dark blue histogram. The mean orientations are indicated by the light blue lines (34° and 32° respectively). On the right, this is shown in 360°-space, illustrating that the grid-pattern tends to align orthogonal to the axis of greater spatial uncertainty.

6.5. Discussion

Using a biologically-inspired computational model, I have demonstrated that when spatial uncertainty is greater in one of a 2D environment's Cartesian axes than the other, errors in a grid cell system's self-location representation can be substantially mitigated by orienting the grid-pattern axes so that they are maximally misaligned (i.e. two of the three axes at 30°, one at 90°) from the environmental axis of greatest spatial uncertainty. My collaborators have tested this prediction and shown that in a polarised virtual environment where the availability of spatial information is anisotropic, the orientations of human subjects' grid-patterns, inferred via fMRI signal, indeed tend to misalign with the axis of greater spatial uncertainty.

6.5.1. Adoption of an adaptive orientation by the grid cell pattern in polarised environments

When an animal is introduced to a new environment, the firing patterns of its grid fields adopt a new orientation and phase relative to the environment – they do this coherently as an ensemble (Fyhn et al., 2007). This investigation shows that when this happens in an environment with polarised, anisotropic spatial information, the grid cell system must be able to orient adaptively relative to this polarisation – i.e. in a way that maximises the fidelity with which it is able to represent self-location. This raises some questions.

First, when does this happen? When an animal enters a new environment, grid cell patterns are established immediately (Hafting et al., 2005). At what point is the adaptive orientation set? The human study reported here did not assess for changes in orientation within a session, so this is a matter for future investigation. It might be set with the initial establishment of the grid-pattern. This would imply that the animal enters an environment with pre-existing knowledge about how environmental

features determine an optimal grid-pattern orientation and can evaluate the environment against this knowledge very rapidly. We might ask whether this knowledge is learned through an animal's life by experience of different environments, or if it is part of an innate, Kantian mental framework (Kant, 1787; Palmer & Lynch, 2010) embedded into the system by developmental processes independent of direct experience. And we might ask by what mechanisms the brain so rapidly assesses the polarisation of the environment in light of this knowledge, selects and imposes an orientation on the grid-patterns.

Alternatively, it might be the case that the very initial orientation of the grid-pattern upon entering a novel environment is more arbitrary, and only subsequently shifts to an adaptive configuration – much as other aspects of grid-pattern configuration shift with experience of an environment, including the contraction of initially-expanded grids (Barry, Ginzberg, et al., 2012) and homogenisation of initially fragmented grid-patterns in connected compartments (Carpenter et al., 2015). In this case we might ask whether the adaptive orientation is selected via some sort of experience-based, trial-and-error process, by assessment of the features of the environment, or some combination of the two – and then how this process is translated into shifting the orientation of the grid-pattern accordingly. In addition, if the grid-pattern orientation does change with experience, does this produce mismatches with the other components of the spatial representation and with learned associations between particular locations and behaviourally relevant features of the environment, how is this resolved, and until any process of resolution is complete, does it manifest in error-prone behaviour?

Second, what is the relation between the orientation of grid-patterns and the anchoring of head direction cells to the environment? At least within each brain area where they have been studied, head direction cells act as an ensemble – that is,

when an animal is moved between environments, the same relative angles between their preferred directions are maintained even as the orientation of the whole system anchors afresh to cues in the new environment, prompting the theory that ensembles of head direction cells are connected together in continuous ring attractor networks (Skaggs et al., 1994). It is as-yet unproven whether the head direction cells and the grid-pattern orientations across brain areas are also anchored together as an ensemble in this way, though in the entorhinal cortex deep layers, conjunctive cells spanning a continuum between "pure" grid-pattern tuning and "pure" head direction tuning do appear to maintain the same relative orientations as an ensemble (Sargolini et al., 2006). Thus the role of head direction cells in the adoption of adaptive grid-pattern orientation remains an open question. Simultaneous electrophysiological recording of grid and head direction cells while animals are introduced to novel, polarised environments could shed light on this issue.

6.5.2. Do all grid-patterns in an animal's entorhinal cortex share the same orientation?

In my *in silico* experiments, grid-pattern orientation was uniform both within and between modules. Is this assumption realistic?

In humans at least, the fact that the predicted hexadirectional modulation of the entorhinal fMRI signal has been detectable in this and multiple previous studies (Doeller et al., 2010; Kunz et al., 2015; Bellmund et al., 2016; Horner et al., 2016) suggests either that grid orientation is uniform, or least that one orientation predominates.

By comparison, a survey capturing the grid-patterns of large numbers of cells within individual animals revealed that variation in grid-pattern orientation between modules exceeded the variation within modules (Stensola et al., 2012). Another study showed that while pairs of simultaneously recorded modules tended to have similar

orientations (within 5°), a subset showed greater differences. These relative orientations remained stable as animals were transferred between environments (Krupic et al., 2015).

Three explanations for this apparent discrepancy are possible.

First, it is possible that there is no real discrepancy: humans' grid cell modules show a similar clustered distribution of orientations as those of rats, and the hexadirectional BOLD signal merely reflects a dominant, but not uniform, orientation. Non-invasive imaging techniques, even with finer spatial resolution, might be insufficient to shed light on this question, if human grid cell modules are as interspersed and overlapping as those of rats. Direct electrophysiological recordings from human grid cells across multiple modules could provide answers, but would be difficult to obtain in the numbers needed.

Second, humans and rats may simply differ, with human grid modules exhibiting more uniformity in orientation than those of rats.

Third, it is conceivable that grid modules' relative orientations can be varied adaptively, permitting them to align in certain circumstances (for instance, where this would maximise coding fidelity) – perhaps variation between grid modules is advantageous in some other circumstances.

To test the third hypothesis, further investigation of rats' grid module orientations in strongly polarised environments is warranted to explore whether inter-module variation in orientation disappears in such environments. There is preliminary evidence of this already. Comparison of the orientations of 62 modules across 41 rats reveals greater clustering in square environments than unpolarised circular environments (Krupic et al., 2015). Stensola et al. (2015) also observed strong clustering

of grid cell module orientations in a square environment. However, simultaneous recordings of multiple modules within the same animal, compared across different types of environment, would provide more conclusive evidence. Further investigation could also compare the results of such experiments to the results of modelling grid cell systems with uniform versus varying grid orientations in different environments, to assess how any observed variability or clustering affects fidelity.

Speculatively, the observable strength of the hexadirectional modulation of the BOLD signal in human entorhinal cortex could be determined by the degree of uniformity of the modules' orientations. If humans virtually navigating an unpolarised environment show a weaker modulation than in a polarised environment, that also would bolster this hypothesis.

If the third hypothesis is indeed correct, a further possibility arises. If adaptively orienting grid-patterns requires experience of many different environments in order to learn the relationships between environmental features and ideal orientations, it is possible that the adult human participants in the fMRI experiments have acquired that experience, while laboratory animals with comparatively limited experience of a small number of relatively small, simple environments are less likely to have done so. This is reflective of a limitation common to almost all studies of rodent spatially-tuned cells – the subjects are reared in environments that are unenriched compared to life in the wild, and experimental arenas are smaller and cue-poor compared to their natural habitats. Many questions in the field will not be conclusively resolved until these experimental limitations are overcome.

6.5.3. Grid-pattern orientation and boundaries

As discussed in the Introduction, in a familiar square environment the axis of the grid-pattern closest to parallel with one of the boundaries tends to be at an angle of

around 7.5°, attributed to a shear transformation that also makes the grid-pattern more elliptical (Krupic et al., 2015; Stensola et al., 2015; Julian et al., 2018), and (as would be expected) travelling close to a wall reduces grid cell self-location error more in the axis perpendicular to the wall (Hardcastle et al., 2015). Whether this orientation and distortion of the grid-pattern is adaptive given the anisotropy in spatial uncertainty near to boundaries is an obvious question that could extend the investigation reported here.

However, without further empirical information, experiments to explore this question would require making modelling assumptions that would be substantial enough to make the model very arbitrary. In particular, simulating spatial uncertainty becomes problematic.

First, a function would have to be specified to set how spatial uncertainty would vary with proximity to a boundary. This would entail an assumption about whether distance to boundary is related linearly to spatial uncertainty or by some more complex function. But the question is more complex still. So far in my investigations, even when the distribution from which erroneous inputs to the grid cell modules were drawn was anisotropic, the distribution in each axis was still described by a symmetrical Gaussian along any linear section. It would be reasonable, however, to assume that the effect of a boundary in reducing spatial uncertainty would not be symmetrical. Rather, when close to a boundary, the information available to an animal might curtail the probability distribution of possible locations more on the side of the animal facing toward the wall than the side facing away from it, with the function reaching zero at or before the wall – after all, the animal must at least know it is not inside the wall! (**Figure 6.6**) If so, modelling would have to make assumptions not only about the degree of anisotropy in the spatial uncertainty, but the asymmetry too.

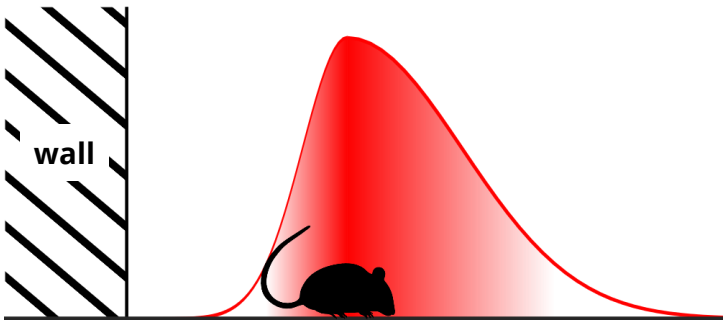

Figure 6.6 – Spatial uncertainty close to a boundary

When close to a boundary, it seems reasonable to speculate that the reduction of spatial uncertainty by the information available would be not only anisotropic but asymmetrical. This cartoon shows an example of a probability distribution (red curve and shading) reflecting how a rat might assess its possible locations close to a wall – on the side closer to the wall, the function drops to zero at or before the boundary, since the animal can at least be confident about which side of the wall it is on.

On the other hand, one could continue to model spatial uncertainty with symmetric Gaussian functions. However, in this case another question arises in the application of the model developed in this work: erroneous locations drawn to input to the grid cell modules from such distributions will, when close to a boundary, frequently fall outside the environment. In the experiments above, such inputs were either left as-is (i.e. the signal fed to the grid cell module indicated a position beyond the boundary) or corrected to the closest location at the edge of the environment before being fed to the grid cells. Another possible solution would be simply to draw replacement location from the distribution until one within the environment was obtained.

Making decisions on these issues in the construction of the model would require more detailed knowledge concerning what information derived from sensory information about boundaries reaches the grid cells and what processing (potentially including error detection) it has undergone upstream of the grid cells. Without such information, assumptions would be very arbitrary.

In the previous investigations, these factors did not have a major impact, since only in a few cases was the simulated location close enough to a boundary them it to be relevant. However, here, it is precisely the locations close to the boundaries that are of interest. Therefore, experimental work to establish a stronger basis for modelling assumptions will be needed before this approach would likely be able to conclusively resolve this question.

7. FURTHER DISCUSSION

This project aimed to investigate how the grid cell system encodes representations of location, and in particular how the configuration of the grid cell ensemble's firing patterns under different conditions contributes to the fidelity of the representation. In Chapter 3, I introduced a biologically-inspired modelling framework which could be used to test the representational fidelity of differently-configured grid cell systems and applied it to establish the separate contributions of errors of precision and of accuracy. In Chapter 4, I used the framework to test and confirm the prediction that the expansion of rodents' grid-pattern scale observed in novel environments (Barry, Ginzberg, et al., 2012) would mitigate the reduction of fidelity caused by spatial uncertainty. In Chapter 5 I applied it to investigate the relationship between a grid cell system's complement of grid-pattern scales and its capacity to represent location across large environments. In Chapter 6 I used it to predict how the orientation of grid-patterns could optimise encoding in an environment with anisotropic spatial uncertainty, and reported experiments by my collaborators indicating that humans virtually navigating such an environment exhibit the predicted optimal grid-pattern orientation. In addition, in Chapter 2 I reported a related project in which preliminary computational analyses indicate that when a rat pauses during locomotion, its grid cells may recapitulate activity they exhibited during movement – foreshadowing more recent work by other investigators illustrating replay in grid cell ensembles.

In this section I will briefly review each of these parts of the investigation and the outstanding areas for further investigation and consideration that they raise, before discussing the project as a whole.

7.1. Grid cells' activity at rest recapitulates the organisation of their activity during movement

Extensive work since the 1990s has revealed place cells participating in non-local representations: replaying sequences reflecting previously-travelled paths, and playing sequences that appear to reflect not-yet travelled paths. Roles in learning, memory, planning and imagination have been proposed for these phenomena. By analysing simultaneous electrophysiological recordings of mEC grid cells in rats running back and forth on a linear track, I demonstrated in Chapter 2 that cells whose spatial firing fields observed during locomotion were close together, also fired in close proximity during clustered spiking events in periods of relative immobility on the same track.

This was a preliminary indication that grid cells exhibit replay analogous to that found in place cells. I noted the difficulty of devising a test for the presence of the complex sequences in which multi-field cells would be expected to fire during an imagined trajectory without making a lot of assumptions about the features of the events being searched for, and argued that one thing needed would be simultaneous recordings of larger numbers of cells, ideally in concert with recordings of place cells and/or SWRs.

Replay in grid cells was subsequently observed by other researchers in experiments that my findings foreshadowed. Their findings indicate that grid cells in the mEC deep layers replay at rest in coordination with hippocampal place cells, while mEC superficial layer grid cells replay during task performance independently of place cells, suggesting a model in which hippocampal-initiated replay, transmitted to the mEC deep layers, is involved in memory consolidation, while independent replay in mEC superficial layers may be more relevant to planning navigation (Ólafsdóttir et al., 2016, 2017; O'Neill et al., 2017). This model, and the claim that deep layer grid

cell replay is coordinated with hippocampal place cell replay, are contested (Trimper et al., 2017), indicating a need for further work.

Of note here is the progressive development of probes allowing simultaneous electrophysiological recording of increasing numbers of cells (Csicsvari et al., 2003; Jun et al., 2017; Chung et al., 2018), and the development of chronic fluorescence microscopy techniques that allow activity to be visualised across large cell ensembles in rodents navigating virtual reality environments (Dombeck et al., 2010; Heys et al., 2014) or even freely moving in real environments (Ghosh et al., 2011), with temporal resolution sufficient to detect hippocampal replay (Malvache et al., 2016). These techniques promise to enable much fuller understanding of non-local spatial representations as phenomena involving coordinated activity across large ensembles of cells.

Also relevant are the refinements and extensions of animal virtual reality techniques, leading to the recent demonstration of place, grid and head direction cell recordings in animals freely navigating a 2D virtual environment rather than the constrained linear tracks so far common in VR studies (Chen et al., 2018), along with the aforementioned techniques for cell-level functional imaging in freely-moving animals. The studies demonstrating grid cell replay so far have been limited to behaviour in very constrained environments – linear tracks and T-maze tasks. Investigators might seek evidence of grid cell participation in 2D navigational planning in VR or the real world, using tasks such as variants of the Morris water maze, the Morris group's "event arena" for what-where paired associate learning (Day et al., 2003) or the O'Keefe group's Honeycomb maze (Wood et al., 2018).

Thus, the field is open for a wide range of possible experiments assessing the role of mEC grid cells in equivalents of all the different types and contexts of non-local place cell firing reviewed in the Introduction.

7.2. A modelling framework for assessing the adaptiveness of grid cell code configurations

The various parameters defining the repeating triangular firing pattern of a grid cell, and the assembly of cells with different such patterns in modules in the mEC, allows for many different configurations that affect how location is encoded by the grid cell system. I have built on an existing modelling framework (Mathis et al., 2012) to develop a framework in which the fidelity of position coding with different configurations can be assessed under different conditions, and applied it to a number of questions.

7.2.1. Trade-offs between precision and accuracy

In Chapter 3, I demonstrated the role of two different types of error: those of *precision*, which are small relative to the grid-pattern scale, clustered close to the true location, and those of *accuracy/ambiguity*, which are larger, resulting in decoding to entirely the wrong part of the environment.

I showed that in the absence of spatial uncertainty and when a grid cell system included a sufficient number of cells to compensate for each others' intrinsic noisiness, the probability of ambiguity errors became negligible and grid codes with smaller scales (whether geometrically progressing scales with a smaller ratio, or random sets of grid scales which happened to have more small scales) experienced smaller precision errors, since they could represent space more finely.

When the number of cells in the system was low enough for accuracy errors to arise, unlike precision errors their magnitude of course scales with the size of the environment. Thus in an environment significantly larger than the smallest grid-pattern scale, they can become orders of magnitude larger than the precision errors. This form of error was, as expected, rife in configurations whose modules had

commensurate grid-pattern scales (i.e. with a geometric ratio of 2, or to a lesser extent √2 since in this scheme alternate scales are commensurate) since, even when intrinsic noise is eliminated, such a "nested" code cannot uniquely represent locations across distances greater than its largest scale.

7.2.2. Grid scale expansion mitigates error when spatial uncertainty increases

Experimental observations in rats have shown that grid cells' firing patterns expand in scale when placed in a novel environment, and gradually contract back to their previous scale with experience of the environment (Barry, Ginzberg, et al., 2012). In Chapter 4, I applied my modelling framework to test the hypothesis that this might be an adaptation to improve fidelity of coding in conditions of spatial uncertainty.

By testing grid cell systems with different degrees of scale expansion under varying levels of spatial uncertainty, I showed that such uncertainty increases errors in self-location representations, and expansion of the grid scale can partially mitigate this effect. For each level of uncertainty, a particular optimal degree of expansion was identifiable, and the relationship between the two appeared linear. This did not rule out other hypotheses about the effect of expansion in novel environments and I noted that they were not mutually exclusive.

The clear next step in this line of investigation will be experimental work asking whether grid scale expands in response to other causes of spatial uncertainty, such as a lack of cues or unreliable landmarks. I noted preliminary evidence that it does – grid scale expands in a 2D VR environment compared to reality (Chen et al., 2018) – and a potential effect of cue richness which was obscured by multiple interacting effects of novelty (Manson, 2017). Further investigation is clearly warranted, and could take advantage of the virtual reality techniques that would now enable precise manipulation of cue richness and reliability in a 2D environment.

There is a clear candidate mechanism for grid scale expansion. Grid scale is influenced by the I_h current dependent on HCN1 channels (Giocomo et al., 2011; Mallory et al., 2018). Cholinergic manipulations modulate this current in layer II mEC stellate cells, and acetylcholine release is known to be associated with novelty. Alternatively, cAMP upregulation also modulates this current in the same cells, and cAMP might in turn be modulated by another neuromodulator noradrenaline (Barry, Heys, et al., 2012; Heys & Hasselmo, 2012).

A more generalised model proposes acetylcholine as a signal for expected uncertainty (due to known unreliability of cues) and noradrenaline as a signal for unexpected uncertainty (due e.g. to a new context) (Yu & Dayan, 2005). I noted that both types of uncertainty, and thus both neuromodulators, may be relevant in a novel environment. Possible experiments to tease out the effects of these neuromodulators on grid cell coding could compare behaviour (perhaps learning of a spatial task) in novel environments, and in familiar environments with varying cue reliability, with and without acute mEC-localised infusions of competitive antagonists blocking the effects of acetylcholine or noradrenaline on grid scale.

7.2.3. A complicated relationship between grid scale configuration and spatial capacity

The field has seen various contributions debating the relationship between the configuration of grid-pattern scales across the modules present in an animal, and the capacity of the grid cell system to uniquely encode locations across large environments. I investigated this question in Chapter 5.

Fiete and colleagues have shown that in an idealised system, a modular arithmetic (MA) code can represent locations up to the lowest common multiple (LCM) of the grid scales – this would make a coprime sequences of scales optimal. They argue that a more realistic system, in which capacity is reached when the environment is

large enough to encompass locations at which the sets of grid module phases are so similar they cannot be reliably distinguished, could still have a capacity many times greater than the largest scale (Fiete et al., 2008).

On the other hand, the research groups of Andreas Herz and Vijay Balasubramanian model the grid cell system as providing a "nested" representation limited in capacity to the largest grid scale present (Mathis et al., 2012; Stemmler et al., 2015; Wei et al., 2015). Using different approaches, they predict geometric sequences of grid scales, defined by ratios of ~1.5 (Stemmler et al., 2015) or – depending on the read-out mechanism – either √e (~1.65) or ~1.44 (Wei et al., 2015).

Finally, a recent contribution defending the MA code hypothesis (Vágó & Ujfalussy, 2018) predicted that with a very small number of grid cell modules, the relationship between scale ratio and capacity is sharply irregular so that even very small deviations in scale can result in dramatic changes in capacity. This would make optimisation of the ratio biologically implausible given the experimentally observed variation in scales (Barry, Ginzberg, et al., 2012; Stensola et al., 2012; Krupic et al., 2015). And in systems with more modules, the influence of ratio on capacity becomes weak, making optimisation marginal or unnecessary.

I applied my modelling framework to investigate this problem. Like Fiete and colleagues, I showed that capacity failures relate to points where the environment is large enough to encompass distances across which the set of grid module phases signalling location are not reliably distinguished. However, unlike previous studies, my approach emphasised that error in the system increases incrementally with increasing environment size, as more sets of locations with similar grid phase signals are encompassed. On the premise that biological systems may be expected to tolerate some degree of errors, I have rejected the "all or nothing" approach of previous investigators who have taken capacity to be the largest range over which the

system can encode location without any ambiguity errors, in favour of assessing varying degrees of accuracy and precision in fallible coding systems.

With this approach I corroborated the prediction by Vágó & Ujfalussy (2018) relating to systems with small numbers of grid cell modules. In such systems, the variation of error with ratio was sharply irregular and non-monotonic. However, my investigation challenged their prediction that the relationship becomes weak in systems with larger numbers of modules – in environments large enough for the increased capacity of such systems to be tested, the same sharp irregularity was observed. This disagreement may be due to the aforementioned differing approach to the question of capacity. However, we agree that optimisation of the ratio between grid scales to maximise capacity is unlikely.

My approach here does prompt the question – what magnitude and frequency of error is tolerable? Here, an arbitrary measure (mean square error) is used, and no threshold is specified – both of these things would be needed to actually estimate the specific capacities of different configurations. Determining these would require a more in-depth knowledge of the downstream read-out systems and the behavioural requirements of the animal.

While corroborating analyses that capacity could in theory far outstrip the largest grid scale, my investigation did not resolve the question of whether it does so biologically. The tolerable level of error may be low enough, and the degree of noise and uncertainty high enough, that the capacity is indeed constrained to roughly the largest grid scale present.

However, as I have discussed, part of this debate relates to estimates of rats' natural behavioural range. Advocates of the "nested code" hypothesis have relied upon an old study based in urban areas which estimated a home range as small as ~$(10\ m)^2$

(Davis et al., 1948). More recent research including more open environments has suggested ranges of $(100m)^2$ to $(1km)^2$ (Recht, 1988; Russell et al., 2005), which could much less plausibly be covered by a single grid-pattern period. I have argued that there is a need in the field to try to characterise grid cell activity in rats navigating larger, natural-sized environments. Key questions would include: is the grid cell representation continuous across environments of this size or splintered into "neighbourhoods" (indeed – is the characteristic pattern observed in laboratory animals raised in stereotyped, limited environments even the same in natural or naturalistic environments, or in animals raised in such environments?), and connected to that, is the animal capable of planning novel trajectories for vector navigation (presumed to rely on a continuous grid cell system representation) across such distances?

7.2.4. Grid-patterns orient adaptively in polarised environments

In Chapter 6, I used the framework to show that when spatial uncertainty is modelled as anisotropic, error can be substantially reduced by orienting the grid-pattern axes so that they are maximally misaligned from the environmental axis of greater uncertainty. I then reported experiments conducted by my collaborators, which took advantage of the ability to infer grid-pattern orientation in human from fMRI data to confirm that subjects' grid-patterns do indeed exhibit such an orientation. I explored a number of questions raised by this finding, which I will briefly review here.

First, how rapidly is this adaptive orientation adopted – immediately upon entering the environment or after a period of time spent in the environment? If the former, what features of the environment are used to make the necessary assessment, and are these criteria learned or a "hard-coded" product of development? And if the latter, again on what features of the environment is the decision based, or is it a trial-and-error process, and what are the consequences of this shifting representation for mismatches with other components of the spatial code? With enough data,

it should be possible to test whether grid cell fields shift during the initial minutes of experience in an environment in a way that reflects rotation of the pattern. The relation of this process to head direction cells and their anchoring to a novel environment is also open to investigation, which would be aided by simultaneous recordings of both cell types.

My experiments made the assumption that grid-pattern orientation was uniform between modules, not just within them. I discussed evidence of a limited degree of variation in orientation across modules (Stensola et al., 2012; Krupic et al., 2015), while the reproducibility of the hexadirectional modulation of the mEC fMRI signal in humans (Doeller et al., 2010; Kunz et al., 2015; Bellmund et al., 2016; Horner et al., 2016) suggests either uniformity or at least the predominance of one orientation. I discussed possible explanations: that humans' grid cell modules show the same variation but the predominance of a single orientation is sufficient to produce the observable hexadirectional modulation; or that rats and humans differ; or that the relative orientations of grid modules' patterns might be adaptively variable for different situations with different coding demands (much like grid scale appears to be adaptively variable for the different demands of familiar and novel environments). I assessed preliminary evidence in favour of the last of these hypotheses (Krupic et al., 2015; Stensola et al., 2015). I also speculated that adaptive flexibility in the orientation of grid-patterns could be the result of extensive life-time experience of diverse and rich environments, and thus might be more limited or absent in most laboratory animals. Future experiments could include modelling different combinations of grid-pattern orientations across modules; assessing grid-pattern orientation in rats in environments with strongly polarised spatial information; assessing the strength of the signature hexadirectional modulation in human entorhinal cortex while navigating polarised vs unpolarised environments, and as mentioned in the previous section, experiments in rats exposed to richer, natural or naturalistic environments.

Finally, I also discussed the possibility of investigating whether the observed 7.5° orientation of grid-patterns to boundary in square enclosures (Krupic et al., 2015; Stensola et al., 2015; Julian et al., 2018) is an adaptive response to the anisotropic spatial information received when an animal moves close to a boundary. I argued that to apply the modelling framework set out here would require an array of assumptions that would have a strong impact on results but for which empirical evidence is lacking.

7.2.5. Some aspects of the grid cell code configuration appear to be adaptive to the changing demands of the environment

In sum, I have established a biologically inspired modelling framework and used it to show that experimentally observed variation in some aspects of the grid code configuration – namely scale expansion and pattern orientation – appear to be adaptive for maximising the fidelity of self-location representations under particular conditions – the uncertainty of novel environments, and the anisotropic information available in polarised environments, respectively. In the case of the former, at least one hypothesised candidate mechanism for this adaptation exists, while the latter finding raises open questions about mechanism. I have also used the modelling framework to contribute to the debate around the spatial capacity of differently configured grid cell systems, emphasising that capacity limits should be considered in terms of tolerable degrees of error and the incremental deterioration of fidelity in environments of increasing size, and showing that the sharply irregular, discontinuous dependence of that fidelity on grid scale ratios in large environments makes optimisation of the ratio for capacity implausible.

Thus, certain features of the grid cell system appear to possess some surprising adaptive flexibility. However, not everything is easily optimised. My findings point to a wide array of possible further *in vivo* experiments, and the modelling framework

set out could be developed to address a range of other questions, some of which will be discussed later in this chapter.

7.2.6. Evolution and Panglossian pitfalls

The substantial majority of this investigation has focussed on asking whether certain features of the grid cell code configuration are adaptive, or adaptively flexible, for high-fidelity representation of self-location. In those cases where I have found evidence that such features are indeed adaptive, it might be tempting to conclude that I have uncovered an evolutionary *cause* – to reason that these features therefore arose due to selection pressures to maximise coding fidelity in the relevant types of environment. Indeed, the quality of spatial representations and thus of the behavioural choices they inform is of clear importance to an animal's ability to survive to reproduce.

However, Gould & Lewontin (1979) rightly warned against the construction of speculative "just-so" stories that conflate evidence for the current utility of a trait, considered in isolation from the organism as a whole, with evidence for the cause of its origin. It is important to remember that an adaptive trait may have arisen as a by-product of other evolutionary pressures or developmental constraints. More evidence than simply the suitability of a trait for a particular purpose is required to reliably infer its evolutionary history. In the case of the grid cell code, two particular areas of investigation could yield somewhat stronger evidence with which to test such hypotheses.

The first is comparative studies of the grid cell system in different animals with different behavioural needs. If different configurations, or different capacities for flexibility of configuration, are present in different clades, then a history of the development of those configurations can be hypothesised.

The second is further exploration of the dual role of the grid cell system in encoding spatial and non-spatial information (discussed in the Introduction). The discovery and initial exploration of the grid cell system was in the spatial context, with non-spatial roles being discovered comparatively recently. However, this alone does not mean that the spatial role is necessarily primary, either historically or functionally – that is the subject of some discussion (debated in Lisman et al., 2017). The particular origin of the grid cell system would have imposed particular pressures, selecting for certain traits and features and (due to the complex developmental processes of biological systems) these could have substantially constrained the possible subsequent evolutionary changes if the system was later applied to different contexts.

7.3. Limitations and opportunities for this modelling framework

As a model, the framework presented here for investigation of the grid cell system is necessarily simplified. Below, I will discuss the simplifications and limitations of the model, as well as possible extensions to it.

7.3.1. Measuring coding fidelity

As discussed in Chapter 3, following Mathis et al. (2012), I used mean square error as a measure of the fidelity of the grid cell system's coding. This is a common measure but an arbitrary one, and other measures would give differing weights to large vs small errors (e.g. mean absolute error would be less strongly affected by infrequent large values). In the context of exploring the adaptiveness of grid cell system configurations, the measure used would ideally reflect more detailed knowledge about the behavioural needs of the animal and the impact of different frequencies and magnitudes of error than is currently available. However, experiments comparing which configurations minimise different measurements could be used to draw conclusions about configurations would better serve different behavioural needs.

7.3.2. Idealised decoding

Again following Mathis et al. (2012), the models used here included an optimal decoding method: this term refers to methods that, by some measure, extract the maximum information possible from a signal to infer the stimulus value. The particular method used was maximum-likelihood (ML) inference. This is not unreasonable: it has been shown that at least one biologically plausible read-out mechanism could come close to this level of performance (Stemmler et al., 2015). However, not only are biological systems still imperfect and subject to noise, it would also be wrong to make the Panglossian assumption that the actual read-out systems present in the animal are necessarily as good as the best plausible ones we can imagine.

Three categories of elaboration on the framework I have built could be fruitful:

7.3.2.1. Bayesian inference: an alternative optimal decoding method

As discussed in Chapter 3, Bayesian inference is an alternative form of optimal decoding, in which a "loss function" describes the expected cost to the organism of estimating $x_{estimate}$ when the true stimulus value is x_{actual}, and a function is found that minimises the average result of the loss function across possible outcomes (Dayan & Abbott, 2001). As argued in that chapter, and similarly to the issues discussed immediately above relating to the selection of an error measurement, this was not used because without more detailed knowledge of the behavioural needs of the animal, selecting a loss function would mean including an additional layer of weakly-justified assumptions to the model. However, it would become a possible option with more experimentally-obtained knowledge.

7.3.2.2. Decoding a path rather than individual locations

In the model set out here, a large number of locations are randomly selected, encoded and decoded independently of one another. In reality, an animal continuously

assessing its location as it navigates an environment would be able to use recent estimates to constrain new estimates, on the basis that it can only travel at limited speeds and cannot teleport. Thus, a decoded output of the grid cell ensemble could be compared with recent self-location estimates, and ruled out as erroneous if too distant. This is facilitated by the fact that with a modular arithmetic code, a small change in the grid-pattern phase read from one module can result in a large change in the location represented by the ensemble. This facility for error correction in the grid cell code has been proposed previously (Fiete et al., 2008; Sreenivasan & Fiete, 2011). It could be implemented by reference to a slower-changing representation of position, potentially the hippocampal place cells (Sreenivasan & Fiete, 2011), or by calculating the vector displacement between successive position estimates in the same ways as theoretically proposed for vector navigation (Kubie et al., 2009; Bush et al., 2015).

A straightforward development of the modelling framework presented in this project could be made in order to model this hypothesised feature of the biological system. Rather than individual independently-generated random locations, the input to the model would be positions on a continuous path through the environment – potentially actual paths recorded experimentally. A simple amendment to the ML inference decoding mechanism would then use this information – the probability density function from which the model estimates the location is simply multiplied by a Gaussian distribution centred on the previous location estimate, which plays the role of a Bayesian prior (not to be confused with Bayesian inference decoding, explained above). Such a decoding mechanism has been used in previous models (Brown et al., 1998).

7.3.2.3. Biologically inspired read-out mechanisms

Finally, rather than an abstractly mathematical decoding algorithm, this model of grid cell activity could be connected to similarly biologically inspired models of downstream systems – or upstream systems, or indeed, systems that are both, since the hippocampal formation circuitry includes various loops. Studying how differently-configured grid cell systems interact with other spatially-tuned cells, and comparing the results to simultaneous recordings of these cell types in vivo, could provide evidence supporting or ruling out different hypothetical configurations of the system.

Combined models like this could also be used to investigate what grid-pattern distortions are realistically possible without disrupting downstream read-out. As mentioned previously, as long as distortions are common to all grid cells within a module, the code can still act as a universal metric in theory (Stemmler et al., 2015) but we do not yet know how far this theoretical possibility is borne out in biological reality. The capacity of different hypothesised read-out mechanisms to account for distortions with minimal error could be compared *in silico*. Evidence of distortions such as shear or warping of the repeating pattern has already been reviewed. A further distortion that could be investigated is the observed heterogeneity of firing rates between spatial fields within individual cells' grid-patterns (Ismakov et al., 2017). A number of hypotheses have been put forward concerning the local information that is thus overlaid on top of the regular grid code. First, it could be merely epiphenomenal, a result of uneven feedback from place cells. Second, it might originate from this but have been co-opted to serve a purpose like contributing to pattern separation. Third, the relationship might be the other way around, with grid cell heterogeneity helping to drive the specificity of place cells. Finally, the relationship might be less hierarchical, with an important role for information exchange in both directions. A combined model including both grid and

place cells could explore these hypothesised interactions and the implications for the fidelity of the representation in each.

7.3.3. Non-uniform allocation of grid cells to modules

Thus far, each modelled module in the grid cell system has contained the same number of cells. However, observations suggest that there may be fewer cells in larger-scale modules (Stensola et al., 2012) – though this could be due to difficulty identifying them in environments of limited size. A grid cell modelling approach in which self-location was decoded dynamically (using the spike information available not just at each step in a path, but from recent steps too) predicted that an efficient allocation of grid cells would result in a geometric trend of decreasing cell numbers for modules with increasing grid-pattern scale (Mosheiff et al., 2017). This makes sense, as the signal from a larger-scale module would change less for a particular displacement in space. This predicted allocation of cells to modules could be tested in the modelling framework I have presented and fidelity compared to that with uniform allocation.

7.3.4. Multi-dimensional stimuli

In Chapter 4, I demonstrated that extending the model from one- to two-dimensional space was simple. In fact, though the simulations would be computationally burdensome, given sufficient resources it can be extended just as straightforwardly to any number of dimensions.

Exploration of the activity of spatial cells during three-dimensional navigation in flying animals (bats), as well as terrestrially-bound ones, is advancing (reviewed by Jeffery et al., 2015). This could allow observations of the configuration of grid cell firing patterns in 3D space to be modelled and assessed in terms of their

implications for the fidelity of self-location representations, in the same way as the different experiments in this project did.

7.4. Non-spatial mapping and grid cell code configuration

Recent evidence has indicated that grid cells also encode “maps” of non-spatial stimuli in rodents and humans (Constantinescu et al., 2016; Aronov et al., 2017; Garvert et al., 2017). It would be worthwhile to investigate whether the predictions made from the modelling experiments reported here hold true for non-spatial representations too. For instance, does the grid-pattern expand in scale when introduced to a new stimulus parameter space, and do they orient in a particular way when more information is available in one dimension than another?

As mentioned above, extending this modelling framework to any number of dimensions is procedurally trivial (albeit computationally burdensome), so it would be applicable even if the grid cell system is discovered to be capable of encoding non-spatial stimulus maps in more than two or three dimensions.

7.5. Conclusion

Spatial cognition has long been recognised as a key area of investigation for behavioural neuroscience. It offers the opportunity of studying, at cell- and circuit-levels, representations of abstract concepts which must be derived from advanced processing of sensory information across multiple modalities, but which can nevertheless be correlated to real world stimuli that can be easily, reliably and quantitatively measured. Thus the study of spatial cognition may be an accessible avenue to potentially generalisable principles about how the brain represents and processes complex, composite information for behaviour. This has become even more true with two discoveries: first, non-local activity of spatially-tuned cells, which

might play roles in learning, memory, planning and imagination; and second, the participation of grid cells in mapping non-spatial information.

This project aimed to examine how the particular configuration of the grid cell ensemble determines how, and with what fidelity, this information is represented, and how different configurations may be adaptive for fidelity given different environmental conditions. I have presented a flexible, biologically inspired modelling framework that permits study of such questions especially in relation to degrees of uncertainty in the spatial information available to an animal, and I have used it to both test and make hypotheses about experimentally measurable aspects of the grid cell system configuration.

By comparing predictions derived from simulations to experimental findings in rodents and humans, I have shown that the configuration of the grid cell code appears to be flexible in ways that improve the fidelity of coding in at least two different circumstances: novel environments and environments in which spatial information is polarised and anisotropic. I have also developed an argument that the spatial capacity of the code needs to be considered from the perspective of what degree of error is tolerable given the behavioural needs of the animal, and confirmed that optimisation of the ratio between grid scales (which has been the subject of various theoretical proposals by other researchers) is not biologically plausible, providing a warning against theoretical approaches that risk inculcating an assumption of optimality in biological systems. Finally, I have proposed a wide range of avenues for future investigation that are raised by my findings and by the development of this modelling framework.

8. REFERENCES

Amaral, D. & Lavenex, P. (2006) 'Hippocampal Neuroanatomy', in Andersen, P. et al. (eds) *The Hippocampus Book*. New York, NY, USA: Oxford University Press, pp. 37–114. doi: 10.1093/acprof:oso/9780195100273.003.0003.

Andersen, P., Bliss, T. V. P. & Skrede, K. K. (1971) 'Lamellar organization of hippocampal excitatory pathways', *Experimental Brain Research*, 13(2), pp. 222–38. doi: 10.1007/BF00234087.

Aronov, D., Nevers, R. & Tank, D. W. (2017) 'Mapping of a non-spatial dimension by the hippocampal–entorhinal circuit', *Nature*, 543(7647), pp. 719–722. doi: 10.1038/nature21692.

Barry, C., Lever, C., Hayman, R., Hartley, T., Burton, S., O'Keefe, J., Jeffery, K. & Burgess, N. (2006) 'The Boundary Vector Cell Model of Place Cell Firing and Spatial Memory', *Reviews in the Neurosciences*, 17(1–2), pp. 71–97. doi: 10.1515/REVNEURO.2006.17.1-2.71.

Barry, C., Hayman, R., Burgess, N. & Jeffery, K. J. (2007) 'Experience-dependent rescaling of entorhinal grids', *Nature Neuroscience*, 10(6), pp. 682–684. doi: 10.1038/nn1905.

Barry, C., Ginzberg, L. L., O'Keefe, J. M. & Burgess, N. (2012) 'Grid cell firing patterns signal environmental novelty by expansion.', *Proceedings of the National Academy of Sciences of the United States of America*, 109(43), pp. 17687–92. doi: 10.1073/pnas.1209918109.

Barry, C. & Bush, D. (2012) 'From A to Z: a potential role for grid cells in spatial navigation', *Neural Systems & Circuits*, 2(1), p. 6. doi: 10.1186/2042-1001-2-6.

Barry, C., Heys, J. G. & Hasselmo, M. E. (2012) 'Possible role of acetylcholine in regulating spatial novelty effects on theta rhythm and grid cells', *Frontiers in Neural Circuits*, 6(February), p. 5. doi: 10.3389/fncir.2012.00005.

Bellmund, J. L. S., Deuker, L., Navarro Schröder, T. & Doeller, C. F. (2016) 'Grid-cell representations in mental simulation', *eLife*, 5(AUGUST), pp. 1–33. doi: 10.7554/eLife.17089.

Bethge, M., Rotermund, D. & Pawelzik, K. (2002) 'Optimal short-term population coding: when Fisher information fails.', *Neural computation*, 14(10), pp. 2317–2351. doi: 10.1162/08997660260293247.

Boccara, C. N., Sargolini, F., Thoresen, V. H., Solstad, T., Witter, M. P., Moser, E. I. & Moser, M.-B. (2010) 'Grid cells in pre- and parasubiculum.', *Nature Neuroscience*, 13(8), pp. 987–994. doi: 10.1038/nn.2602.

Bonnevie, T., Dunn, B., Fyhn, M., Hafting, T., Derdikman, D., Kubie, J. L., Roudi, Y., Moser, E. I. & Moser, M.-B. (2013) 'Grid cells require excitatory drive from the hippocampus.', *Nature neuroscience*, 16(3), pp. 309–17. doi: 10.1038/nn.3311.

Bostock, E., Muller, R. U. & Kubie, J. L. (1991) 'Experience-dependent modifications of hippocampal place cell firing', *Hippocampus*, 1(2), pp. 193–205. doi: 10.1002/hipo.450010207.

Brown, E. N., Frank, L. M., Tang, D., Quirk, M. C. & Wilson, M. A. (1998) 'A statistical paradigm for neural spike train decoding applied to position prediction from ensemble firing patterns of rat hippocampal place cells.', *Journal of Neuroscience*, 18(18), pp. 7411–25. Available at: http://www.jneurosci.org/content/18/18/7411 (Accessed: 25 March 2018).

Brun, V. H., Solstad, T., Kjelstrup, K. B., Fyhn, M., Witter, M. P., Moser, E. I. & Moser, M.-B. (2008) 'Progressive increase in grid scale from dorsal to ventral medial entorhinal cortex', *Hippocampus*, 18(12), pp. 1200–1212. doi: 10.1002/hipo.20504.

Burgess, N. (2008) 'Grid cells and theta as oscillatory interference: Theory and predictions', *Hippocampus*, 18(12), pp. 1157–1174. doi: 10.1002/hipo.20518.

Burgess, N., Barry, C. & O'Keefe, J. (2007) 'An oscillatory interference model of grid cell firing', *Hippocampus*, 17(9), pp. 801–812. doi: 10.1002/hipo.20327.

Bush, D., Barry, C., Manson, D. & Burgess, N. (2015) 'Using Grid Cells for Navigation', *Neuron*, 87(3), pp. 507–520. doi: 10.1016/j.neuron.2015.07.006.

Bush, D., Barry, C. & Burgess, N. (2014) 'What do grid cells contribute to place cell firing?', *Trends in Neurosciences*, 37(3), pp. 136–145. doi: 10.1016/j.tins.2013.12.003.

Buzsáki, G. (1989) 'Two-stage model of memory trace formation: A role for "noisy" brain states', *Neuroscience*, 31(3), pp. 551–570. doi: 10.1016/0306-4522(89)90423-5.

Buzsáki, G. (2002) 'Theta oscillations in the hippocampus', *Neuron*, 33(3), pp. 325–340. doi: 10.1016/S0896-6273(02)00586-X.

Byrne, P., Becker, S. & Burgess, N. (2007) 'Remembering the past and imagining the future: A neural model of spatial memory and imagery.', *Psychological Review*, 114(2), pp. 340–375. doi: 10.1037/0033-295X.114.2.340.

Carpenter, F., Manson, D., Jeffery, K., Burgess, N. & Barry, C. (2015) 'Grid Cells Form a Global Representation of Connected Environments', *Current Biology*, 25(9), pp. 1176–1182. doi: 10.1016/j.cub.2015.02.037.

Carpenter, F. & Barry, C. (2016) 'Distorted Grids as a Spatial Label and Metric', *Trends in Cognitive Sciences*, 20(3), pp. 164–167. doi: 10.1016/j.tics.2015.12.004.

Carpenter, F., Burgess, N. & Barry, C. (2017) 'Modulating medial septal cholinergic activity reduces medial entorhinal theta frequency without affecting speed or grid coding', *Scientific Reports*, 7(1). doi: 10.1038/s41598-017-15100-6.

Carr, M. F., Jadhav, S. P. & Frank, L. M. (2011) 'Hippocampal replay in the awake state: a potential substrate for memory consolidation and retrieval', *Nature Neuroscience*, 14(2), pp. 147–153. doi: 10.1038/nn.2732.

Cashin-Garbutt, A. (2017) *Professor Loren Frank gives scintillating talk on neural substrates of memories and decisions*. Available at: http://www.ucl.ac.uk/swc/sainsbury-wt-news-pub/professor-loren-frank-gives-scintillating-talk-on-neural-substrates-of-memories-and-decisions (Accessed: 13 February 2018).

Chen, G., King, J. A., Lu, Y., Cacucci, F. & Burgess, N. (2018) 'Spatial cell firing during virtual navigation of 2 open arenas by head-restrained mice', *bioRxiv*. doi: 10.1101/246744.

Chen, L. L., Lin, L. H., Green, E. J., Barnes, C. A. & McNaughton, B. L. (1994) 'Head-direction cells in the rat posterior cortex - I. anatomical distribution and behavioral modulation', *Experimental Brain Research*, 101(1), pp. 8–23. doi: 10.1007/BF00243212.

Chung, J. E. et al. (2018) 'High-density, long-lasting, and multi-region electrophysiological recordings using polymer electrode arrays', *bioRxiv*. doi: 10.1101/242693.

Constantinescu, A. O., O'Reilly, J. X. & Behrens, T. E. J. (2016) 'Organizing conceptual knowledge in humans with a gridlike code.', *Science*, 352(6292), pp. 1464–8. doi: 10.1126/science.aaf0941.

Csicsvari, J., Henze, D. A., Jamieson, B., Harris, K. D., Sirota, A., Barthó, P., Wise, K. D. & Buzsáki, G. (2003) 'Massively Parallel Recording of Unit and Local Field Potentials With Silicon-Based Electrodes', *Journal of Neurophysiology*, 90(2), pp. 1314–1323. doi: 10.1152/jn.00116.2003.

Csicsvari, J., O'Neill, J., Allen, K. & Senior, T. (2007) 'Place-selective firing contributes to the reverse-order reactivation of CA1 pyramidal cells during sharp waves in open-field exploration', *European Journal of Neuroscience*, 26(3), pp. 704–716. doi: 10.1111/j.1460-9568.2007.05684.x.

Davidson, T. J., Kloosterman, F. & Wilson, M. A. (2009) 'Hippocampal Replay of Extended Experience', *Neuron*, 63(4), pp. 497–507. doi: 10.1016/j.neuron.2009.07.027.

Davis, D. E., Emlen, J. T. & Stokes, A. W. (1948) 'Studies on Home Range in the Brown Rat', *Journal of Mammalogy*, 29(3), pp. 207–225. doi: 10.2307/1375387.

Day, M., Langston, R. & Morris, R. G. M. (2003) 'Glutamate-receptor-mediated encoding and retrieval of paired-associate learning', *Nature*, 424, p. 205. Available at: http://dx.doi.org/10.1038/nature01769.

Dayan, P. & Abbott, L. F. (2001) *Theoretical Neuroscience: Computational and Mathematical Modeling of Neural Systems*. MIT Press.

Derdikman, D., Whitlock, J. R., Tsao, A., Fyhn, M., Hafting, T., Moser, M.-B. & Moser, E. I. (2009) 'Fragmentation of grid cell maps in a multicompartment environment', *Nature Neuroscience*, 12(10), pp. 1325–1332. doi: 10.1038/nn.2396.

Diba, K. & Buzsáki, G. (2007) 'Forward and reverse hippocampal place-cell sequences during ripples.', *Nature neuroscience*, 10(10), pp. 1241–2. doi: 10.1038/nn1961.

Doeller, C. F., Barry, C. & Burgess, N. (2010) 'Evidence for grid cells in a human memory network', *Nature*, 463(7281), pp. 657–661. doi: 10.1038/nature08704.

Dombeck, D. A., Harvey, C. D., Tian, L., Looger, L. L. & Tank, D. W. (2010) 'Functional imaging of hippocampal place cells at cellular resolution during virtual navigation.', *Nature neuroscience*, 13(11), pp. 1433–40. doi: 10.1038/nn.2648.

Dragoi, G. & Tonegawa, S. (2011) 'Preplay of future place cell sequences by hippocampal cellular assemblies', *Nature*, 469(7330), pp. 397–401. doi: 10.1038/nature09633.

Dudchenko, P. (2010) *Why People Get Lost : The Psychology and Neuroscience of Spatial Cognition Abstract and Keywords Taxonomies of wayfinding*. Oxford University Press.

Dupret, D., O'Neill, J., Pleydell-Bouverie, B. & Csicsvari, J. (2010) 'The reorganization and reactivation of hippocampal maps predict spatial memory performance.', *Nature Neuroscience*, 13(8), pp. 995–1002. doi: 10.1038/nn.2599.

Ego-Stengel, V. & Wilson, M. A. (2010) 'Disruption of ripple-associated hippocampal activity during rest impairs spatial learning in the rat', *Hippocampus*, 20(1), pp. 1–10. doi: 10.1002/hipo.20707.

Erdem, U. M. & Hasselmo, M. E. (2012) 'A goal-directed spatial navigation model using forward trajectory planning based on grid cells', *European Journal of Neuroscience*, 35(6), pp. 916–931. doi: 10.1111/j.1460-9568.2012.08015.x.

Fiete, I. R., Burak, Y. & Brookings, T. (2008) 'What Grid Cells Convey about Rat Location', *Journal of Neuroscience*, 28(27), pp. 6858–6871. doi: 10.1523/JNEUROSCI.5684-07.2008.

Foster, D. J. & Wilson, M. A. (2006) 'Reverse replay of behavioural sequences in hippocampal place cells during the awake state', *Nature*, 440(7084), pp. 680–683. doi: 10.1038/nature04587.

Foster, D. J. & Wilson, M. A. (2007) 'Hippocampal theta sequences', *Hippocampus*, 17(11), pp. 1093–1099. doi: 10.1002/hipo.20345.

Fuhs, M. C. & Touretzky, D. S. (2006) 'A Spin Glass Model of Path Integration in Rat Medial Entorhinal Cortex', *Journal of Neuroscience*, 26(16), pp. 4266–4276. doi: 10.1523/JNEUROSCI.4353-05.2006.

Fyhn, M., Hafting, T., Treves, A., Moser, M.-B. & Moser, E. I. (2007) 'Hippocampal remapping and grid realignment in entorhinal cortex', *Nature*, 446(7132), pp. 190–194. doi: 10.1038/nature05601.

Garvert, M. M., Dolan, R. J. & Behrens, T. E. J. (2017) 'A map of abstract relational knowledge in the human hippocampal–entorhinal cortex', *eLife*, 6, pp. 1–20. doi: 10.7554/eLife.17086.

Ghosh, K. K., Burns, L. D., Cocker, E. D., Nimmerjahn, A., Ziv, Y., Gamal, A. El & Schnitzer, M. J. (2011) 'Miniaturized integration of a fluorescence microscope', *Nature Methods*, 8(10), pp. 871–878. doi: 10.1038/nmeth.1694.

Giocomo, L. M., Zilli, E. A., Fransén, E. & Hasselmo, M. E. (2007) 'Temporal frequency of subthreshold oscillations scales with entorhinal grid cell field spacing.', *Science*, 315(5819), pp. 1719–22. doi: 10.1126/science.1139207.

Giocomo, L. M., Hussaini, S. A., Zheng, F., Kandel, E. R., Moser, M.-B. & Moser, E. I. (2011) 'Grid cells use HCN1 channels for spatial scaling', *Cell*, 147(5), pp. 1159–1170. doi: 10.1016/j.cell.2011.08.051.

Girardeau, G., Benchenane, K., Wiener, S. I., Buzsáki, G. & Zugaro, M. B. (2009) 'Selective suppression of hippocampal ripples impairs spatial memory', *Nature Neuroscience*, 12(10), pp. 1222–1223. doi: 10.1038/nn.2384.

Goodridge, J. P., Dudchenko, P. A., Worboys, K. A., Golob, E. J. & Taube, J. S. (1998) 'Cue control and head direction cells.', *Behavioral Neuroscience*, 112(4), pp. 749–761. doi: 10.1037/0735-7044.112.4.749.

Gould, S. J. & Lewontin, R. C. (1979) 'The Spandrels of San Marco and the Panglossian Paradigm: A Critique of the Adaptationist Programme', *Proceedings of the Royal Society B: Biological Sciences*, 205(1161), pp. 581–598. doi: 10.1098/rspb.1979.0086.

Gupta, A. S., van der Meer, M. A. A., Touretzky, D. S. & Redish, A. D. (2010) 'Hippocampal Replay Is Not a Simple Function of Experience', *Neuron*, 65(5), pp. 695–705. doi: 10.1016/j.neuron.2010.01.034.

Hafting, T., Fyhn, M., Molden, S., Moser, M.-B. & Moser, E. I. (2005) 'Microstructure of a spatial map in the entorhinal cortex', *Nature*, 436(7052), pp. 801–806. doi: 10.1038/nature03721.

Hafting, T., Fyhn, M., Bonnevie, T., Moser, M.-B. & Moser, E. I. (2008) 'Hippocampus-independent phase precession in entorhinal grid cells', *Nature*, 453(7199), pp. 1248–1252. doi: 10.1038/nature06957.

Hardcastle, K., Ganguli, S. & Giocomo, L. M. (2015) 'Environmental Boundaries as an Error Correction Mechanism for Grid Cells', *Neuron*, 86(3), pp. 827–839. doi: 10.1016/j.neuron.2015.03.039.

Hartley, T., Burgess, N., Lever, C., Cacucci, F. & O'Keefe, J. (2000) 'Modeling place fields in terms of the cortical inputs to the hippocampus', *Hippocampus*, 10(4), pp. 369–379. doi: 10.1002/1098-1063(2000)10:4<369::AID-HIPO3>3.0.CO;2-0.

Hassabis, D., Kumaran, D., Vann, S. D. & Maguire, E. a (2007) 'Patients with hippocampal amnesia cannot imagine new experiences.', *Proceedings of the National Academy of Sciences of the United States of America*, 104(5), pp. 1726–1731. doi: 10.1073/pnas.0610561104.

Heys, J. G. & Hasselmo, M. E. (2012) 'Neuromodulation of I h in layer II medial entorhinal cortex stellate cells: A voltage-clamp study', *Journal of Neuroscience*, 32(26), pp. 9066–9072. doi: 10.1523/JNEUROSCI.0868-12.2012.

Heys, J. G., Rangarajan, K. V. & Dombeck, D. A. (2014) 'The Functional Micro-organization of Grid Cells Revealed by Cellular-Resolution Imaging', *Neuron*. Elsevier, 84(5), pp. 1079–1090. doi: 10.1016/j.neuron.2014.10.048.

Horner, A. J., Bisby, J. A., Zotow, E., Bush, D. & Burgess, N. (2016) 'Grid-like Processing of Imagined Navigation', *Current Biology*, 26(6), pp. 842–847. doi: 10.1016/j.cub.2016.01.042.

Ismakov, R., Barak, O., Jeffery, K. & Derdikman, D. (2017) 'Grid Cells Encode Local Positional Information', *Current Biology*, 27(15), p. 2337–2343.e3. doi: 10.1016/j.cub.2017.06.034.

Jacobs, J. et al. (2013) 'Direct recordings of grid-like neuronal activity in human spatial navigation', *Nature Neuroscience*, 16(9), pp. 1188–1190. doi: 10.1038/nn.3466.

Jadhav, S. P., Kemere, C., German, P. W. & Frank, L. M. (2012) 'Awake Hippocampal Sharp-Wave Ripples Support Spatial Memory', *Science*, 336(6087), pp. 1454–1458. doi: 10.1126/science.1217230.

Jeffery, K. J., Wilson, J. J., Casali, G. & Hayman, R. M. (2015) 'Neural encoding of large-scale three-dimensional space—properties and constraints', *Frontiers in Psychology*, 6. doi: 10.3389/fpsyg.2015.00927.

Johnson, A. & Redish, A. D. (2007) 'Neural ensembles in CA3 transiently encode paths forward of the animal at a decision point.', *Journal of Neuroscience*, 27(45), pp. 12176–89. doi: 10.1523/JNEUROSCI.3761-07.2007.

Joint Committee for Guides in Metrology (2012) *International vocabulary of metrology - Basic and general concepts and associated terms (VIM)*. 3rd edn. Available at: https://www.bipm.org/en/publications/guides/vim.html.

Julian, J. B., Keinath, A. T., Frazzetta, G. & Epstein, R. A. (2018) 'Human entorhinal cortex represents visual space using a boundary-anchored grid', *Nature Neuroscience*, 21(February). doi: 10.1038/s41593-017-0049-1.

Jun, J. J. et al. (2017) 'Fully integrated silicon probes for high-density recording of neural activity', *Nature*, 551(7679), pp. 232–236. doi: 10.1038/nature24636.

Kant, I. (1787) *Critique of Pure Reason*. 2nd edn.

Karlsson, M. P. & Frank, L. M. (2009) 'Awake replay of remote experiences in the hippocampus.', *Nature neuroscience*, 12(7), pp. 913–918. doi: 10.1038/nn.2344.

Killian, N. J., Jutras, M. J. & Buffalo, E. A. (2012) 'A map of visual space in the primate entorhinal cortex', *Nature*, 491(7426), pp. 761–764. doi: 10.1038/nature11587.

Kluger, C., Mathis, A., Stemmler, M. B. & Herz, A. V. M. (2010) 'Movement Related Statistics of Grid Cell Firing', in *Frontiers in Computational Neuroscience Conference Abstract: Bernstein Conference on Computational Neuroscience*. doi: 10.3389/conf.fncom.2010.51.00134.

Knierim, J. J. (2009) 'Imagining the Possibilities: Ripples, Routes, and Reactivation', *Neuron*, 63(4), pp. 421–423. doi: 10.1016/j.neuron.2009.08.002.

Knierim, J. J., Kudrimoti, H. S. & McNaughton, B. L. (1995) 'Place cells, head direction cells, and the learning of landmark stability.', *Journal of Neuroscience*, 15(3 Pt 1), pp. 1648–1659.

Koenig, J., Linder, A. N., Leutgeb, J. K. & Leutgeb, S. (2011) 'The Spatial Periodicity of Grid Cells Is Not Sustained During Reduced Theta Oscillations', *Science*, 332(6029), pp. 592–595. doi: 10.1126/science.1201685.

Kropff, E. & Treves, A. (2008) 'The emergence of grid cells: Intelligent design or just adaptation?', *Hippocampus*. Wiley-Blackwell, 18(12), pp. 1256–1269. doi: 10.1002/hipo.20520.

Krupic, J., Bauza, M., Burton, S., Lever, C. & O'Keefe, J. (2014) 'How environment geometry affects grid cell symmetry and what we can learn from it', *Philosophical Transactions of the Royal Society B: Biological Sciences*, 369(1635), p. 20130188. doi: 10.1098/rstb.2013.0188.

Krupic, J., Bauza, M., Burton, S., Barry, C. & O'Keefe, J. (2015) 'Grid cell symmetry is shaped by environmental geometry', *Nature*, 518(7538), pp. 232–235. doi: 10.1038/nature14153.

Krupic, J., Bauza, M., Burton, S. & O'Keefe, J. (2018) 'Local transformations of the hippocampal cognitive map', *Science*, 359(6380), pp. 1143–1146. doi: 10.1126/science.aao4960.

Kubie, J. L., Fenton, A. A., Lytton, W. W., Park, E. H. & Burgess, N. (2009) 'Grid Cell Models for Navigation and Context Discrimination (Poster)', in *Society for Neuroscience Annual Meeting 2009*.

Kubie, J. L. & Fenton, A. A. (2012) 'Linear Look-Ahead in Conjunctive Cells: An Entorhinal Mechanism for Vector-Based Navigation', *Frontiers in Neural Circuits*, 6(20), pp. 1–15. doi: 10.3389/fncir.2012.00020.

Kudrimoti, H. S., Barnes, C. A. & McNaughton, B. L. (1999) 'Reactivation of hippocampal cell assemblies: effects of behavioral state, experience, and EEG dynamics', *Journal of Neuroscience*, 19(10), pp. 4090–4101. Available at: http://www.jneurosci.org/content/19/10/4090.long.

Kunz, L. et al. (2015) 'Reduced grid-cell-like representations in adults at genetic risk for Alzheimer's disease.', *Science*, 350(6259), pp. 430–3. doi: 10.1126/science.aac8128.

Langston, R. F., Ainge, J. A., Couey, J. J., Canto, C. B., Bjerknes, T. L., Witter, M. P., Moser, E. I. & Moser, M.-B. (2010) 'Development of the Spatial Representation System in the Rat', *Science*, 328(5985), pp. 1576–80. doi: 10.1126/science.1188210.

Lashley, K. S. (1929) *Brain mechanisms and intelligence: A quantitative study of injuries to the brain.* Chicago: University of Chicago Press. doi: 10.1037/10017-000.

de Lavilléon, G., Lacroix, M. M., Rondi-Reig, L. & Benchenane, K. (2015) 'Explicit memory creation during sleep demonstrates a causal role of place cells in navigation', *Nature Neuroscience*, 18(4), pp. 493–495. doi: 10.1038/nn.3970.

Lee, A. K. & Wilson, M. A. (2002) 'Memory of sequential experience in the hippocampus during slow wave sleep', *Neuron*, 36(6), pp. 1183–1194. doi: 10.1016/S0896-6273(02)01096-6.

Lever, C., Burton, S., Jeewajee, A., O'Keefe, J. M. & Burgess, N. (2009) 'Boundary vector cells in the subiculum of the hippocampal formation.', *Journal of Neuroscience*, 29(31), pp. 9771–9777. doi: 10.1523/JNEUROSCI.1319-09.2009.

Lisman, J., Buzsáki, G., Eichenbaum, H., Nadel, L., Ranganath, C. & Redish, A. D. (2017) 'Viewpoints: how the hippocampus contributes to memory, navigation and cognition', *Nature Neuroscience*, 20, p. 1434. Available at: http://dx.doi.org/10.1038/nn.4661.

Louie, K. & Wilson, M. A. (2001) 'Temporally structured replay of awake hippocampal ensemble activity during rapid eye movement sleep', *Neuron*, 29(1), pp. 145–156. doi: 10.1016/S0896-6273(01)00186-6.

Mallory, C. S., Hardcastle, K., Bant, J. S. & Giocomo, L. M. (2018) 'Grid scale drives the scale and long-term stability of place maps', *Nature Neuroscience*, p. 1. doi: 10.1038/s41593-017-0055-3.

Malvache, A., Reichinnek, S., Villette, V., Haimerl, C. & Cossart, R. (2016) 'Awake hippocampal reactivations project onto orthogonal neuronal assemblies', *Science*, 353(6305), pp. 1280–1283. doi: 10.1126/science.aaf3319.

Manson, D. (2017) *The Role of Grid Cells in Spatial Localisation and Computation*. UCL. Available at: http://discovery.ucl.ac.uk/id/eprint/1542147.

Markus, E. J., Barnes, C. A., McNaughton, B. L., Gladden, V. L. & Skaggs, W. E. (1994) 'Spatial information content and reliability of hippocampal CA1 neurons: Effects of visual input', *Hippocampus*, 4(4), pp. 410–421. doi: 10.1002/hipo.450040404.

Mathis, A., Herz, A. V. M. & Stemmler, M. B. (2012) 'Optimal Population Codes for Space: Grid Cells Outperform Place Cells', *Neural Computation*, 24(9), pp. 2280–2317. doi: 10.1162/NECO_a_00319.

McNaughton, B. L., Battaglia, F. P., Jensen, O., Moser, E. I. & Moser, M.-B. (2006) 'Path integration and the neural basis of the "cognitive map"', *Nature Reviews Neuroscience*, 7(8), pp. 663–678. doi: 10.1038/nrn1932.

Morris, R. G. M. (1981) 'Spatial localization does not require the presence of local cues', *Learning and Motivation*, 12(2), pp. 239–260. doi: 10.1016/0023-9690(81)90020-5.

Mosheiff, N., Agmon, H., Moriel, A. & Burak, Y. (2017) 'An efficient coding theory for a dynamic trajectory predicts non-uniform allocation of entorhinal grid cells to modules', *PLOS Computational Biology*, 13(6), p. e1005597. doi: 10.1371/journal.pcbi.1005597.

Mulders, W. H. A. M., West, M. J. & Slomianka, L. (1997) 'Neuron numbers in the presubiculum, parasubiculum, and entorhinal area of the rat', *Journal of Comparative Neurology*, 385(1), pp. 83–94. doi: 10.1002/(SICI)1096-9861(19970818)385:1<83::AID-CNE5>3.0.CO;2-8.

Muller, R. U. & Kubie, J. L. (1987) 'The effects of changes in the environment on the spatial firing of hippocampal complex-spike cells', *Journal of Neuroscience*, 7(7), pp. 1951–1968.

Muller, R. U., Kubie, J. L. & Saypoff, R. (1991) 'The hippocampus as a cognitive graph (abridged version)', *Hippocampus*, 1(3), pp. 243–246. doi: 10.1002/hipo.450010306.

Nau, M., Navarro Schröder, T., Bellmund, J. L. S. & Doeller, C. F. (2018) 'Hexadirectional coding of visual space in human entorhinal cortex', *Nature Neuroscience*. doi: 10.1038/s41593-017-0050-8.

Navarro Schroeder, T., Towse, B. W., Burgess, N., Barry, C. & Doeller, C. F. (2017) 'Optimal decision making using grid cells under spatial uncertainty', *bioRxiv*. doi: 10.1101/166306.

O'Keefe, J. & Burgess, N. (1996) 'Geometric determinants of the place fields of hippocampal neurons', *Nature*, 381(6581), pp. 425–428. doi: 10.1038/381425a0.

O'Keefe, J. & Dostrovsky, J. (1971) 'The hippocampus as a spatial map. Preliminary evidence from unit activity in the freely-moving rat', *Brain Research*, 34(1), pp. 171–175. doi: 10.1016/0006-8993(71)90358-1.

O'Keefe, J. M. & Burgess, N. (2005) 'Dual phase and rate coding in hippocampal place cells: Theoretical significance and relationship to entorhinal grid cells', *Hippocampus*, 15(7), pp. 853–866. doi: 10.1002/hipo.20115.

O'Keefe, J. M. & Recce, M. L. (1993) 'Phase relationship between hippocampal place units and the EEG theta rhythm', *Hippocampus*, 3(3), pp. 317–330. doi: 10.1002/hipo.450030307.

O'Keefe, J. & Nadel, L. (1978) *The Hippocampus as a Cognitive Map*. Oxford University Press. Available at: http://www.cognitivemap.net/.

O'Neill, J., Boccara, C. N., Stella, F., Schoenenberger, P. & Csicsvari, J. (2017) 'Superficial layers of the medial entorhinal cortex replay independently of the hippocampus', *Science*, 355(6321), pp. 184–188. doi: 10.1126/science.aag2787.

Ólafsdóttir, H. F., Barry, C., Saleem, A. B., Hassabis, D. & Spiers, H. J. (2015) 'Hippocampal place cells construct reward related sequences through unexplored space', *eLife*, 4(JUNE2015), pp. 1–17. doi: 10.7554/eLife.06063.

Ólafsdóttir, H. F., Bush, D. & Barry, C. (2018) 'The Role of Hippocampal Replay in Memory and Planning', *Current Biology*, 28(1), pp. R37–R50. doi: 10.1016/j.cub.2017.10.073.

Ólafsdóttir, H. F., Carpenter, F. & Barry, C. (2016) 'Coordinated grid and place cell replay during rest.', *Nature neuroscience*, (April), pp. 1–6. doi: 10.1038/nn.4291.

Ólafsdóttir, H. F., Carpenter, F. & Barry, C. (2017) 'Task Demands Predict a Dynamic Switch in the Content of Awake Hippocampal Replay', *Neuron*, pp. 925–935. doi: 10.1016/j.neuron.2017.09.035.

Palmer, L. & Lynch, G. (2010) 'A Kantian View of Space', *Science*. AAAS, 328(5985), pp. 1487–1488. doi: 10.1126/science.1191527.

Pfeiffer, B. E. & Foster, D. J. (2013) 'Hippocampal place-cell sequences depict future paths to remembered goals', *Nature*, 497(7447), pp. 74–79. doi: 10.1038/nature12112.

Ranck Jr, J. B. (1984) 'Head-direction cells in the deep cell layers of dorsal presubiculum in freely moving rats', *Society for Neuroscience Abstracts*, 10(176.12), p. 599.

Recht, M. A. (1988) 'The biology of domestic rats: telemetry yields insights for pest control', in *Thirteenth Vertebrate Pest Conference*. DigitalCommons@University of Nebraska - Lincoln, pp. 98–100. Available at: http://digitalcommons.unl.edu/vpcthirteen/21 (Accessed: 1 February 2013).

Russell, J. C., Towns, D. R., Anderson, S. H. & Clout, M. N. (2005) 'Intercepting the first rat ashore', *Nature*, 437(7062), pp. 1107–1107. doi: 10.1038/4371107a.

Salinas, E. & Abbott, L. F. (1994) 'Vector reconstruction from firing rates', *Journal of Computational Neuroscience*, 1(1–2), pp. 89–107. doi: 10.1007/BF00962720.

Sargolini, F., Fyhn, M., Hafting, T., McNaughton, B. L., Witter, M. P., Moser, M.-B. & Moser, E. I. (2006) 'Conjunctive Representation of Position, Direction, and Velocity in Entorhinal Cortex', *Science*, 312(2006), pp. 758–763. doi: 10.1126/science.1099901.

SAS Institute (2009) 'Mean Squared Error', in *SAS/STAT ® 9.2 User's Guide*. 2nd edn. Cary, NC: SAS Institute Inc., p. 60. Available at: https://support.sas.com/documentation/cdl/en/statug/63033/PDF/default/statug.pdf.

Savelli, F., Yoganarasimha, D. & Knierim, J. J. (2008) 'Influence of boundary removal on the spatial representations of the medial entorhinal cortex', *Hippocampus*, 18(12), pp. 1270–1282. doi: 10.1002/hipo.20511.

Singer, A. C., Carr, M. F., Karlsson, M. P. & Frank, L. M. (2013) 'Hippocampal SWR Activity Predicts Correct Decisions during the Initial Learning of an Alternation Task', *Neuron*, 77(6), pp. 1163–1173. doi: 10.1016/j.neuron.2013.01.027.

Skaggs, W. E., Knierim, J. J., Kudrimoti, H. S. & McNaughton, B. L. (1994) 'A model of the neural basis of the rat's sense of direction.', in Tesauro, G., Touretzky, D. S., and Leen, T. K. (eds) *Advances in neural information processing systems*. Neural Information Processing Systems Foundation, Inc., pp. 173–180. Available at: https://papers.nips.cc/paper/890-a-model-of-the-neural-basis-of-the-rats-sense-of-direction (Accessed: 25 March 2018).

Skaggs, W. E. & McNaughton, B. L. (1996) 'Replay of neuronal firing sequences in rat hippocampus during sleep following spatial experience.', *Science*, 271(5257), pp. 1870–1873. doi: 10.1126/science.271.5257.1870.

Solstad, T., Boccara, C. N., Kropff, E., Moser, M.-B. & Moser, E. I. (2008) 'Representation of Geometric Borders in the Entorhinal Cortex', *Science*, 322(5909), pp. 1865–1868. doi: 10.1126/science.1166466.

Sreenivasan, S. & Fiete, I. R. (2011) 'Grid cells generate an analog error-correcting code for singularly precise neural computation.', *Nature neuroscience*, 14(10), pp. 1330–7. doi: 10.1038/nn.2901.

Stackman, R. W. & Taube, J. S. (1998) 'Firing properties of rat lateral mammillary single units: head direction, head pitch, and angular head velocity.', *Journal of Neuroscience*, 18(21), pp. 9020–37. doi: 10.3389/fnbeh.2016.00040.

Stemmler, M. B., Mathis, A. & Herz, A. V. M. (2015) 'Connecting multiple spatial scales to decode the population activity of grid cells', *Science Advances*, 1(11), pp. e1500816–e1500816. doi: 10.1126/science.1500816.

Stensola, H., Stensola, T., Solstad, T., Frøland, K., Moser, M.-B. & Moser, E. I. (2012) 'The entorhinal grid map is discretized.', *Nature*, 492(7427), pp. 72–8. doi: 10.1038/nature11649.

Stensola, T., Stensola, H., Moser, M.-B. & Moser, E. I. (2015) 'Shearing-induced asymmetry in entorhinal grid cells', *Nature*, 518(7538), pp. 207–212. doi: 10.1038/nature14151.

Stewart, S., Jeewajee, A., Wills, T. J., Burgess, N. & Lever, C. (2014) 'Boundary coding in the rat subiculum.', *Philosophical transactions of the Royal Society of London. Series B, Biological sciences*, 369(1635), p. 20120514. doi: 10.1098/rstb.2012.0514.

Taube, J. S. (2007) 'The head direction signal: origins and sensory-motor integration.', *Annual review of neuroscience*, 30, pp. 181–207. doi: 10.1146/annurev.neuro.29.051605.112854.

Taube, J. S., Muller, R. U. & Ranck, J. B. (1990) 'Head-direction cells recorded from the postsubiculum in freely moving rats. II. Effects of environmental manipulations.', *Journal of Neuroscience*, 10(2), pp. 436–47. Available at: http://www.jneurosci.org/content/10/2/436.

Tolman, E. C. (1948) 'Cognitive maps in rats and men.', *Psychological review*, 55(4), pp. 189–208. doi: 10.1037/h0061626.

Towse, B. W., Barry, C., Bush, D. & Burgess, N. (2014) 'Optimal configurations of spatial scale for grid cell firing under noise and uncertainty.', *Philosophical transactions of the Royal Society B*, 369(1635). doi: 10.1098/rstb.2013.0290.

Trettel, S. G. & Colgin, L. L. (2014) 'Grid cells in superficial layers of medial entorhinal cortex replay waking activity patterns during subsequent rapid eye movement sleep', in *Poster: Society for Neuroscience Annual Meeting 2014*. Washington D.C. Available at: http://www.sfn.org/~/media/SfN/Documents/AnnualMeeting/FinalProgram/NS2014/FullAbstractPDFs_2014/SFN2014_Abstracts_PDF_Wed_AM.ashx.

Trimper, J. B., Trettel, S. G., Hwaun, E. & Colgin, L. L. (2017) 'Methodological Caveats in the Detection of Coordinated Replay between Place Cells and Grid Cells', *Frontiers in Systems Neuroscience*, 11(August), pp. 1–14. doi: 10.3389/fnsys.2017.00057.

Vágó, L. & Ujfalussy, B. B. (2018) 'Robust and efficient coding with grid cells.', *PLoS computational biology*, 14(1), p. e1005922. doi: 10.1371/journal.pcbi.1005922.

Wei, X.-X., Prentice, J. & Balasubramanian, V. (2015) 'A principle of economy predicts the functional architecture of grid cells', *eLife*, 4(September), pp. 1–29. doi: 10.7554/eLife.08362.

Wikenheiser, A. M. & Redish, A. D. (2015) 'Decoding the cognitive map: ensemble hippocampal sequences and decision making', *Current Opinion in Neurobiology*, 32, pp. 8–15. doi: 10.1016/j.conb.2014.10.002.

Wills, T. J., Cacucci, F., Burgess, N. & O'Keefe, J. M. (2010) 'Development of the hippocampal cognitive map in preweanling rats.', *Science*, 328(5985), pp. 1573–1576. doi: 10.1126/science.1188224.

Wilson, M. A. & McNaughton, B. L. (1993) 'Dynamics of the hippocampal ensemble code for space', *Science*, 261(5124), pp. 1055–1058. doi: 10.1126/science.8351520.

Wilson, M. & McNaughton, B. (1994) 'Reactivation of hippocampal ensemble memories during sleep', *Science*, 265(5172), pp. 676–679. doi: 10.1126/science.8036517.

Witter, M. P., Naber, P. A., van Haeften, T., Machielsen, W. C., Rombouts, S. A., Barkhof, F., Scheltens, P. & Lopes da Silva, F. H. (2000) 'Cortico-hippocampal communication by way of parallel parahippocampal-subicular pathways.', *Hippocampus*, 10(4), pp. 398–410. doi: 10.1002/1098-1063(2000)10:4<398::AID-HIPO6>3.0.CO;2-K.

Wood, R. A., Bauza, M., Krupic, J., Burton, S., Delekate, A., Chan, D. & O'Keefe, J. (2018) 'The honeycomb maze provides a novel test to study hippocampal-dependent spatial navigation', *Nature*, 554(7690), pp. 102–105. doi: 10.1038/nature25433.

Yartsev, M. M., Witter, M. P. & Ulanovsky, N. (2011) 'Grid cells without theta oscillations in the entorhinal cortex of bats', *Nature*, 479(7371), pp. 103–107. doi: 10.1038/nature10583.

Yoon, K., Buice, M. A., Barry, C., Hayman, R., Burgess, N. & Fiete, I. R. (2013) 'Specific evidence of low-dimensional continuous attractor dynamics in grid cells.', *Nature Neuroscience*, 16(8), pp. 1077–1084. doi: 10.1038/nn.3450.

Yu, A. J. & Dayan, P. (2005) 'Uncertainty, neuromodulation, and attention', *Neuron*, 46(4), pp. 681–692. doi: 10.1016/j.neuron.2005.04.026.